Physical modeling of the organization and dynamics of intracellular organelles

Jean-Patrick Vrel

Université de Paris
École Doctorale 474, Frontière du Vivant

UMR 168, Physico-Chimie
Institut Curie
Physical Approach of Biological Problems

Thèse de doctorat en Biophysique

Physical modeling of the organization and dynamics of intracellular organelles

Modélisation physique de l'organisation et de la dynamique de organites intracellulaires

Jean-Patrick Vrel

Rapporteurs Pr. Nicolas Destainville
Laboratoire de Physique Théorique – UMR 5152
Université Toulouse III – Paul Sabatier

Dr. David Lacoste
Laboratoire Gulliver – UMR 7083
ESPCI – Paris

Directeur Dr. Pierre Sens

Examinateurs Dr. Anne-Florence Bitbol
Dr. Cathy Jackson
Dr. Stephanie Miserey-Lenkei

Septembre 2019

Jean-Patrick Vrel

Physical modeling of the organization and dynamics of intracellular organelles

Modélisation physique de l'organisation et de la dynamique de organites intracellulaires

Thèse de doctorat en Biophysique, Septembre 2019
Rapporteurs: Pr. Nicolas Destainville and Dr. David Lacoste
Directeur: Dr. Pierre Sens

Université de Paris
École Doctorale 474, Frontière du Vivant
Physical Approach of Biological Problems
Institut Curie
UMR 168, Physico-Chimie
11 Rue Pierre et Marie Curie
75005, Paris

“For doubt can exist only where a question exists, a question only where an answer exists, and an answer only where something can be said.”

(6.51) – Tractatus Logico-Philosophicus

“My difficulty is only an – enormous – difficulty of expression.”

Notebooks 1914-1916

Ludwig Wittgenstein

Abstract

Eukaryotic cells are highly compartmentalized into intracellular organelles, such as the endoplasmic reticulum, the Golgi apparatus, endosomes and lysosomes. These are dynamical structures bounded by lipid membranes, within which components undergo biochemical modification by enzymes, and between which components are constantly being exchanged. Despite their highly dynamical nature, their spatial organization is fairly well conserved over time, so that they could be seen as stationary states of a highly non-equilibrium, and multi-component system. On the other hand, this organization has been observed to be totally disorganized in pathologies or drug treatments.

Self-organization in equilibrium systems is fairly well understood by means of phase diagrams where the occurrence of different phases (dispersed, condensed, phase separated) depends on physical parameters (concentrations, interaction energy between components). The situation is much less clear for non-equilibrium systems. It is therefore an exciting challenge to reach a quantitative understanding of the mechanisms dictating the intra-cellular organization, where active transport and biochemical modification by energy-consuming enzymes compete with purely passive phenomena such as diffusion. We design and study, both analytically and numerically, simple models of self-organization and transport in systems where a limited number of components may self-organize into larger structures by means of stochastic reactions. Our main fundamental question is to determine how the interplay between the dynamics of inter-organelle exchange (by means of vesicle secretion, transport and fusion) and the kinetics of biochemical maturation within organelles may yield a precise and robust organelle network. To this end we focus on one “stereotype” organelle, that is already multi-compartments and with a very rich dynamics of vesiculation, fusion and maturation: the Golgi Apparatus.

We describe and understand the steady-state organization of such systems, in term of compartments’ size and purity – how big and well sorted are the different compartments. From this steady-state, a vesicular transport spontaneously emerges, whose directionality is linked to the steady-state organization. It is anterograde in a pure regime, and retrograde in a mixed configuration. We also show that local interaction between components being transported, and membranes are sufficient to

bias their transport, such that given proteins may undergo anterograde or retrograde transport depending on their interactions with the different membrane identities present in the system. This in turns influences the steady-state localization of these proteins. This both change the kinetics of transport in the system, and thus their location in the compartments. How efficient the system is in sorting these elements, strongly relies on the steady-state organization and the vesicular transport. Our work demonstrates the intimate link that exists between structure and transport dynamics in the Golgi apparatus, and can be extrapolated to other cellular organelles implicated in intracellular transport.

Résumé des travaux de thèse

Contexte

Les cellules eukaryotes sont compartimentées en réseaux d'organites intracellulaires, qui délimitent des territoires sub-cellulaires spécialisés. Même si la définition stricte est plus large, on entend par organites des compartiments intracellulaires délimités par des membranes, compartiments dotés d'une structure et d'une fonction propres. Ces structures communiquent les unes avec les autres et sont organisées en réseaux. L'un de ces organites, l'appareil de Golgi (ou Golgi), est un exemple réduit de ces réseaux, et à ce titre, un système de choix pour toute étude sur les organites intracellulaires et leur fonctionnement.

Le Golgi est en effet lui-même constitué d'un ensemble de compartiments distincts, appelés citernes, présentant chacun une identité biochimique propre : *cis* lorsque proche du réticulum endoplasmique et du noyau, *trans* proche de la membrane cellulaire, et *medial* entre deux. Cette structure est continuellement traversée d'un flux de protéines que l'organite trie et modifie, protéines entrant dans le Golgi par sa face *cis*, pour le quitter à sa face *trans*. C'est une structure dynamique dont les composants sont renouvelés continuellement, et dans laquelle s'organise un important transport de vésicules entre les citernes.

Une question se pose : comment stabiliser la polarité $cis \rightarrow medial \rightarrow trans$ alors même que le système est brassé par de tels flux ? C'est une question importante car la structure et la polarité de cet organite sont cruciales à sa fonction, et celles de la cellule en générale. Et on peut citer par exemple certaines maladies neurodégénéra-

tives où la structure golgienne est altérée. C'est cependant une question difficile, car les techniques de microscopie *in vivo* n'offrent pas la résolution spatiale nécessaire à l'observation des transports qui y prennent place. En conséquence, comment cet organite s'organise et fonctionne, notamment dans son transport des cargos, est une question ouverte. Deux hypothèses s'opposent pour y répondre. L'une postule que les citernes sont continuellement formées à la face *cis* et se déplacent avec les cargos à mesure que leurs identités maturent vers une composition *trans*. Un transport rétrograde de vésicules empêchent dans cette hypothèse les constituants du Golgi d'en échapper. L'autre postule que les citernes sont des entités fixes, avec une composition fixe, et que les cargos transitent d'un compartiment à l'autre en suivant un flux antérograde de vésicules.

L'une et l'autre de ces hypothèses ayant trouvé des preuves indirectes de leur véracité [Los+06; Dun+17], trancher cette question est aujourd'hui impossible par l'expérience. Modéliser ce système pour en comprendre les lois générales a donc toute sa pertinence, aussi bien pour comprendre le Golgi que pour créer de nouveaux paradigmes sur l'organisation et la fonction des organites. C'est un travail intéressant aussi bien pour les biologistes à la recherche de nouveaux outils conceptuels, mais aussi pour les physiciens pour qui l'organisation de systèmes hors équilibre est une question non-triviale. C'est pourquoi nous étudions un modèle simple du Golgi, en ne faisant que le minimum d'hypothèses. L'objectif est de voir si ces dynamiques de transports vésiculaires peuvent émerger d'un Golgi théorique, dont l'état stationnaire s'auto-organise à partir de mécanismes simples. Et si oui, quelles sont les conditions nécessaires à leur émergence.

Résultats

Le modèle

Le modèle se focalise sur trois mécanismes généraux, observés dans quasiment tous les organites, et communs aux appareils de Golgi de toutes les cellules eukaryotes :

- la conversion des membranes d'une identité biochimique à une autre au cours du temps [GON06].
- la scission des compartiments pour former un sous-compartiment plus petit (typiquement une vésicule) [MM04].
- la fusion des compartiments entre eux, que ce soit des vésicules entre elles, des vésicules avec un compartiment, ou des compartiments entre eux. Plus

ces compartiments ont des compositions proches, plus probable est leur fusion, phénomène observé *in vivo* et nommé fusion homotypique [Pfe10].

Aucune contrainte ni de structure, ni de directionalité pour le transport vésiculaire, n'est imposée. Les seuls paramètres sont les taux associés au processus stochastiques de maturation, de fusion et de vésiculation. Aussi bien la structure que le transport vésiculaire émergent par auto-organisation des composants du Golgi, qui ne sont soumis qu'aux 3 mécanismes cités. Nous étudions ce modèle numériquement (simulations codées et réalisées durant la thèse) et analytiquement (calculs effectués durant la thèse) pour caractériser la structure et le transport vésiculaire dans cet organite théorique.

Premier objectif : caractériser la structure du Golgi théorique

Le premier objectif pour comprendre ce Golgi théorique, est d'en caractériser la structure à l'état stationnaire. Cette structure est définie par la taille des compartiments, ainsi que leur pureté (forte pureté pour une membrane décorée d'une unique identité, faible pureté pour un mélange). On montre que la taille des compartiments est impactée par le rapport du taux de scission sur le taux de fusion. Plus rapide est la scission ou plus lente est la fusion entre les compartiments, plus petite est leur taille. La pureté des compartiments est quant à elle impactée par le rapport du taux de maturation sur le taux de scission. Plus rapide est la vésiculation, plus vite les compartiments éliminent les éléments de membrane ayant subi une maturation, étant donc devenus contaminants dans le compartiment.

Le taux de scission impacte donc à la fois la taille et la pureté des compartiments, ce qui permet de distinguer trois régimes d'état stationnaire en fonction du taux de scission (à taux de fusion et de maturation fixés) : un régime ***mixé*** avec de gros compartiments impurs (faible taux de scission), un régime ***vésiculaire*** avec de petits compartiments purs (fort taux de scission), et un régime ***trié*** où les compartiments sont à la fois gros et purs (taux de scission intermédiaire). Ce résultat est particulièrement intéressant car il explique avec peu d'hypothèses pourquoi diminuer le taux de vésiculation augmente la taille des compartiments (ce à quoi on pourrait s'attendre) mais aussi pourquoi il en diminue la pureté [Pap+15]. Il explique également pourquoi accélérer la maturation diminue cette même pureté [Kim+16].

Deuxième objectif : caractériser le transport vésiculaire émergent

On montre avec ce modèle, que les deux hypothèses généralement avancées quant au transport vésiculaire, sont possibles au sein du même système. La direction du transport vésiculaire peut en effet être anterograde ou rétrograde selon les régimes d'état stationnaire. Un transport rétrograde émerge dans les régimes *mixés* ; tandis qu'un transport antérograde émerge dans les régimes *triés* et *vésiculaires*.

C'est encore une fois le rapport du taux de maturation sur le taux de vésiculation qui définit la direction du transport vésiculaire. Pour une vésicule nouvellement formée, deux épisodes de fusion sont possibles : si la vésicule est de la même composition que le compartiment dont elle est issue, elle peut fusionner homotypiquement avec ce dernier ; mais si elle est contaminante (didentité minoritaire) dans son compartiment, elle doit alors trouver un autre compartiment avec qui fusionner homotypiquement. On remarque que le premier cas ne crée pas de transport vésiculaire net, alors que le second si. La question est donc de savoir si les espèce contaminantes des compartiments sont en moyenne plus matures ou moins matures que le compartiment qui les crée. Plus matures et elles fusionnent homotypiquement avec un compartiment plus mature (transport antérograde), et inversement. Dans le cas d'un régime *mixé* à fort taux de maturation, l'espèce contaminante est celle qui n'a pas encore subit de maturation : le transport est donc rétrograde. A l'inverse, dans un régime *trié* ou *vésiculaire*, l'espèce contaminante est celle qui vient juste de mûrir : le transport est antérograde.

De façon intéressante, une analyse de la littérature montre que le transport vésiculaire rétrograde, avec maturation des citernes, est souvent inféré chez des organismes ayant un Golgi plutôt mixé (colocalisation de plusieurs marqueurs golgiens) [Los+06]. En revanche, chez les eukaryotes supérieurs, dont le Golgi est supposé davantage trié, c'est davantage le transport anterograde qui y est inféré [Dun+17]. Ce modèle est donc cohérent avec les observations expérimentales, et explique qualitativement et avec peu d'hypothèses ces variations entre espèces.

Troisième objectif : le tris et l'adressage des protéines

Le dernier objectif de cette thèse est de voir si différents types de cargos peuvent avoir différentes voies de transport vésiculaire, différentes localisations dans le Golgi, ainsi que différentes cinétiques de transport en fonction de leur affinité. Pour ce faire, nous suivons des cargos qui interagissent de manière spécifique avec les différentes identités membranaires qu'ils peuvent rencontrer. Ces cargos ont en effet une forte

affinité pour l'une des identités membranaires, et sont donc appelés cargos *cis*, *medial* et *trans* en fonction de la membrane pour laquelle ils sont affins.

Le transport vésiculaire des régimes *mixés* (initialement rétrograde) et *triés* (initialement antérograde) est flexible dans cette implémentions. Dans ces deux régimes, un cargo *cis* suit toujours un transport rétrograde, un *trans* toujours anterograde, et un *medial* est acheminé vers le centre de l'organite. En revanche, les régimes vésiculaires contraignent tous les cargos à un transport antérograde. Ces flux vésiculaires, qui diffèrent d'un cargo à l'autre, les répartissent dans des compartiments d'identités moyennes différentes. Ce tri est d'autant plus efficace que le transport vésiculaire est important, et on les montre tous deux maximaux dans le régime *trié*. Cette répartition impacte le temps de résidence des cargos dans le Golgi. Un cargo *trans* est plus vite au contact de la sortie. À l'inverse, les cargos *cis* et *medial* sont maintenus plus longtemps dans le Golgi.

Ce modèle démontre donc que de simples interactions locales sont suffisantes pour générer des voies de transport différentes au sein d'un même organite. Ce concept peut à la fois expliquer la répartition différentielle des enzymes dans les compartiments du réseau d'organites, mais aussi les temps de résidence mesurés expérimentalement pour différents types de cargos.

Perspectives

Les mécanismes très élémentaires de vésiculation, fusion et maturation des identités membranaires, sont suffisants pour comprendre une part importante de l'organisation et de la dynamique des organites. La structure et le transport vésiculaire sont intimement liés : un transport vésiculaire antérograde émergeant dans les régimes *triés*, alors qu'un transport rétrograde émerge dans les régimes *mixés*. Les deux hypothèses adverses sont donc possiblement les deux faces d'une même réalité biologique. C'est d'autant plus vrai que de simples interactions locales entre le cargo et l'identité de membrane golgienne peuvent créer plusieurs routes d'adressage au sein de la même structure.

Ce modèle nécessite cependant de nombreux ajouts pour permettre des prédictions, non plus qualitatives, mais quantitatives. C'est là une étape nécessaire pour que cette approche très conceptuelle puisse servir la biologie cellulaire, et à terme, permette de comprendre les effets des dérèglements d'organites en pathologie. Une analyse plus poussée des différents acteurs au sein du Golgi, qui agissent sur les 3 mécanismes présentés, comme le contenu en enzymes des compartiments, les mécanismes de maturation sur les cargos eux-mêmes, ou même le rôle de la

matrice golgienne dans l'adressage des vésicules, sont donc indispensables. Il s'agit cependant là du premier modèle non biaisé et auto-organisé des organites intracellulaires, qui lie à la fois structure, transport vésiculaire et tri des cargos. Une extensions plus fine de cette approche permettra sans doute à terme de mieux comprendre ces systèmes, et d'en prédire les comportements.

Acknowledgement

I first would like to thank the rapporteurs Nicolas Destainville and David Lacoste who accepted to read the manuscript and to evaluate this work. Thanks to all the jury members Anne-Florence Bitbol, Cathy Jackson (thanks a lot for your help during the whole thesis), Stephanie Miserey-Lenkei and Franck Perez who kindly accepted my invitation. I met some of you before and really enjoyed our discussions. I am very pleased that you joined this jury, and hope you will find this work interesting.

I spent long days writing in English for this manuscript and I would like to switch back to French for this section. Before I do, I would like to thank all non French-speakers in the lab and outside the lab for their discussion and the time we spent together during these three years. I will probably forget some names in all the wonderful persons I met, and my apologies if I do. But thanks to Niladri, Amit (from who I got my title of “princess”), Carles, Ander, Gert-Jan, Samy, Sergio (thanks angain for the metal bands) Veronika and many others for your time and discussion around beers or in front of a computer when I needed help. This was intense, and you are definitely part of the reasons why it was worth it. Thanks also to Rachele Alena, Mathiew Turner and Bruno Goud for stimulating discussions.

Un immense merci à Pierre de m’avoir donné cette chance. Peu de gens auraient accepté un apprenti médecin dans un laboratoire de théorie, et je te suis très reconnaissant pour ça. Je ne vais pas m’étendre trop longuement sachant que j’aurais le plaisir de continuer de travailler avec toi dans les prochaines années, mais j’ai beaucoup apprécié t’avoir comme encadrant. Un grand merci à mon deuxième “chef”, Quentin, qui m’a quasiment porté à bout de bras au début de ma thèse et à la fin de la sienne. Tu as beaucoup aidé tout au long de ces trois ans, et je t’en serais toujours redevable.

Un grand merci à tous ceux qui ont contribué à la bonne ambiance du laboratoire, et qui ont fait que jamais venir au travail n’a été difficile. La liste est longue, mais dans un ordre alphabétique qui évitera tout conflit, merci à Aléria, Antoine, Camille, Efe, Louis, Maj, Marie, Mathieu, Michele, Philippe, Remy, Thomas (avec qui jamais on ne parle politique), Tommaso et tellement d’autres que je suis sûr d’avoir oublié ici. Une pensée pour mes camarades de rédaction que sont Elie, Laura et Alicia,

qui ont rendu cette période beaucoup moins douloureuse que prévu, et entretenu une toxicomanie au café de circonstance.

Merci à mes amis en dehors du laboratoire, qui me rappelaient qu'il existe un monde par delà ces murs. Je pense surtout aux énergumènes de médecine avec qui j'adore passer du temps, à des amis plus anciens comme ceux du lycée avec qui je suis resté très proche, et même des très anciens comme Ben et Olivier qui me ramènent un peu de philosophie à chaque fois que j'ai le plaisir de les voir.

Quelques mots pour mes proches, et ceux de ma compagne qui ont été très aidants. À mes deux frères avec qui je rigole toujours autant. À mes parents qui ont beaucoup sacrifié pour que j'en sois là aujourd'hui et qui m'ont toujours aidé à aller plus haut. Et à Angèle pour m'avoir supporté, soutenu et tout simplement avoir été là à mes côtés tout ce temps.

Contents

1 Introduction

Contents for this chapter

1.1 Organelles structure and function

1.1.1 Historical and general considerations

When observing living systems, one can note that organisms tend to spatially segregate their functions into smaller specialized structures we call organs. For example, bones are the frame of our bodies, leafs are specialized in capturing the light to produce energy, and shells protect clams from predators. But big organisms

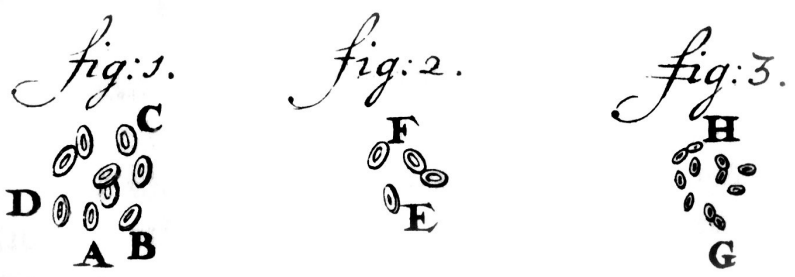

Fig. 1.1: Oldest known drawing of cells with an intracellular structure, called "lumen". Red blood cell of salmons, A. van Leeuwenhoek, 1719. From [Van22], source: wikipedia.org

like mammals or trees are not the only forms of living species, and unicellular organisms are very common [BPM18]. And even for large organisms, one should bear in mind that their absolute living units are still cells. These cells assemble to form tissues, constituting organs, and finally constituting organisms, but the units of these structures remain cells. One can thus ask whether the observation we had for macroscopic organisms, is really a general rule to understand living systems, and thus is still true for cellular structures. Do microscopic systems dedicate some intracellular regions to specific functions, the same way our bodies dedicates muscles to movement? Do the cells have organs?

This rather philosophical question became a practical one in XVIIs century, when the first optical microscopes were built. At that time, microscopists described that the cytoplasm – the inner part of the cell – was not homogeneous. There was indeed a "lumen" in the intracellular liquid – liquid called cytosol – whose first known drawing (Figure, Fig.1.1) was done by Antonie van Leeuwenhoek, in 1719 [Van22]. This lumen took the name "nucleus" more than a century after, under the studies of Robert Brown, in 1831 [Maz99]. However, this intracellular structure did not have any known function before 1877, when Oscar Hertwig showed that fertilization was performed when the nucleus of the sperm fuses with the nucleus of the oocyte (History of the discovery of fertilization in [CS13]). The role of the nucleus in heredity was thus established, validating the fact that cells can have organ-like structures, with a particular shape, and dedicated to a cellular function.

Other cellular organelles – literally tiny organs – have been discovered after the nucleus. For example, Richard Altmann showed in 1890 that nucleated cells also present "bioblasts" in the cytoplasm, later called "mitochondria"[ES81]. One can also cite Camillo Golgi, who observed an "internal reticular apparatus" in 1898 [Maz99]. This organelle has been later named after him the "Golgi body", or "Golgi Apparatus". It was thus showed that some cells, typically the ones with a nucleus, had multiple organ-like structures in the cytosol.

But the constrains that are applied to macroscopic organs are very different from the ones applied to microscopic organelles. And despite the proximity we see between organs and organelles, the justifications for their existence are very different. One argument to understand why compartmentalization is necessary in some cells is the following. Cellular systems have to struggle against two antagonistic phenomena:

- Microscopic systems are very sensitive to thermal fluctuations. These fluctuations make cellular components randomly move – diffuse – in the cytoplasm. All elements explore their surrounding environment, with a speed one can characterize using a coefficient: the diffusive coefficient. The larger this coefficient, the faster an element explores the cytosol.

- However, cells also need to make its components to interact with one another, in an efficient manner. For example, sugar molecules need to interact with the correct enzyme for the cell to produce energy, and this reaction should occur quickly enough for the cell to stay alive.

The question is thus the following: what is the maximum size a compartment can have, if one wants diffusion time and reaction time to be of the same order? Enzymes have to find their substrate randomly, and the larger the compartment, the longer the meeting time. But these enzymes work at a given speed in the cell: so what the size a compartment can have, to optimize the system by keeping the diffusion timescale compatible with the kinetics of enzymatic reactions? Considering a typical diffusive coefficient in the cytoplasm $D = 1\mu m^2/s$ [Küh+11], a slow enzymatic kinetics $k_{\text{cat}} = 1s^{-1}$ [ABW90], the typical size of compartments should be around $1\mu m$.

For cells whose size is around $1\mu m$, there is no need to compartmentalize. Following this argument, diffusion is sufficient for metabolic processes to occur efficiently at this scale. This is typically the case for the large majority of procaryotes like bacteria. And we observe that these cells do not have organelles *per se*. There can be an intracellular organization, with subcellular structures like nucleoids and carboxysomes. But these sub-units are made of proteins, or encapsulated in a shell of proteins, and are out of all proportions to membrane-bound organelles.

The term “organelle” is indeed usually used to describe the intracellular organization of eukaryotic cells. This *domain* – formally, family of cells – is actually named after one of these organelles, eukaryote coming from the Greek “karyon” that means “nut” or “kernel”, and by extension nucleus. The membrane constituting these compartments prevents diffusion of soluble proteins, helping the creation of different biochemical environments inside the cytoplasm. Freed from diffusion limitations, eukaryotics cells can grow dramatically, and reach an average volume that is 10000

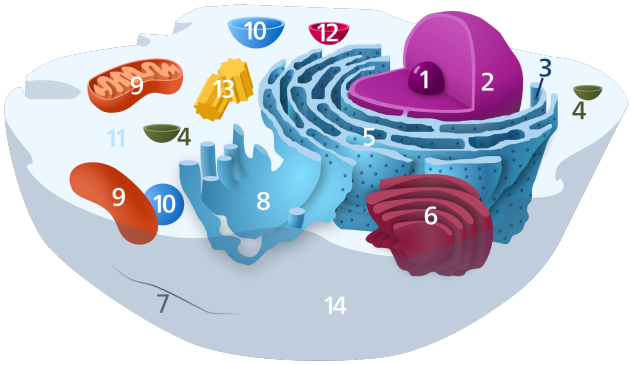

Fig. 1.2: Components of a typical animal cell (from wikipedia.org). The major membrane bounded organelles are:

- 2: the nucleus, which stores the majority of the genome
- 5: the rough endoplasmic reticulum, which is a site of protein synthesis
- 6: the golgi apparatus, which plays a role in proteins processing and sorting
- 8: the smooth endoplasmic reticulum, which plays a role in lipid synthesis
- 9: the mitochondrion, dedicated to energy conversion
- 10: the endosomes, that brings components from outside, inside the cell
- 12: the lysosomes, that degrade and digest unused elements

times greater than the prokaryotic cells' one [YW14]. Because these compartments are well isolated from one another, this allows great specialization of these structures. For example, DNA is protected in the nucleus from aggressive metabolisms performed in mitochondria or lysosomes. A scheme of the major organelles and their functions (with a focus on animal cells) can be found in Fig.1.2. Compartmentalization also allows specialization between cellular types, with intracellular organelles that are exclusive to some species:

- melanosomes store pigments in our skin and skin of other animals,
- chloroplasts in plants and protists convert light to chemical energy
- hydrogenosomes allows some eukaryotes to grow in an oxygen-depleted environment
- etc...

These are very rich and interesting structures, but difficult to investigate and understand. Indeed, the study of these systems asks a lot of both biological and physical questions. On a biological point of view, one can ask what are the structures and cellular functions of organelles, and what are the actors inter-playing to build these structures and maintain their functions. On a physical point of view, one could ask what are the general laws constraining these systems and the rules dictating their formation, maintenance and dynamics. This is particularly relevant because, despite the increasing knowledge we have about these biological actors – like proteins, lipids, and others – we are still far from understanding how these actors are sufficient to build such organelles.

As we will see, acquiring more data on those systems is facing some limitations like the diffraction limit of light microscopy. It is even not clear whether such data could explain by themselves organelles' organization and dynamics. These structures are indeed very challenging to model as they use energy to build, stabilize and perform their functions. This prevents any use of classical physical approaches that rely on equilibrium descriptions. Besides, there is no clear pattern on which organelles build, and it seems they self-organize only by the mean of local interactions between biochemical partners [Gli02; Bev+02; Mis01]. But before proposing a modeling approach for these systems, it is necessary to present them in more details. As we want to build a general, bottom-up model of those intracellular compartments, one should first describe what they have in common among all the organelles' diversity.

1.1.2 Defining organelles identity

Different approaches can be used in order to identify organelles. One of the most obvious way when one gets confronted to microscopic images (Fig.1.3) is to define organelles by their anatomy. Some of them are bounded by one layer of biological membrane, like the Golgi apparatus (Golgi), some other have more than one, like the chloroplast. Some of them are vesicular, like the endosomes, others are tubular, like the endoplasmic reticulum (ER).

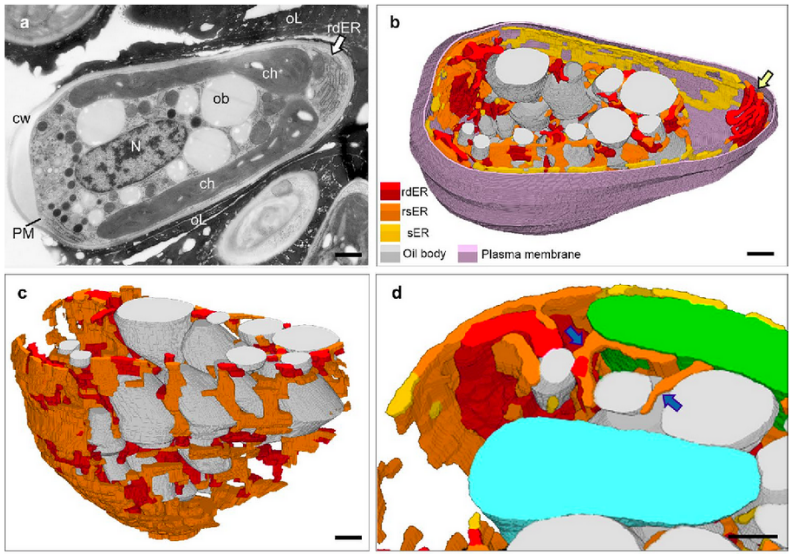

Fig. 1.3: 3D segmentation of some organelles in green alga, Botryococcus braunii, from [Suz+17]. (a) Electron microscopy image of the cell. (b-d) 3D segmentation of the organelles. rdER: Endoplasmic reticulum (ER) with ribosomes on both sides. rsER: ER with ribosomes on one side. sER: ER without ribosomes. PM: plasma membrane. cw: cell wall. ob: oil body. N: nucleus. ch: chloroplast. oL: extra-cellular oil layer.

This anatomic description is a mesoscopic one, with structures that are of a couple of micrometers. Considering how cells work, this is actually a large scale description, as these structures are order of magnitude larger than the size of its typical biochemical actors, like proteins. And as the cell needs to keep control on organelles' organization, there are other scales at which compartments' identities are defined. For example, one can cite the biochemical composition of membranes itself, the proteins acting in and on the compartments bounded by the membrane, or even the physico-chemical properties of the compartment's inner space – points we review in some details below.

Biological membranes

The membrane constituting organelles is a sheet of lipids. These molecules are composed of a hydrophilic or polar head (soluble in water) and a hydrophobic tail, for which it is energetically costly to be in contact with aqueous components of the cell. Lipids self-organize in cells following three typical patterns: micelles, liposomes and bilayers (Fig.1.4). The two latter are defining two domains around the lipids structure, across which aqueous components cannot diffuse. Practically speaking this creates a frontier, a membrane, between two media in the cell, which is the very basis of compartmentalization. These two structures are thus the ones used to bound organelles.

Composition of lipids may vary between organelles. This is a very large and complicated topic if one considers the actual composition in each lipid, the fraction of cholesterol, the charge of the lipids, the steric repulsions between the tails, their complexion with sugar complexes, etc... All these have actual effects on proteins, such as their ability to form rafts in the membrane [Lor+17], or their affinity for the membrane thickness [SSM10]. To simplify this complex picture, one can consider the cell presents two major territories. One that has a low membrane order, little cholesterol, little thickness, neutral charge and lots of packing defects; and the other that has a high order in lipids, more cholesterol, higher thickness, negative charges and very few packing defects [JWV16]. The first one is composing the membrane of the ER, the nucleus and part of the Golgi, the other is found in the plasma membrane, endosomes and the other part of the Golgi. All these lipids are created in the ER, but distributed in other compartments using contact sites. These contact sites are proteic bridges between organelles, that consume energy to maintain the heterogeneity in lipids composition between compartments.

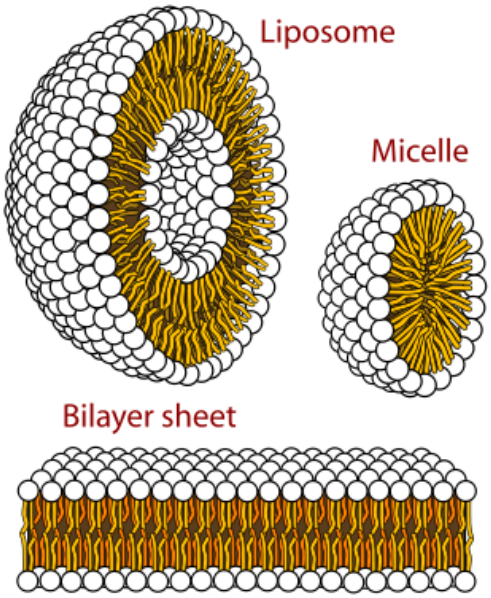

Fig. 1.4: Self-organization of lipids in cells (water-rich environments), exposing their polar head (white) in the aqueous medium, and hiding the hydrophobic tails (orange/yellow) in the structure. Drawing realized by Mariana Ruiz Villarreal, released into the public domain by the author.

Physico-chemical properties of organelles' lumen

The physical environment encapsulated in compartments can be dramatically different between organelles. For example, the pH in the ER is neutral, it is acid in the lysosome, and basic in mitochondria [She+13]. This has many implications, such as activating enzymes when they enter the acid lumen of lysosomes, and not before, which prevents them from degrading substrate as soon as they are created [Tur+12]. Some organelles have really extreme physical environments, such as mitochondria that have a field strength of about 30 million volt per metre ($150 - 200mV$ over a $5nm$ membrane) [LM10]. This field modulates the activity of some actors, such as cytochrome C, to trigger apoptosis if mitochondria get damaged [De +09].

Proteins decorating organelles' membrane

Approximately half of the membrane mass is composed of proteins. There are many ways a protein get attached to membranes, from being restrained by the mean of weak interactions, to be fully integrated in the membrane. These proteins are particularly interesting in defining organelles identities, as they are major biochemical actors allowing organelles to function. Some of them are specific to certain organelles – like rhibosomes that are mostly attached to the ER, or Vacuolar-type proton

ATPases that are used in mitochondria or lysosomes. But some other classes of proteins are ubiquitous in all compartments, with sometimes variants for each organelle. When such variants exist, they are very interesting proteins to define organelles' identity. One of these is the RAB family of proteins.

These proteins are small guanine nucleotide-binding proteins, cellular switches that can be either in an active (three-phosphate, GTP form) or inactive (diphosphate, DGP form) [SO01]. RABs have the ability to bind membranes by their C-terminus part, with preference for some organelles. Different RABs bind different organelles. They are shown to be important in regulating dynamics of the secretory (ER, Golgi, secretory vesicles) and endosomal pathways [Pfe01]. But they also play a role in the nucleus [Pyl+18], lysosomes [Buc+00] and mitochondria functions [Yam+14]. RABs have a crucial importance in anchoring compartments to the cytoskeleton, targeting vesicles to the correct compartment, and even budding elements out of a compartment [GON06]. As they tune what membrane is getting removed, transported, or fused to a target compartment, they can be seen as proteins specialized in defining membranes' identity. They are thus extremely relevant actors to consider when defining organelles.

But if one agrees to see RAB proteins as markers of membrane identities, one should then accept the fact membrane identities are extremely dynamical. In fact, RAB proteins function in cycle of attachment/detachment from the membrane. Two cofactors play a role in this cycle: a GTP exchange factor (GEF) that activates them on the membrane, and a GTPase-activating protein (GAP) that processes them into their GDP inactive form and detaches RABs from the membrane. Interestingly, it has be shown that GEFs can be recruited by another RAB, of a variant that is

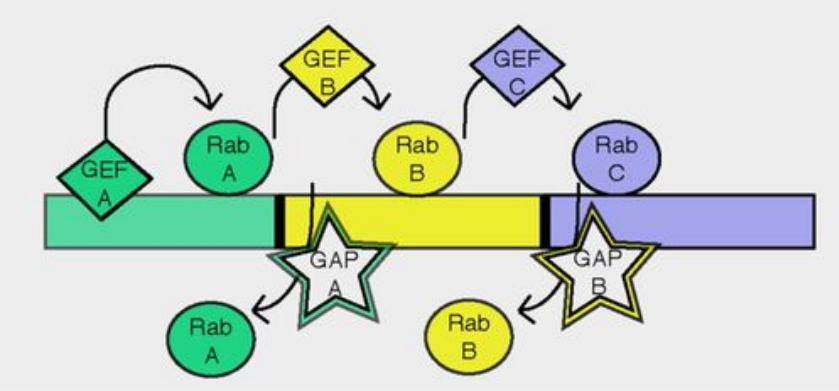

Fig. 1.5: **RAB cascade**, from [Pfe17]. RAB protein (A) gets phosphorylated by its GEF (A), promoting its activity and anchoring it on the membrane. This RAB (A) then recruits another GEF (B) which itself recruits its respective RAB (B), yielding to its accumulation on the membrane. The GAP of the first RAB removes it by promoting its dephosphorylation. The overall process matures the membrane from the first (A) identity to another (B) identity.

different from the one activated by the said GEF [Del+08]. When coupled to the removal of the previous RAB using the proper GAP, it overall acts as a maturation process of the membrane identity [Sud+13; Pfe17] (Fig.1.5).

1.1.3 Inter-organelles communication

Proteins decorating membranes are thus possibly subjected to biochemical conversion over time. But a steady-state can be observed in organelles' identities, and thus, there should be other fluxes counterbalancing maturation.

One of these fluxes is the transport of material between organelles. Lipid bilayers prevent any passive processes to transport components between organelles. If proteins have to move from the compartment they are created in, to the compartment they are active in, other mechanisms than diffusion have to be used. This is of course the case for polar components that cannot cross the hydrophobic boundary of compartments, but also for trans-membrane or anchored proteins in the bilayer.

Many strategies are explored by the cell. The first one is a direct communication between compartments, by putting them in close proximity from one another. For example, the ER is creating contact sites with lots of organelles, contact sites that allow lipids to be transported in between these compartments [JWV16]. This process uses energy and specific proteins to mechanically remove one component of one compartment and put it in the one apposed. This works for lipids, that can be access outside of the compartment, but not for polar elements that are hidden in the lumen. For the latter ones, an effective transport strategy relies on creating a continuity between the intra-compartment's spaces. This can be achieved in a temporary manner, by "kiss-and-run" fusion between the compartments [Fes+94], or irreversibly by fusing a compartment into another, like lysosomes with endocytic vesicles. The latter is particularly efficient in releasing components into another organelle, but it relies on loosing one of the compartments. To prevent this, sub-compartments can be used as carriers, a strategy largely used and called vesicular transport.

Many proteins can be used to create such vesicles, from coats directly deforming the membrane to bud vesicles (one can cite COP and clathrin proteins [MM04]), to scission of membrane tubes, as these tubes get elongated using proteic motors [Sci+97]. This budding machinery strongly interacts with proteins decorating membrane, which allows a great specificity in what is taken out from the budding organelle [GON06]. The same proteins also interacts with the machinery responsible for vesicles fusion with the target compartment – like tethers and SNAREs proteins [CRF07]. This is thought to increase fusion rates between compartments of the same biochemical identity, a process often called homotypic fusion [ZH13; Pap+15].

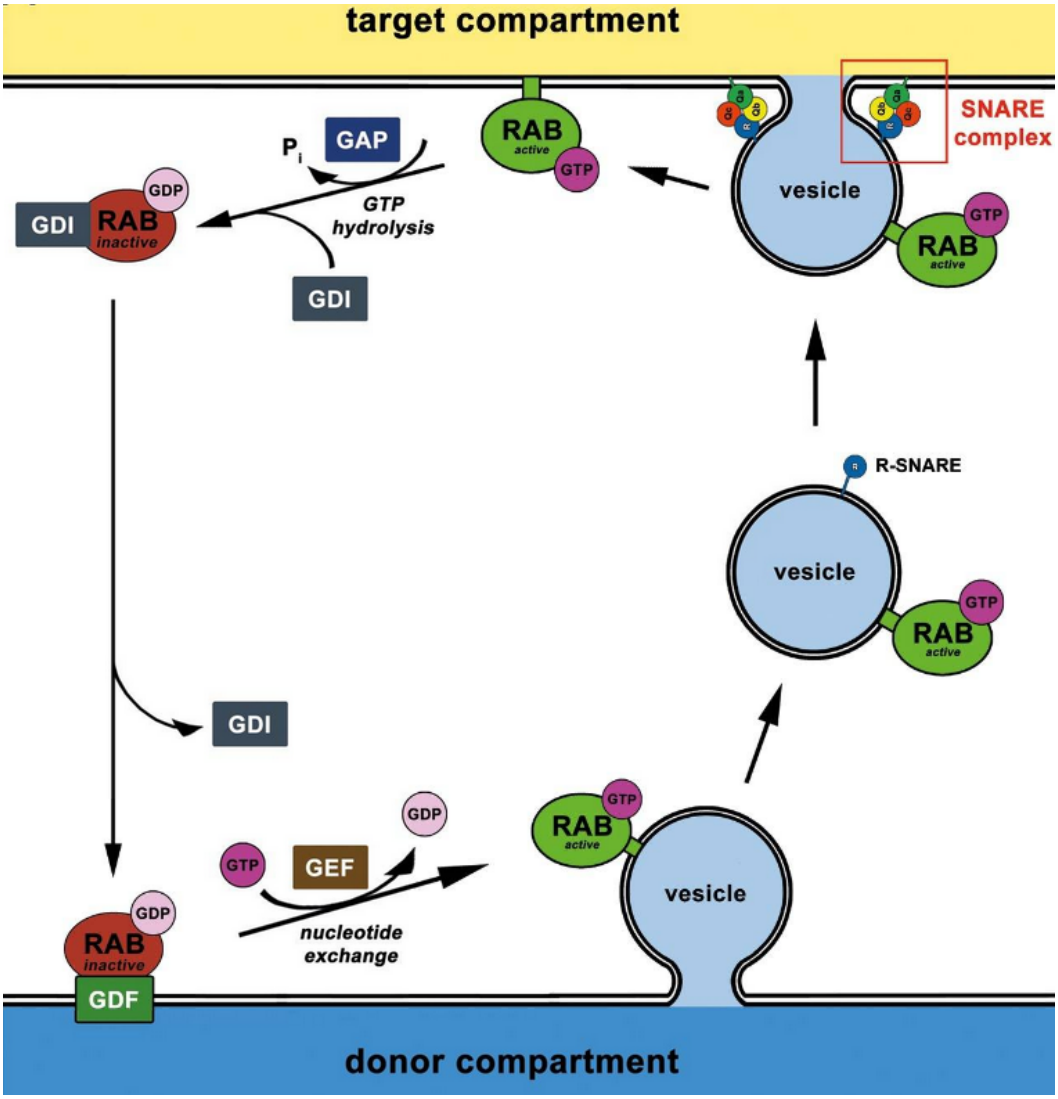

Fig. 1.6: The role of RAB proteins in vesicular traffic. From [Hoe+14]. RAB proteins cycle between GTP-bound (green) and GDP-bound (dark red). GAP (dark blue) increases GTP hydrolysis on active GTP RAB. GDP dissociation inhibitor (GDI, dark gray) prevents RABs from biding the membrane. GDF (dark green) removes the GDI. GEF (dark brown) changes the bound GDP to GTP which activates the RAB protein. SNAREs (red box in A) enable fusion of vesicles into the target compartment. GTP, magenta; GDP, light pink.

In brief, membrane identity – and particularly the one defined by RAB proteins – is very important at all stages of the vesicular transport (Fig.1.6).

1.1.4 The challenges of studying organelles

We see that organelles are complicated and extremely dynamical systems. But they display a robust organization, meaning a steady-state can be described. This steady-state should not be understood as fixed, passive organization of compartments, but as the interplay of counterbalancing fluxes. Two of them are the one we already discussed: identities maturation and components transport between organelles. And as everything is linked to other compartments, whether to fulfill its task or to maintain a steady-state by renewing its components, this system should be seen as a network.

This is thus very challenging to investigate *in vivo*. The amount of interconnected pathways involved in organelles bio-genesis, maintenance and functions can be intimidatingly large. Everything can potentially interact with everything, directly or indirectly, and the amount of actors tuning the organization of the system is enormous. Besides, these events involve small structures like vesicles, or very close to one another, like tubules in the ER. These can be resolved using electron microscopy, but not with live microscopy. In other words, one can either observe the coarse-grain dynamics of organelles, or their fine structure, but not together.

And even if we could, it is not clear we would be able to understand what we see. Such systems are indeed conceptually complicated to understand. Each action performed by a protein consumes energy, which breaks the detailed balance as these actions are irreversible. Organelles are out-of-equilibrium systems, that are the result of the interplay between contradictory fluxes mixing them: in a sense, self-organized structures. Self-organization is fairly well understood for equilibrium systems, but there is no clear answer on how such an open and energy consuming system behaves. What are the general rules constraining the organelles' structure and dynamics is thus an open question.

And this is this question we are trying to tackle with this work. But before going further, we will focus on a more specific system. Organelles are indeed very diverse, and modeling the whole network with one unique model is unfeasible. That is why we focus on a stereotype organelle that has all the features we are interested in, but in a smaller version. It is already a multi-compartment system, with different identities for each compartment that mature over time, displaying important vesicular transport between those compartments or even direct fusion between them. It is at the crossroad of the two lipidic territories we discussed in Section, Sec.1.1.2, and is

also at a transition in pH in the cell. This organelle we choose for the rest of this study is the Golgi apparatus.

1.2 The Golgi apparatus

1.2.1 General structure and role of the Golgi

The Golgi apparatus is an organelle involved in the secretory pathway (creation and secretion of proteins by the cell), in which it plays a role in the processing and sorting proteins synthesized in the ER. It is a multi-compartment system, that is (in most eukaryotes) organized in stacks of flattened disks called “cisternae”. Each cisterna is a closed compartment, bounded by a biological membrane (Fig.1.7). This organelle can be roughly seen as a sorting and processing hub, traversed by a constant flux of proteins (called cargo-proteins, or cargo) following a route coming from the ER, and going to the plasma membrane and other organelles, like endosomes. It has an entry and an exit which define its polarity. The entry, close to the ER, is called the *cis*-Golgi, the exit, close to the plasma membrane, is called the *trans*-Golgi. Note that there is at least one intermediate compartment between the Golgi and the plasma membrane – the *trans*-Golgi network (TGN) [GS86]; and

Fig. 1.7: Electron microscopy image of the Golgi apparatus. In a human leukocyte, using a high magnification transmission electron microscope. Louisa Howard, source: dartmouth.edu.

possibly one between the ER and the Golgi (mostly in mammalian cells) – the ER-Golgi intermediate compartment (ERGIC) [PM06].

Golgi's polarity can be characterized by different means. Structurally speaking, the *cis*-Golgi part presents more vesicles and less tubular fenestrations than the *trans*-Golgi [Lad+99]. This change in structure goes with a change in lipid composition. The *trans*-Golgi is indeed much richer in cholesterol and poor in packing defects that the *cis*-Golgi. One of the main mechanisms explaining the transition in lipid composition, between the two territories we discussed before, takes place at contact sites between the ER and the *trans*-Golgi [JWV16]. The same goes with the intra-compartment pH, that is more acid at the *trans*-Golgi than the *cis*-one [CGO10]. But it is probably more by looking at the proteic actors, that one can reach a fine description of this polarity.

Membranes of the Golgi apparatus are indeed decorated with different RABs, depending on their location in the *cis* $\rightarrow$ *trans* polarity [PG14]. RAB1 (Ypt1 in yeast) is related to the identity of the ER to the Golgi's *cis*-face membranes. RAB6 (Ypt6 in yeasts) is related to the identity for the *trans* to TGN membranes. Interestingly, one can define an intermediate identity between these two, a *medial*-Golgi, assumed by the RAB33B (Ypt32 in yeasts). This three identity model explains how Golgi's functions are spatially segregated. Different processes are indeed applied to the transported cargo crossing the Golgi, processes that require a *cis* to *trans* polarity (see below).

1.2.2 Secretory role of the Golgi Apparatus

One of the roles of the Golgi apparatus is to process and sort cargo coming from the ER. This processing is a maturation mechanism during which proteins and lipids get glycosylated by a sequential binding of sugars to the cargo. Glycosylation process starts in the ER, but the elongation of the sugars polymer and quality control of that maturation is assumed by the Golgi. This is a very large and complicated topic that we won't discuss in detail here. We will just consider the following simplistic, and protein-focused picture of glycosylation.

One can distinguish two major types of glycosylation: *N*-glycosylation and *O*-glycosylation, depending on the residue from which the glycosylation starts [Sta11].

- *N*-glycosylation – attached to a nitrogen of asparagine or arginine side-chains – is ubiquitous in eukaryotes. It starts in the ER before the cargo get addressed to the *cis*-Golgi. Cargo arriving in this compartment are of high mannose (Man) type with eight to nine Man residues. In the *cis*-Golgi, a set of α-mannosidases

remove some Man residues. It allows the Golgi to initiate the synthesis of "hybrid" and "complex" *N*-glycans, by adding a *N*-Acetylglucosamine residue (GlcNAc) in the *medial*-Golgi. "Hybrid" glycans are extended by adding galactose (Gal) and sialic acid (Sia) in the *trans*-Golgi. "Complex" *N*-glycans loose more Man residues and acquire a second GlcNAc. This organization of residues allow high branching of sugars, followed by elongation using GlcNAc – in the *medial/trans*-Golgi; *N*-Acetylgalactosamine (GalNAc), fucose (Fuc), Sia and galactose (Gal) – in the *trans*-Golgi.

- *O*-glycosylation – attached to the hydroxyl oxygen of serine, threonine, tyrosine, hydroxylysine, or hydroxyproline – also starts in the ER and consists of the addition of only a single sugar residue: GalNAc, or glycosaminoglycan (GAG). They can be extended in the Golgi by the addition of GlcNAc – in the *medial/trans*-Golgi; Gal, Sia and Fuc – in the *trans*-Golgi. GAG chains can also be extended in the *cis*-Golgi to form long linear polymers, before being modified by blocks at specific positions of the glycan. The latter mechanism of great specificity is totally absent in yeasts.

To get processed, cargo have to meet the correct enzyme, and thus be in the correct compartment with the correct identity, and this, in a specific order. Deregulation of the glycosylation can have dramatic consequences. As this process is crucial in extracellular matrix production, cell-cell interaction including immune recognition, and many other functions. Any modification of the Golgi structure or enzymes acting on glycosylation can lead to severe diseases [BS13; RC12].

Processed cargo are then addressed to the TGN and sorted to other compartments, like the endosomes or the plasma membrane. Other proteins such as the resident Golgi enzymes get retained in the structures. Some materials can be addressed back to the ER, following specific pathways such as the KDEL one [Orc+97].

This is a brief and simplistic view of what we know about the Golgi complex, keeping a focus on its secretory role in the cell. To be exhaustive, we probably should discuss other aspects of the Golgi polarity, such as the different budding actors used at different Golgi parts, or its other roles in cells, such as the endosomes to Golgi pathway, how glycosylation can be used as a bar-code to sort proteins, other proteins tuning the Golgi's very particular shape, like golgins, etc... But the aim of this section was not to introduce what we know about the Golgi, but more what we still do not understand.

Indeed, despite the increasing knowledge we have about the actors organizing the Golgi, we still lack of a global understanding on how it behaves. Such basic questions as how cargo-proteins get transported from one identity to the next in still

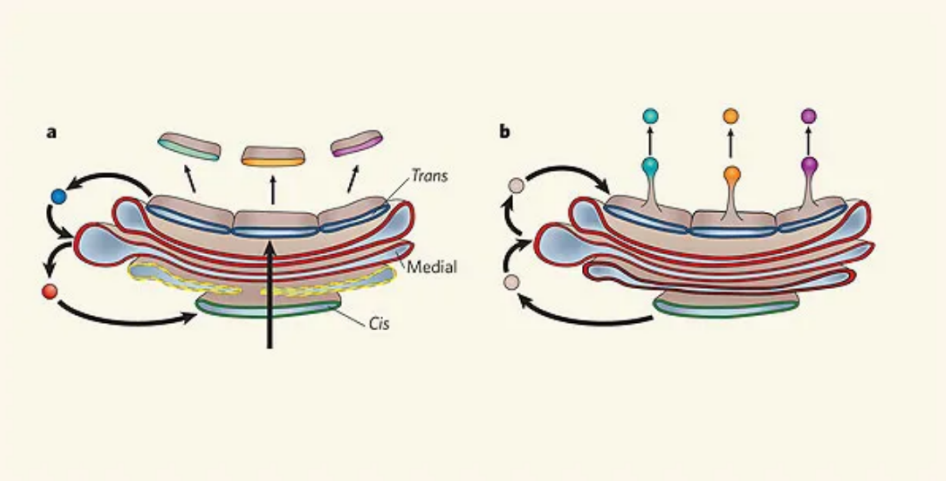

Fig. 1.8: The two major models of the Golgi organization and dynamics. From [MM06]. **a**, The cisternal maturation model. **b**, The vesicular exchange model.

strongly debated. As a matter of fact, no direct observation of such phenomenon is possible: the typical thickness of a cisterna, and the distance to its neighbors is around tens of nanometers (Fig.1.7), whereas optical microscopes hardly resolve structures smaller than few hundreds of nanometers. Super resolution microscopy or electron microscopy can image the fine structure of the Golgi, but the temporal resolution is either not good enough, or abolished because cells need to be fixed.

Fortunately, this lack of experimental data did not prevent scientists to hypothesize how the Golgi works, and many models have been proposed to explain how it fulfills its secretory role [GL11]. Two of them have particularly marked the field: the vesicular exchange model, and the cisternal maturation model (Fig.1.8).

Vesicular exchange model (Fig.1.8b)

This is the historical model of the Golgi apparatus. It postulates cisternae are fixed with fixed composition. To get processed, cargo have to move from one compartment to the next using an anterograde flux of vesicles.

This model explains well how different identities are segregated in the Golgi, its polarity, how residing enzymes are sequestered while cargo get transported from one identity to the next. It also explains how different cargo can have different residing time in the Golgi. But it fails to predict how new cisternae can be formed, particularly after mitosis, during which the Golgi gets disassembled before reforming *de-novo* [WS17; Gli02]. Besides, it fails to explain how cargo larger than a vesicle (typically procollagen) get processed in this system.

Cisternal maturation model (Fig.1.8a)

This is the currently most accepted model of the Golgi. It assumes cisternae are mobile elements that are getting formed at the *cis*-pole of the Golgi, before continuously getting transported to the *trans*-face of the Golgi. During the process, their identity matures from a *cis* to a *trans*-identity. Cargo, that are blocked in the cisternae, see all the identities in a *cis* $\rightarrow$ *trans* order, to get matured. A retrograde flux of vesicles retains the Golgi's residing enzymes.

This model explains well the Golgi's polarity, how cargo-proteins – including very large ones – get processed, how enzymes remain in the compartments of the correct identity, and how new cisternae can be formed. It however fails to predict how different cargo can be transported with different kinetics as they should remain in a cisterna.

1.2.3 Other model adaptations

Other models have been proposed. Some are just slight modifications of the previous ones, like adding heterotypic (between compartments of different identities) tubular connections between cisternae. Others are drastic alterations of the textbook picture we have of the Golgi, like the rapid partitioning in a mixed Golgi, hypothesizing that the Golgi works as unique compartment. But unfortunately, none of these models allows a complete description of the Golgi. For this reason, we will stick to the two most accepted ones for the rest of this manuscript.

1.2.4 Diversity and common Golgi's phenotypes across organisms

As we saw, there is no consensus on how the Golgi couples its structure and vesicular transport to fulfill its function. It is even more challenging, considering the fact that the Golgi's structure can vary a lot between different species, or even different cell types in a unique organism. Even if many of them consist in a stack of cisternae, many stacks can assemble to form a ribbon in mammals [WS10], and some species do not have any stack at all but a dispersed Golgi through the cell [PG09].

Interestingly, it seems that this diversity of morphology goes with the diversity of models proposed in the literature. The cisternal maturation has been directly observed in yeast [Los+06; Mat+06], whereas the vesicular transport model has

been indirectly inferred in stacked Golgis [Dun+17; DRS13]. However, the main elements constituting the Golgi are well conserved over species, and if there exists variations around the stacked morphology, these are the results of adaptations and not profound rebuilds of the organelle [Bar+18].

This suggests that the different models of the Golgi are indeed fine-tuning of a unique, more general reality about these systems. All Golgis should thus have the capacity to exhibit both regimes – fixed compartments with an anterograde flux of vesicles / maturing compartments with a retrograde flux of vesicles – slightly adapting the mechanisms taking place in the system. And this is this kind of general description we are trying to reach in this work.

1.3 Modelling the Golgi

Because of its central role in the cell, the controversy surrounding it, and its intriguing shape, the Golgi apparatus received quite a lot of attention from biophysicists. Lots of questions have been asked with modelling approaches tuned to answer these questions. All these models – including the one we propose – face an important problem: the scales that are relevant to understand the Golgi are too broad. In the following section, we present some quantifications about the Golgi to highlight this point.

Golgi's membranes are in close proximity from one another (see Fig.1.7), around tens of nanometers between two cisternae. But the nanometer scale is not sufficient to describe this structure, as we also see on the same picture that the average diameter of the cisternae is around $1\mu m$. If we approximate cisternae as flat pancakes, this gives an average area per cisterna around $0.5\mu m^2$. Multiplied by the number of cisternae (here between 3 and 4 full cisternae on that section plane), we get a Golgi total area of a couple of micrometers. This surface has to be compared with the area of vesicles travelling in the system, with a diameter around $50nm$, which gives a vesicle surface of around 1% of the Golgi surface. But the gap between these two orders of magnitude is nothing compared to the one between the Golgi's surface, and the size of the lipids or proteins constituting the membrane. Each of these elements contribute to an area between 0.1 and a couple of nm^2 and are thus 10^5 to 10^7 smaller than the Golgi. A quick ratio gives a number of bio-molecular actors to consider that is of a couple of millions at minimum, to which one must add the cargo inside the compartments, and the extra-cisternae actors tuning the system. In other words, one does not simply model the Golgi by modeling all its components.

The same problem shows up when considering the time scales defining the system. We said that the maximum time scale k_{cat} defining an enzymatic reaction is about $1s^{-1}$. But they can be much quicker with time scales of the order of $1ms^{-1}$. This has to be compared to the diffusion timescale that we saw to be around $1s$, as compartments characteristic size is $1\mu m$. But there are much larger timescales defining the systems, like the typical transport time of cargo protein across the structure, of order 20 minutes, which matches the typical time of golgi reformation after mitosis 20min [PL03]. The largest timescale for which a Golgi is defined is the time after the last cellular division, and thus the Golgi's reformation. And that timescale can be of tens of year for non dividing cells – like some neurons – that are formed during development and never divide after.

In brief, one should bear in mind that no model of the Golgi can consider all these scales together in a unified approach. All models of these systems are a coarse-grained representation of the organelle, with approximations that strongly depend on the scientific question asked. Each time the terms "organization" or "dynamics" are used, one should remember they can mean dramatically different things. To better contrast the way we will define these terms, we propose a rapid overview of the approaches that have been tried to model the Golgi. What are the scientific questions they ask, the main results they get, and the limitations they face.

1.3.1 Structure as the Golgi's shape

Because their beautiful shapes were a very obvious way to identity organelles, defining organization by the spatial steady-state structure has been extensively proposed. And because of the very particular of the Golgi, multi-cisterna and fattened compartments shaped organization, it is an organelle of choice for such approaches.

The first question one could ask is how to stabilize such a non-trivial structure. The first thing we could anticipate is that dynamics of diffusion and identity changes compete with adhesion and fusion of elements to stabilize the structure. Whether such structure can be built in a self-organized way, and the quantification of the relative impact of the said competing mechanisms has been assessed by [Küh+10]. In short, they conclude the structure can form *de novo* and a steady-state can emerge. They quantify and explain the relevant parameters such as the ratio of injection of new elements over the decay of the Golgi components which defines the Golgi's mass, the importance of tethering to maintain the stacked structure, and the importance of the proximity to the ER exit site to prevent the diffusion from being dominant over stacking.

The flattened structure is however assumed in the previous modeling, and mechanical properties of the membrane have been neglected. Others studies have aimed to quantify whether our understanding of membrane mechanics was compatible with the steady-state structure of the Golgi [TM17]. They show vesicles aggregation models can yield a stacked Golgi, with the necessary assumptions that proteins in the Golgi spontaneously prefer high curvature regions and stabilize the rim of compartments, rim where all the fusion events occur. The stacked Golgi is here seen as a steady-state where vesicle aggregation, membrane fusion, and shape relaxation compete. Interestingly, they show that Golgi formation is relatively resistant to physical parameters changes, which is consistent with the fact such systems are robust.

These approaches are important to understand the physical impact of space and mechanics on such structures. It is however very difficult to infer those physical properties. For example, the diffusion in the cytoplasm is a really non-trivial topic, as cytosol can be seen as a gel, with a mesh-grid that prevent passive movement of components larger than a threshold size. For these components, interactions with the cytoskeleton, and the proteins of the Golgi matrix, for the case of interest here, are dominant. And again, because of the complexity of the system, and the very high specificity of interaction between biochemical components, it is very easy to end up with tens of parameters to fit. For all these reasons, this approach is not the one we choose for this study.

1.3.2 Structure as the Golgi's polarity

Another approach is to consider the Golgi's structure, not as how different compartments are shaped and placed in space, but how these compartments adjust their identities to define a polarity ER to TGN, polarity that is crucial in the Golgi's functions. Coarse-graining spatial and mechanical components of the problem of course limits our understanding on these points. But it allows a finer, and sometimes easier modeling of the fluxes within the system.

Two of these fluxes, that are particularly relevant to the Golgi, are maturation of cisternae versus vesicular transport. One way to investigate their interplay is to see the Golgi as a 1D structure, defined by the ER $\rightarrow$ TGN axe. The amount of each component of the Golgi can be represented as a number on this axe. We can then coarse-grain the effect of maturation and vesicular transport by quantifying how they impact the position and amount of components on this axis. Maturation moves components closer to the TGN, and vesicular transport closer to the ER or TGN, depending on whether it is a retrograde or anterograde vesicular transport. This simplicity allows proposing models with very limited number of parameters

[DRS13], that can then be used to fit real data and infer whether the observed *in vivo* Golgi is more of a "Vesicular exchange" or "Cisternal maturation" Golgi. In this publication for example, they show that a purely cisternal maturation model is not sufficient to explain the kinetics of cargo transport in the mammalian Golgi. By comparing biological data to their modeling, they indeed conclude there are intercisternal exchanges of cargo.

Such reductionist approaches allow very fundamental questions of the type: what are the very minimal ingredients one needs to recreate a given phenomenon in the Golgi? It can be linked to experimental data like the previous example, or it can be more conceptual. For example, two previous publications in the lab asked what are the mandatory rules for the vesicular transport, so that this transport drives sorting in the system [DS11], and what is the role of stochasticity on such sorting [VS18b]. The first publication shows us that vesiculation and fusion are not always sufficient to drive sorting, and one need to be in particular regimes (we will discuss in the chapter Ch.2) to promote such sorting. The latter shows that stochastic sorting of compartments is only efficient when budding kinetics are faster than fusion kinetics. Comparable approaches have been tried on open systems, to see what types of mechanisms one should apply to get a self-organized Golgi that sorts its budding and fusion actors [Bin+09]. They show that cooperation between fusion actors (which ensure compartments of comparable affinity fuse faster than compartments of different identities) is key to build a sorted system.

While reviewing organelles' common properties, we saw that maturation of membranes' identities constitutes an important flux in the Golgi. This flux has been less studied than budding and fusion mechanisms, but one could however cite [IM13] that includes a protein degradation in the cisternae, which can be seen as identity changes of the said cisternae. This gives interesting insights on how such maturation process can initiate and maintain a polarity in the system. They also show that maturation affects vesicular transport – which in the present is implemented as a SNAREs degradation mechanism – creating an interplay between these two features, enhancing and stabilizing the polarity. It however defines the Golgi in a continuous manner, which should not dramatically change the results (see [Gon+10] to have a comparison of different approaches in simulating the Golgi) but has to be assessed. This work has been performed in the lab [VS18a], but this time ignoring the impact of vesicular transport.

Some works have combined both budding, fusion and maturation in a unified model, but they are much less common. One can however cite [SBR16] which is a perfect example of this approach. The idea of this publication is to fix the rules dictating maturation and vesicular transport, and see what steady-state in possible, when *de novo* formation is permitted. They show that "Cisternal maturation" and "Vesicular

transport" models of the Golgi indeed exhibit very different phenotypes: the first one requires a much less fine-tuning of the parameters, which goes with fewer restrictions on the steady-state, whereas the second one needs its identities to be well sorted to stabilize the steady-state.

1.3.3 Our modelling approach

We want to build a bottom up model of the Golgi apparatus, focusing on some very fundamental mechanisms, and in a very minimalist way. The aim is to reach a qualitative understanding on how organelles work in general, apart from the enormous diversity one can find in these systems. We thus will not consider fitting approaches of biological data. For a comparable reason, we will neglect mechanical and spatial dependencies that are both very difficult to implement – and an efficient way to multiply the number of parameters to investigate, a fact we want to avoid in a minimalist approach.

The model will have to coarse-grain the spatial and mechanical dependencies. Structure of the Golgi will be defined by the composition and size of compartments in the system, and not their shape or respective places in the organelle. We will implement all the mechanisms discussed before, that are affected by the composition or size of compartments: budding, fusion and membrane maturation. And because of the capacity to rebuild after mitosis, we want this model of Golgi to be a self-organized description based on local interactions.

In a sense, we want to do the exact opposite of what has been done by [SBR16]. They indeed implement global mechanisms tuning the system, to see how they influence the composition of compartments, and whether the steady-state of such systems can be described. And they do it in a continuous description of the Golgi, where its composition is projected on a 1D, *cis* $\rightarrow$ *trans* axe. On the contrary, we build a model where local interactions can self-organize a Golgi structure, and where global mechanisms emerge from the structure. And we do it in a discrete and stochastic description of the phenomena.

1.4 Structure of the manuscript

This manuscript is organized as follows:

- Chapter 2 is dedicated to present the model used in this thesis.

- Chapter 3 is dedicated to present the results we submitted recently. In this publication, we investigate how fusion, budding and maturation are sufficient to build a *de novo* Golgi. Once we characterize the steady-state, we describe how vesicular transport emerges from the said steady-state using the very same mechanisms, and the directionality of this transport.

- In chapter 4, we study how local interactions between cargo and the biological identity of membrane can affect the system. We use a slight adaptation of the previous implementation and add cargo that can feel identities of the compartment in which they are. They have an affinity for some identities and not for the others, and we study how this affinity can affect their transport and addressing in the Golgi.

- The last chapter is dedicated to a global discussion of the presented works, and the next problems that could be addressed in order to continue this research work.

Methods: the model

2

Contents for this chapter

2.1 Biological background – main points of Introduction chapter

The Golgi apparatus is an intracellular organelle at the crossroad of the secretory, lysosomal and endocytic pathways [HC14]. One of its most documented functions is the sorting and processing of many proteins synthesized by eukaryotic cells [LRH00]. Proteins translated in endoplasmic reticulum (ER) are addressed to the Golgi, where they undergo post-translational maturation and sorting, before being exported to their final destination. During this process, they interact in a predetermined order with Golgi resident enzymes. This is made possible by the peculiar organization of the Golgi, which is composed of distinct sub-compartments, called cisternae, of different biochemical identities [Sta11]. From the ER, cargo successively reside in cisternae of the *cis*, *medial* and *trans*-identities, after which they exit Golgi via the *trans*-Golgi network (TGN). In some organisms such as the yeast Saccharomyces

cerevisiae, cisternae are dispersed throughout the cell and each cisterna undergoes maturation from a *cis* to a *trans*-identity [SN11]. In most other eukaryotes, cisternae are stacked in a polarized fashion, with cargo-proteins entering via the *cis*-face and exiting via the *trans*-face [BP13]. This polarity is robustly conserved over time, despite cisternae constantly exchanging vesicles with each other, the ER and the TGN [LRH00].

Although there is a large diversity in Golgi structures and dynamics among different species, the organelle's physiological function as a sorting and processing hub is common to all species, suggesting that important mechanisms controlling Golgi dynamics are conserved. Works in evolutionary biology and biophysics have attempted to describe these mechanisms [KMD11; SR13]. Different classes of mathematical models have been proposed, from models of vesicle budding and fusion based on rate equations [Bin+09; IM13; MO14] – some specifically including space [SBR16], to continuous, discrete and stochastic models of protein sorting in the Golgi [Gon+10; VS18a] and computer simulations based on membrane mechanics [TM17]. To account for the Golgi's ability to reassemble after mitosis [WS17], many of these studies have sought to describe the Golgi as a self-organized system [Bin+09; Küh+10]. However, the manner in which the kinetics of the Golgi two main functions (namely the transport and biochemical maturation of its components) interplay with one another to yield a robust steady-state has so far received much less attention [SBR16; VS18a].

We propose here a model in which both Golgi self-organization and vesicular transport are solely directed by (local) molecular interactions resulting in composition-dependent budding and fusion. Thus, the directionality of vesicular transport is an emergent property of the self-organization process that co-evolves with the size and number of Golgi sub-compartments, rather than being fixed by arbitrary rules.

2.2 Nomenclature

Tab. 2.1: Steady-state description

c_n	Size distribution of compartments in the system
n_c	Cutoff in the size distribution of compartments, namely the maximum size of compartments before the distribution collapses for higher values
N	Total number of membrane patches, in all compartments, in the steady-state system
N_i	Total number of patches of the i species (*cis*, *medial* or *trans*)

Tab. 2.2: System's parameters

K_{b}	Budding rate per patches of membrane in a compartment
K_{m}	Maturation rate for each patch of membrane (*cis* $\rightarrow$ *medial* $\rightarrow$ *trans*)
K_{f}	Maximum fusion rate between two compartments
K_{i}	Injection rate of *cis*-vesicles from the ER
K	Budding rate normalized by the fusion rate ($K_{\mathrm{b}}/K_{\mathrm{f}}$)
k_{m}	Maturation rate normalized by the fusion rate ($K_{\mathrm{m}}/K_{\mathrm{f}}$)
J	Injection rate normalized by the fusion rate ($K_{\mathrm{i}}/K_{\mathrm{f}}$)
α	Fraction of *cis* (*trans*) species in the ER (TGN)
α_i	When different between boundaries, α in the boundary i (i = ER or TGN)

Tab. 2.3: Compartments' description

ϕ_i	Fraction of a given species i (*cis*, *medial* or *trans*) in a compartment
$\vec{C}$	Composition of a compartment, whose components are the fractions ϕ_i
n	Size of a compartment, (*i.e.* number of membrane patches in the compartment)
n_i	Number of membrane patches of the i identity, in a compartment
n_{id}	Number of different identities (from 1 to 3) in a single a compartment
n_{v}	Number of vesicles surrounding a compartment that share the same composition
P	Purity of a compartment
$J_{\mathrm{b},i}$	Budding flux of vesicles decorated by the *i*-identity, from a given compartment
ξ_i	Cargo's affinity for patches of the i-identity
$\vec{\xi}$	Cargo's affinity, whose components are the affinities for each patch of the i-identity
$P(i)$	Probability for a cargo to be in contact with the i-identity in a compartment
$P_{\mathrm{v}}(i)$	Probability for a cargo to be taken out of a compartment, in a vesicle of the i-identity
$S_{\mathrm{c}}(\vec{\xi},\vec{C})$	Sorting for a cargo of a $\vec{\xi}$ affinity, in a compartment of a $\vec{C}$ composition

2.3 Model overview

The model of organelle self-organization – with a focus on the Golgi apparatus – is shown in Figure Fig.2.1, introduced below, and fully described in the next sections of this chapter. The building blocks are vesicles that can be of three identities, corresponding to the *cis*, *medial* and *trans*-identities of the Golgi. A compartment is an assembly of fused vesicles. The identity of a membrane patch is defined in a very broad sense by its composition in lipids and proteins that influence its interaction with other patches, such as RAB GTPases [GON06] or fusion proteins such as SNAREs [CRF07]. We describe compartments' dynamics using only three mechanisms – budding, fusion and maturation – defined below:

- **Budding**: Composition-dependent vesicular budding is an important sorting mechanism in cellular traffic [BG04]. Here we adopt a non-linear budding scheme that relies on both the compartment's size and its contamination state, which promotes efficient sorting [DS11]. Analytical developments on why such approach is relevant can be found in section Sec.2.8.2.
- **Fusion**: Homotypic fusion – the higher probability of fusion between compartments of similar identities – is a feature of cellular organelles in general [Ant+00] and the Golgi apparatus in particular [Pfe10; Bha+14]. This is controlled here by a fusion rate between compartments proportional to the probability that they present the same identity at the contact site. We stress that this homotypic fusion mechanism (relying on local interactions) allows vesicular transport between compartments of different identities – a process that may be regarded as heterotypic fusion [GL11]. It merely requires that the receiving compartment contains some membrane patches of identity similar to that of the emitted vesicle.
- **Maturation**: Each membrane patch undergoes stochastic maturation from a *cis* to a *medial* to a *trans*-identity, in agreement with *in vivo* observations [Los+06; Mat+06]. This is a local mechanism of identity conversion, consistent with processes such as the RABs cascade [GON06; Pfe10]. It is distinct from the maturation of entire compartments, which is also affected by the dynamics of budding and fusion.

These mechanisms of compartment self-organization are applied to an open system that interacts with two boundaries: the ER, from which newly synthesized material is injected in the system, and the TGN, through which processed material can leave the system. Vesicles and entire compartments can exit the system by homotypic fusion with either boundaries, following the rules described above. Boundaries' composition

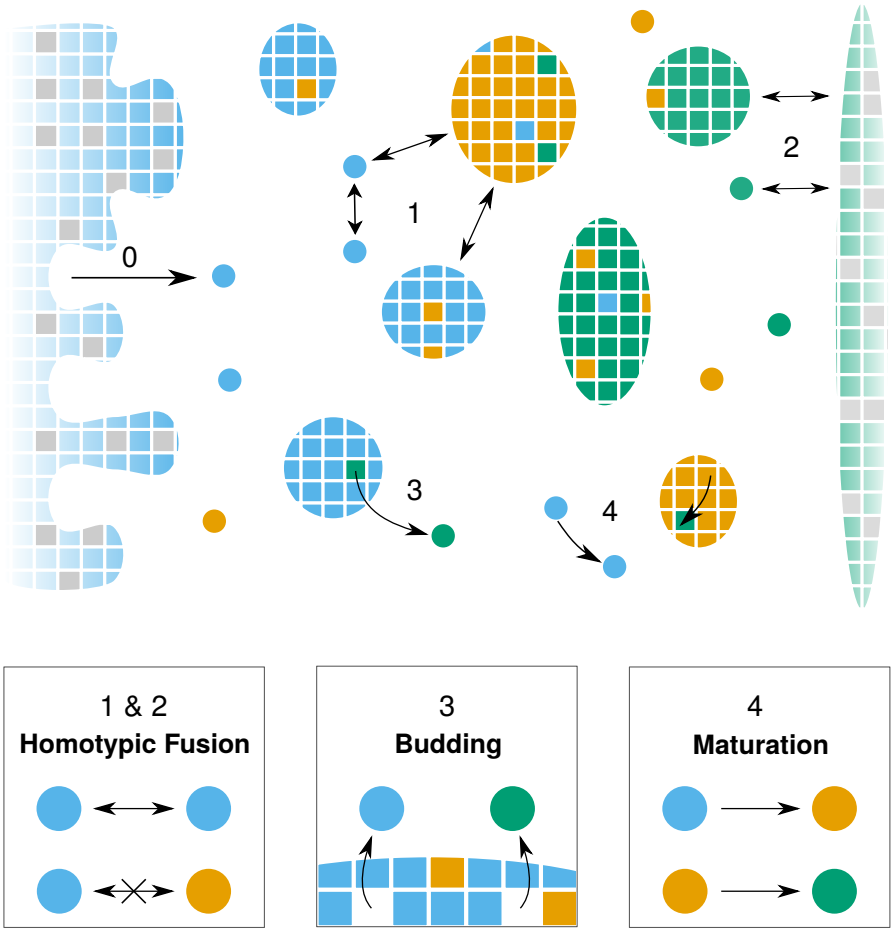

Fig. 2.1: Model of self-organization of the Golgi apparatus. The system includes three membrane identities (*cis*: blue, *medial*: orange, *trans*: green). It self-organizes between two boundaries: the ER (left) is composed of a *cis*-membrane identity, and the TGN (right) is composed of a *trans*-membrane identity. Golgi's compartments self-organize *via* three stochastic mechanisms: **Fusion**: (1) All compartments can aggregate using homotypic fusion mechanisms: the more identical they are, the higher the fusion rate. (2) Each compartment can exit the system by fusing homotypically with one of the two boundaries. **Budding:** (3) Each compartment larger than a vesicle can create a vesicle by losing a patch of membrane. **Maturation:** (4) Each patch of membrane matures from a *cis* to a *trans*-identity. New *cis*-vesicles (0) bud from the ER at a constant rate. In the sketch, the boundaries also contain neutral (gray) membrane species that dilute their identity.

is defined by a parameter α (varying between 0 and 1) which characterizes the fraction of *cis* (*trans*) identity in the ER (TGN).

In its simplest form, our model contains only four parameters: the rates of injection, fusion, budding, and maturation ($K_\mathrm{i},\ K_\mathrm{f},\ K_\mathrm{b},\ K_\mathrm{m}$). By normalizing time with the fusion rate, we are left with three parameters: $K = K_\mathrm{b}/K_\mathrm{f}$, $k_\mathrm{m} = K_\mathrm{m}/K_\mathrm{f}$ and $J = K_\mathrm{i}/K_\mathrm{f}$. The systems' dynamics is entirely governed by these stochastic transition rates, and can be simulated exactly using a Gillespie algorithm [Gil77]

2.4 Detailed mechanisms

2.4.1 Maturation mechanism

In the Golgi, it is known that cargo-proteins [Kel85] and cisternae [DSG13] undergo biochemical modifications over time. If we focus on membrane's identity changes, these are driven by maturation cascades of proteins such RAB GTPases [Sud+13]. These biochemical conversions can be directly observed using live microscopy, and have been best characterized in the yeasts' Golgi [Mat+06]. Biochemical maturation of membrane identity is a complex and possibly multi-step process involving different kinds of enzymes. As we are mostly interested in the interplay between maturation (which mixes different identities within a single compartment) and sorting mechanisms, we coarse-grain the maturation events into simple, one step, stochastic processes: *cis*→*medial* and *medial*→*trans*. To simplify the model, we choose the same maturation rate for both conversions, K_{m}. Each patch of membrane (in a vesicle or a compartment, and whatever the surrounding patches are) has the same transition rate.

2.4.2 Fusion mechanism

Intracellular transport strongly relies on vesicular trafficking [Tak+06]. This involves at least two steps: the budding of a vesicle from a donor compartment (described in the next section), and its fusion with a receiving compartment. The fusion process itself requires close proximity between the receiving compartment and the vesicle, followed by the pairing of fusion actors resulting in membrane fusion. In the current model, the rate of encounter of two compartments is constant, and equal to K_{f}, while the actual fusion event depends on the biochemical composition of the fusing compartments. *In vivo*, some of the key proteins involved in the fusion process, such as the SNAREs or tethering proteins are known to closely interact with membrane markers like RAB proteins [CRF07]. This is thought to accelerate fusion events between compartments of similar biochemical identities and decrease it between compartments of different identities, a process often called homotypic fusion [Mar+07]. To take this into account, fusion is modulated by the probability that both compartments exhibit the same identity at the contact site. The total fusion rate for two compartments (a) and (b) with composition $\phi_i^{(a)}$ and $\phi_i^{(b)}$ for each identity i (with i equals *cis*, *medial* and *trans*) is then:

$$K_{\mathrm{f}} \times \sum_i \phi_i^{(a)} \phi_i^{(b)} \tag{2.1}$$

The fusion rate is maximum (K_{f}) for two identical compartments, and vanishes between two compartments with no common identity. The exchange of vesicles

between compartments of different identities [GL11], or the fusion of compartments of different identities [Mar+04], are sometimes regarded as heterotypic fusion. Such processes are allowed within our homotypic fusion model, provided the different compartments share at least some patches of similar identities. But because of the lower probability to find the same identity-patches at the contact site between two compartments, this process is slower, and thus less probable.

2.4.3 Budding mechanism

Budding is the formation of new vesicles from a large compartment. We assume that each budding vesicle is composed of a single membrane identity, which is consistent with the high specificity of the *in vivo* budding machinery [BG04]. In our model, the flux of vesicles budding from a compartment depends on the compartment's size and composition. Compartments smaller than 2 cannot bud a vesicle. Compartments of size 2 can split into two vesicles. For larger compartments, we consider a general budding flux for vesicles of identity i (for $i =$ *cis*, *medial* and *trans*) of the form:

$$J_{\mathrm{b},i} = K_{\mathrm{b}} \times n \times f(\phi_i) \tag{2.2}$$

with n the compartment's size, K_{b} a constant and $f(\phi_i)$ a function of the compartment's composition.

If the budding machinery, for a given membrane identity, is exclusively recruited on membrane patches with this identity, one expects a linear budding scheme: $f(\phi) = \phi$, yielding a budding flux for identity i proportional to the number patches of identity i: $J_{\mathrm{b},i} = K_{\mathrm{b}} n \phi_i = K_{\mathrm{b}} n_i$. Previous theoretical works suggest that efficient sorting of different membrane species by vesicular budding requires non-linear budding $f(\phi_i) \neq \phi_i$ [DS11]. An extension of this model can be found in Sec.2.8.2. One of the Golgi's main features is to segregate different biochemical species into different compartments. In order to reproduce this feature, we choose a highly non-linear budding scheme, setting $f(\phi_{\mathrm{species}}) = 1$ if $\phi_{\mathrm{species}} > 0$ and $f(\phi_{\mathrm{species}}) = 0$ otherwise. This leads to a total budding flux $K_{\mathrm{b}} \times S \times n_{\mathrm{id}}$ for a compartment carrying n_{id} different identities. The budding flux for a given identity depends on the compartment's total size rather than on the amount of that particular identity. This budding kinetics corresponds the case where budding actors (*e.g.* coat proteins) bind non-specifically to the compartment's membrane and find their budding partners (a patch of a particular identity) by diffusion [VS18a]. This scenario is consistent with the fact that budding proteins interact very dynamically with the membrane, attaching and detaching multiple times before budding a vesicle [Hir+98]. We can however implement linear budding schemes to compare the two implementation, which is done in next chapter.

2.5 Interactions with the boundaries

2.5.1 Exit of compartments

In cells, the Golgi is placed between two intra-cellular structures that are the ER and the TGN [Pre+97; Kle+09]. Fluxes of material leaving the Golgi include retrograde fluxes toward the ER, carrying immature components such as *cis* and *medial*-Golgi enzymes or recycling ER enzymes, and anterograde fluxes toward the TGN of mature components, such as processed cargo that properly underwent all their post-translational maturation steps [BP13]. The exiting fluxes are accounted for by allowing the different compartments in the system to fuse with the boundaries. All compartments, from vesicles to the largest ones, can fuse homotypically with the ER or the TGN to exit the system. Thus, these boundaries are modeled as stable compartments, containing a fraction α of *cis* (*trans*) components for the ER (TGN). This allows immature (*cis*) compartments to undergo retrograde exit, and mature (*trans*) components to undergo anterograde exit. We focus on the case $\alpha = 1$, that is the default value when nothing is specified. But one should bear in mind that lower values of α reduce fusion with the boundaries and increase the residence time of components in the system. The effect of such modifications are studied in the next chapter.

2.5.2 Influx to the Golgi

The Golgi receives material from different compartments like the endosomal network, lyzosomes, etc... [BP13]. As we are primarily interested in characterizing the relationship between the Golgi's structure and dynamics, and in relating these to the rates of individual maturation and transport processes, we focus here on the secretory role of the Golgi, and only account for the incoming flux of immature components coming from the ER. We define a rate K_{i} of injection of *cis*-vesicles in the system. As the system's parameters are varied, the injection rate is varied as well in order to keep the total amount of mass in the system to an almost constant value. This constraint is only approximately enforced using the relationship between the steady-state system's size and the different rates that can be computed analytically in the simple limit where all compartments are pure (see the model in Sec.2.8.1, Equation Eq.2.7).

In the majority of the simulations, we restrict ourselves to a system size of $N = 300$. This is suitable for Golgi ministacks whose total area is of the order of $1\mu\mathrm{m}^2$ (the area of a mammalian Golgi ribbon is much larger) [YHW09], corresponding to about a few hundreds of vesicles of diameter $\sim 10 - 50\mathrm{nm}$.

One should remember that the equation used to predict the system's mass N assumes that compartments are pure (perfectly sorted). We will later show that this assumption fails to predict N for systems where the budding rate is low compared to the fusion rate (highly interacting compartments). In this regime, compartments have a great probability to fuse together, creating hybrid *cis/medial/trans*-structures. This makes *medial*-patches sensitive to the interaction with the ER and the TGN, and creates an exit flux for these patches that is not observed in a pure regime. Such systems exhibit a larger exit flux and thus a lower N. Note this is only true for maturation rates lower than the fusion rate, as the system is saturated with *trans*-patches for high k_{m} (Sec.2.8.1).

2.6 Cargo-proteins

We design cargo-proteins (cargo) as objects blocked inside compartments and vesicles, that can interact locally with the surrounding membrane. They indeed have an affinity for each membrane identities, ξ_i – i equals *cis*, *medial* or *trans* – that is implemented as a number between 0 and 1: the higher ξ_i the greater the chance a cargo is in contact with an i-identity membrane patch. In a compartment composed of n_i patches of each i-identity, the probability $P(j)$ for a cargo to be in contact with a j identity is:

$$P(j) = \frac{n_j \times \xi_j}{\sum_i n_i \times \xi_i} \tag{2.3}$$

When this compartment buds a vesicle of the j-identity, the probability $P_{\mathrm{v}}(j)$ for the cargo to be taken in the budded vesicle is:

$$P_{\mathrm{v}}(j) = \frac{\xi_j}{\sum_i n_i \times \xi_i} \tag{2.4}$$

A passive cargo has the same affinity for all identities, so its probability to exit a compartment is $1/n$ – n being the compartment's size. Cisternal cargo cannot exit a compartment (except the ER) by getting taken in a budding vesicle. If not precised, *cis*-cargo (*medial* | *trans*) have an affinity ξ_{cis} (ξ_{medial} | ξ_{trans}) that equals 1, and 0 for the others.

One way to picture this affinity is to assume cargo dynamics inside a compartment is an equilibrium process, and that each affinity is as a Boltzmann weight $k_i = \exp\left(-\frac{E_i}{k_{\mathrm{b}}T}\right)$ where E_i is the energy of a cargo in contact with the i-identity. In that framework, neutral cargo have the same energy associated to their interaction with *cis* and *trans* membrane-species. On the contrary, *cis* and *trans*-cargo have an infinite energetic preference for one identity.

Source Code

Codes used for the simulation can be found on the UMR168 Curie website, section `team-sens/software`. **Click to access**
A more recent implementation, used in chapter 4, can be found on Github (as soon as it get published, please contact *jean-patrick.vrel@curie.fr* if not accessible yet). **Click to access**

2.7 Gillespie algorithm and Software implementation

All rates in the system are normalized by the fusion rate: $K = K_\mathrm{b}/K_\mathrm{f}$, $k_\mathrm{m} = K_\mathrm{m}/K_\mathrm{f}$ and $J = K_\mathrm{i}/K_\mathrm{f}$. The dynamics of the system can be exactly simulated (to yield the correct trajectories, stochastic noise, etc...) using a Gillespie algorithm [Gil77], also known as stochastic simulation algorithm. After choosing the initial state of the system (see below), the algorithm is implemented as follows:

1. The rates of all possible events (be it the input of a new vesicle in the system, the fusion between two compartments or between a compartment and one boundary, the budding of a vesicle, or the maturation of a membrane patch) are calculated. The time interval δt for the next reaction to occur is randomly picked from an exponential distribution with mean $1/R_\mathrm{TOT}$, where R_TOT is the sum of the reaction rates of all possible reactions. The reaction that actually occurs is randomly picked with a probability equal to the rate of this reaction, normalized by R_TOT.

2. The state of the system is modified according to the picked reaction. The rates of all events in the modified system are calculated, and the current time of the simulation is incremented by δt.

3. The program comes back to step 1 `IF` the predefined maximum number of iterations has not been reached, `AND` there is at least one reaction that has a non-zero rate ($R_\mathrm{TOT} \neq 0$).

Depending on the required precision, the maximum number of time-steps is typically set to 10^6 or 10^7 in order to reach steady-state and accumulate enough statistics on all the measured quantities. The time needed to reach steady-state can be shortened by starting the simulation from a vesicular system with the predicted amount of *cis*, *medial* and *trans*-species (see Sec.2.8.1).

2.8 Analytical models used to build the simulation

2.8.1 System's steady-state composition in the well-sorted limit

To anticipate the influx from the ER in order to fix the Golgi's mass, one should compute its steady-state composition. But this system's composition at steady-state is difficult to compute due to the fact that the exit of components from the system, through fusion with the boundaries, depends on the composition of the exiting compartments, which cannot be derived analytically. This calculation becomes straightforward if the system is well sorted and all compartments are pure. In that case, mean-field equations can be derived for the total amount N_{cis}, N_{medial} and N_{trans} of the respective species:

$$\begin{aligned} \frac{\partial N_{cis}}{\partial t} &= J - N_{cis}(\alpha_{\text{ER}} + k_{\text{m}}) \ , \ \frac{\partial N_{medial}}{\partial t} = k_{\text{m}}(N_{cis} - N_{medial}) \ , \\ \frac{\partial N_{trans}}{\partial t} &= k_{\text{m}} N_{medial} - \alpha_{\text{TGN}} N_{trans} \end{aligned} \tag{2.5}$$

With J the injection rate of new *cis*-vesicles in the system and k_{m} the maturation rates, both normalized by the fusion rate, and α_{ER} (α_{TGN}) is the fraction of *cis* (*trans*) species promoting homotypic fusions with Golgi's components in the ER (TGN). At steady-state, the system's composition satisfies:

$$N_{cis} = N_{medial} = \frac{J}{\alpha_{\text{ER}} + k_{\text{m}}} \ , \ N_{trans} = \frac{k_{\text{m}}}{\alpha_{\text{TGN}}} \frac{J}{\alpha_{\text{ER}} + k_{\text{m}}} \tag{2.6}$$

In order to fix the total system's size $N = N_{cis} + N_{medial} + N_{trans}$ to a predetermined value (typically 300) while changing the other parameters, the influx J should vary according to:

$$J = \frac{N \ (\alpha_{\text{ER}} + k_{\text{m}}) \ \alpha_{\text{TGN}}}{2\alpha_{\text{TGN}} + k_{\text{m}}} \tag{2.7}$$

2.8.2 Why a non-linear budding rate?

Previous works performed in the lab showed that a budding and a homotypic fusion mechanisms are not sufficient in all regimes, to sort biochemical identities between two compartments of fixed sizes [DS11]. To be efficient, these two mechanisms need to be in a non-linear regime. Here, we propose an extension of this modeling approach, relaxing the hypothesis of compartments of fixed sizes. We more precisely want to know whether it changes the required non-linearity on the budding rate to sort species in the system.

We consider two compartments composed of two mixed species. One species is active, meaning it can drive budding homotypic fusion, with a total amount A, the other is passive, meaning it acts as a solvent, with a total amount O. The first compartment is composed of a active and o passive species, and the second compartment is composed of $A-a$ active and $O-o$ passive species. Both compartments can exchange materials by budding a vesicle from one of them and fusing this vesicle with the other. These mechanisms change the s of a, o, $A-a$ and $O-o$ in a continuous manner. Both fusion and budding mechanisms are non-linear:

- For the budding rate, the flux of elements leaving the compartment does not scale linearly with the number of element in the compartment. We consider two contributions to the budding flux, one that scales with the compartment size, one with the concentration of active species in the compartment. The latter is non-linear, and saturates at large values of the concentration of active species. We thus need to define two constants: K_b the maximum budding rate per unit surface, and ϕ_b the concentration beyond which the budding flux saturates at its maximum value. The lower ϕ_b, the higher the non-linearity in the budding rate. The non-linear dependency in the budding flux $S[\phi_\mathrm{b},\phi]$ is then:

  $$S[\phi_\mathrm{b},\phi] = \phi\,\frac{\phi_\mathrm{b}+1}{\phi_\mathrm{b}+\phi} \tag{2.8}$$

  One way of picturing this equation is to consider a system in which budding flux scales linearly with the compartment's size, but sorts active species while creating a vesicle. The concentration of active species in the vesicle is higher than the one in the compartment: there is an enrichment in the vesicle. The flux of active species leaving the compartment is the budding rate, times the size of the compartment, times the amount of active species in the vesicle, yielding the exact same equation we derive below.

- Fusion occurs in a homotypic way, meaning a vesicle is more likely to fuse with a compartment that shares the same identity. We define one constant: ϕ_f the typical concentration beyond which homotypic fusion becomes relevant.

The probability for a vesicle, that budded from a compartment with a fraction ϕ_1 of active species, to fuse with a second compartment of a fraction ϕ_2 is then:

$$P_{\phi_1\to\phi_2} = \frac{\phi_\mathrm{f} + S[\phi_\mathrm{b},\phi_1]\,\phi_2}{2\phi_\mathrm{f} + S[\phi_\mathrm{b},\phi_1]\,(\phi_1+\phi_2)} \tag{2.9}$$

In the following, the system unit size is defined by vesicle so that compartments' size are multiples of the vesicle size. We can now write the time derivative of a and o:

$$\begin{aligned}\dot{a} =& - K_\mathrm{b} \times (a+o)\, S\left[\phi_\mathrm{b}, \frac{a}{a+o}\right] P_{1\to 2} \\ &+ K_\mathrm{b} \times (A+O-a-o)\, S\left[\phi_\mathrm{b}, \frac{A-a}{A+O-a-o}\right] P_{2\to 1} \qquad (2.10)\\ \dot{o} =& - K_\mathrm{b} \times (a+o) \left(1 - S\left[\phi_\mathrm{b}, \frac{a}{a+o}\right]\right) P_{1\to 2} \\ &+ K_\mathrm{b} \times (A+O-a-o) \left(1 - S\left[\phi_\mathrm{b}, \frac{A-a}{A+O-a-o}\right]\right) P_{2\to 1} \qquad (2.11)\end{aligned}$$

For a mixed system, with $o = O/2$ and $a = A/2$, we get $\dot{a} = \dot{o} = 0$, meaning it is an equilibrium point. The question is then whether it is a stable or an unstable one. To answer this question, we compute the Jacobian matrix around this point.

$$J = \begin{pmatrix} \left.\frac{\partial \dot{a}}{\partial a}\right|_{a\to\frac{A}{2},o\to\frac{O}{2}}, & \left.\frac{\partial \dot{a}}{\partial o}\right|_{a\to\frac{A}{2},o\to\frac{O}{2}} \\ \left.\frac{\partial \dot{o}}{\partial a}\right|_{a\to\frac{A}{2},o\to\frac{O}{2}}, & \left.\frac{\partial \dot{o}}{\partial o}\right|_{a\to\frac{A}{2},o\to\frac{O}{2}} \end{pmatrix} \qquad (2.12)$$

Assuming $\phi_A = \frac{A}{A+O}$, we get:

$$\det(J) = \frac{K_b^2\, \phi_\mathrm{b}(1+\phi_\mathrm{b})}{(\phi_A+\phi_\mathrm{b})^2} \qquad (2.13)$$

$$\begin{aligned}\mathrm{Tr}(J) =& K_b \left(-2 + \phi_A \frac{1-\phi_A}{(\phi_A+\phi_\mathrm{b})^2} + \frac{\phi_A}{\phi_A+\phi_\mathrm{b}}\right. \\ &\left. -\phi_\mathrm{f} \frac{1-\phi_A}{\phi_A(\phi_A+\phi_\mathrm{f}) + \phi_\mathrm{b}(\phi_A^2+\phi_\mathrm{f})}\right)\end{aligned} \qquad (2.14)$$

The determinant is always positive, meaning the real part of the eigenvalues are always of the same sign. If the trace is positive, then both eigenvalues are positive and the system is unstable. We thus need to compute for which ϕ_b the trace is positive. To get an analytical result we consider the limit of a purely selective fusion with $\phi_\mathrm{f} = 0$. If it does not segregate in this regime of high specificity, it will not for higher ϕ_f. We show that even in this limit, for the system to be unstable, ϕ_b must satisfy:

$$\phi_\mathrm{b} \leq \frac{1}{4}\left(-3\phi_A + \sqrt{8\phi_A - 7\phi_A^2}\right) \qquad (2.15)$$

This never exceed 0.15, when ϕ_b must tend to infinity for the budding flux to be linear. The budding rate has to be very non-linear.

To conclude, for a system containing passive species, even if fusion occurs in a perfectly homotypic way, we still need a highly non-linear budding for the system to

keep sorted. That is why we implement a non-linear budding rate in the simulation, and to remove a parameter in the system, we take it the most non-linear way possible, $\phi_{\mathrm{b}} = 0$.

3

Steady-state organization and emergent vesicular transport in a self-organized Golgi apparatus

Contents for this chapter

In the current Chapter, we discuss how the model yields a steady-state in organization and vesicular transport. These results have been submitted, that is why the way they are reported follows the “main text” – “Supplemental information” convention. It has however been reworked to ease reading.

3.1 Chapter’s abstract

The design principles dictating the spatio-temporal organization of eukaryotic cells, and in particular the mechanisms controlling the self-organization and dynamics of membrane-bound organelles such as the Golgi apparatus, remain elusive. Although this organelle was discovered 120 years ago, such basic questions as whether vesicular transport through the Golgi occurs in an anterograde (from entry to exit) or retrograde fashion are still strongly debated. Here, we address these issues by studying a quantitative model of organelle dynamics that includes: *de-novo* compartment generation, inter-compartment vesicular exchange, and biochemical maturation of membrane components. This model is described in the previous chapter, chapter 2. We show that purely anterograde or retrograde vesicular transports are asymptotic behaviors of a much richer dynamical system. Indeed, the structure and composition of cellular compartments and the directionality of vesicular exchange are intimately linked. They are emergent properties that can be tuned by varying the relative rates of vesicle budding, fusion and component maturation.

3.2 Main results

The steady-state organization and dynamics of the system is described in terms of the average size and purity of compartments, and the directionality of vesicular transport between them (introduced here and detailed in the Sec.3.3.2):

- The typical compartment’s size is defined as the ratio of the second over the first moments of the size distribution [VTS15].

- The purity of a given compartment is defined as the (normalized) Euclidean distance of the compartment’s composition (the fractions ϕ_i in the different i-identities, $i =$ *cis*, *medial* and *trans*) from a perfectly mixed composition. $P = 0,\ 1/2,\ 1$ correspond respectively to compartments that contain the same amount of the three identities, the same amount of two identities, and a single

identity (see Figure Fig.3.1). The system's purity is the average purity of each compartment weighted by its size, ignoring vesicles.

- Finally, to characterize the directionality of vesicular transport, the dynamics of passive cargo injected from the ER is followed over time. Each cargo in a compartment of size n has a probability $1/n$ to join a vesicle budding from this compartment. When this vesicle fuses with another compartment or a boundary, the composition difference $\Delta\phi_i$ between the receiving and emitting compartment (a number between -1 and 1) is recorded for the three i-identities ($i =$*cis*, *medial*, *trans*). Averaged over all budding/fusion events, this defines the *enrichment vector* $\vec{E}$, whose three components E_i are normalized for readability so that $\sum_i |E_i| = 1$ (see Fig.3.7A – Sec.3.3.4, p.54 for non-normalized enrichment). Vesicular flux is anterograde if $E_{cis} < 0$ and $E_{trans} > 0$, while it is retrograde if $E_{cis} > 0$ and $E_{trans} < 0$.

3.2.1 Steady-state organization

The compartment size distribution shows a power law with an exponential cutoff (Fig.3.2A), as expected for a non-equilibrium steady-state controlled by scission and aggregation. With our definition, the characteristic compartment size is close to half the cut-off size (see Sec.3.3.2 for details about this quantification). The way it depends on the model parameters is shown in Fig.3.2B. Increasing the ratio of budding to fusion rate K decreases the compartment size [TSS05]. The size

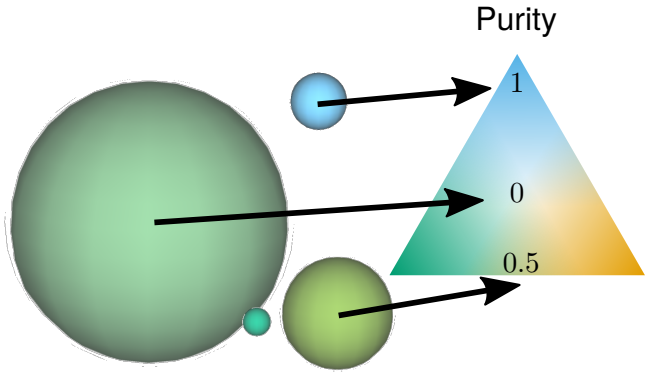

Fig. 3.1: Graphical representation of the size and purity of compartments. Each compartment is represented as a sphere with an area equal to the area of a vesicle (the smallest elements in this snapshot) times the number of vesicles that fused together to create the compartment. The color of the compartment reflects its composition, according to the color code on the triangular composition phase space: 100% *cis* at the top, *medial* at the bottom right, *trans* at the bottom left. The purity of each of these compartments is its distance from a perfectly mixed compartment at the center of the triangle (middle arrow). This distance is normalized so that it equals 1 for a perfectly pure compartment (bottom arrow).

depends on the maturation rate k_{m}, which controls the compartment's composition and hence the fusion probability, in a non-monotonic manner: for a given budding rate, the size is smallest for intermediate values of the maturation rate ($k_{\mathrm{m}} \simeq 1$). This is well explained by a simple analytical model (discussed in Sec.3.3.7) that approximates the system by three pure compartments interacting with a pool of vesicles (solid lines in Fig.3.2B). The system is mostly composed of *cis* and *medial*-components for low maturation rates and of *trans*-components for high maturation rates. If compartments are well sorted, the mean compartment size is limited by the amount of each species in the system, which is smallest when the three identities are in equal amount, that is when $k_{\mathrm{m}} \simeq 1$.

The dependency of the compartments' purity with the parameters is shown in Fig.3.2C. As for the compartments' size, it is non-monotonic in the maturation rate, and regions of low purity are found for intermediate maturation rates $k_{\mathrm{m}} \simeq 1$, when all three identities are in equal amount. The purity increases with the budding rate K in a sigmoidal fashion (see Fig.3.3). This can be understood by analyzing the processes involved in mixing and sorting of different identities. In a first approximation, mixing occurs by maturation and sorting occurs by budding of contaminating species, suggesting a transition from low to high purity when the budding rate reaches the maturation rate ($K \simeq k_{\mathrm{m}}$). A "purity transition" is indeed observed in an intermediate range of maturation rates ($0.1 < k_{\mathrm{m}} < 10$, see Fig.3.2C). It is most pronounced for $k_{\mathrm{m}} \simeq 1$. Beyond this range, the system is dominated by one identity and compartments are always pure. The purity variation can be qualitatively reproduced by an analytical model (Sec.3.3.7, p.62) that accounts for the competition between maturation and budding, but also includes fusion between compartments and with the exits (solid lines in Fig.3.2C.).

In summary, three types of organization can be found, mostly controlled by the ratio of budding over fusion rate K: a *mixed regime* at low K, where compartments are large and contain a mixture of identities, a *vesicular regime* at high K, where compartments are made of only a few vesicles and are very pure, and a *sorted regime* for intermediate values of K, where compartments are both rather large, and rather pure. Snapshots of these three steady-states are shown in Fig.3.2D. Non-linear budding is essential to the existence of the intermediate *sorted* regime. With a linear budding scheme Sec.3.3.6, p.59), the purity transition occurs for larger values of the budding rate K, where compartments are already small.

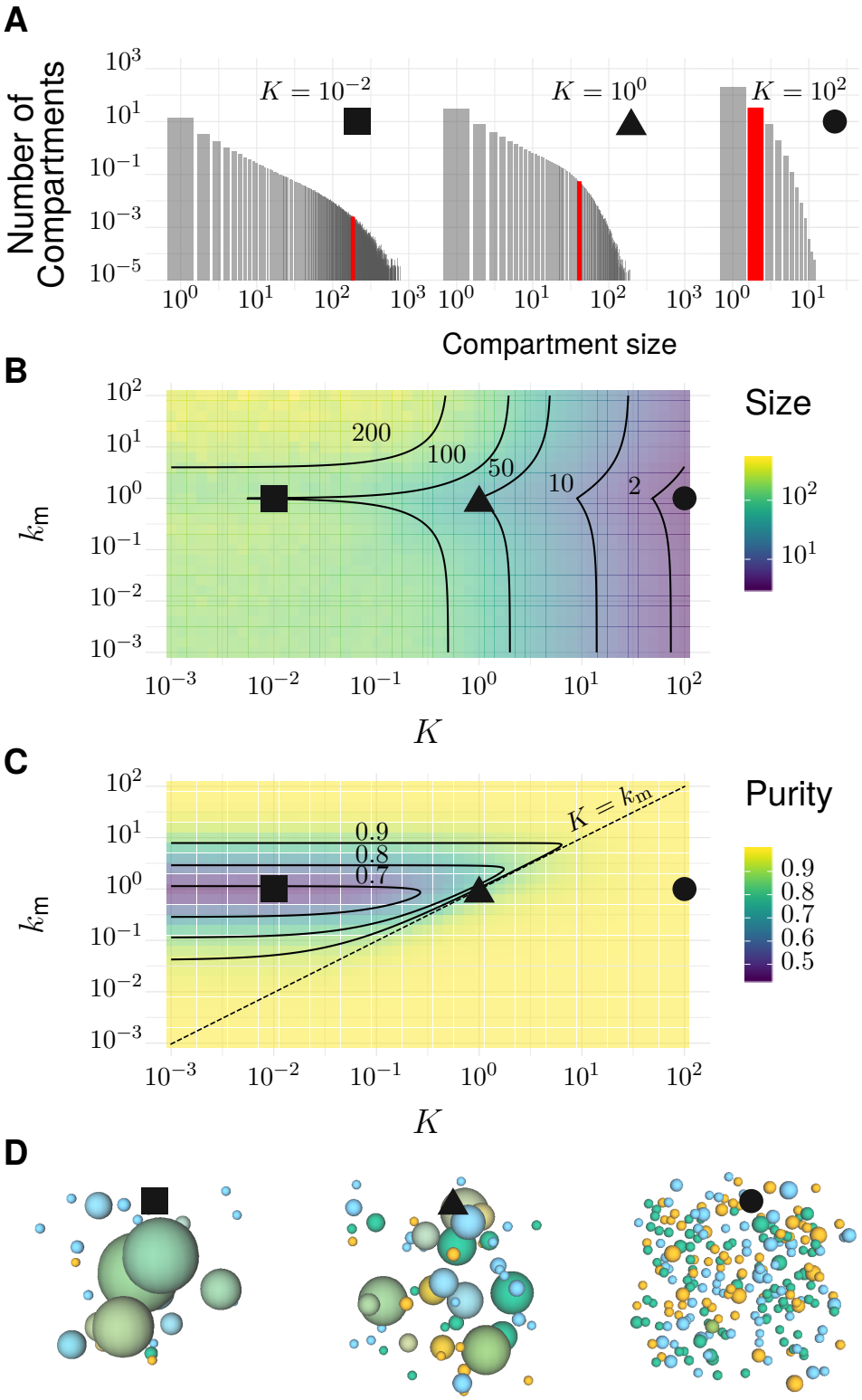

Fig. 3.2: Steady-state of the self-organized model of Golgi apparatus. **A** Size distribution of compartments for a maturation rate $k_m = 1$ and different values of the budding rate K. The red bar shows the characteristic compartment size. **B** Phase diagram of the compartments' size as the function of K and k_m. Black lines: theoretical prediction (introduced in text, developed in Sec.3.3.7, p.48). **C** Phase diagram of the system's purity as a function of K and k_m. Dashed line is $k_m = K$, black lines are a theoretical prediction (see Sec.3.3.7, p.63). **D** System snapshots for $k_m = 1$ showing the *mixed regime* (square - $K = 10^{-2}$), the *sorted regime* (triangle - $K = 1$), and the *vesicular regime* (circle - $K = 10^{2}$) - see text. See also Sec.3.3.3, p.51 for further characterizations of the steady-state organization, Sec.3.3.5, p.57 for the role of exits' composition, and Sec.3.3.6, p.60 for results with alternative budding and fusion kinetics.

3.2.2 Vesicular Transport

We compute the mean enrichment in *cis*, *medial* and *trans*-identities during vesicular exchange from a donor to a receiving compartment. We focus on systems containing comparable amounts of each species at steady-state ($k_{\mathrm{m}} = 1$ – as discussed in the Methods chapter, Sec.2.8.1). The enrichment in *cis*, *medial* and *trans*-identities are shown in Fig.3.3 as a function of the budding rate K. The most striking result is the high correlation between compartment's purity and the directionality of vesicular transport. For low values of the budding rate ($K \ll 1$), compartments are well mixed (purity $\simeq 1/2$) and the vesicular flux is retrograde, with a gain in *cis*-identities and a loss in *trans*-identities. For high values of the budding rate ($K \gg 1$), compartments are pure (purity $\simeq 1$) and the vesicular flux is anterograde, with a gain in *trans*-identities and a loss in *cis*-identities. The archetypal behaviors most often discussed in the literature are thus, within the limits of our model, asymptotic regimes for extreme values of the ratio of budding to fusion rates. Remarkably, the cross over between these two asymptotic behaviors is rather broad ($K \sim 0.1$) and displays a more complex vesicular transport dynamics, mostly oriented toward medial compartments.

In our model organelle, vesicle budding and fusion are biased solely by local compositions, which is subjected to irreversible biochemical maturation. The interplay between these microscopic processes gives rise to an irreversible flux of vesicles across the system. To better understand the directionality of vesicular exchanges, we represent on Fig.3.4 the vesicular fluxes between compartments as a vector field on the compartments' composition space. This is shown as a triangle plots in which each point corresponds to a fraction of *cis* (100% at the top), *medial* (100% at the bottom right) and *trans* (100% at the bottom left) components in a compartment (Sec.3.3.2, for details about this quantification). The net vesicular flux leaving compartments with a given composition is represented as a vector field. The variation of the vesicular flux with the budding rate K (Fig.3.4) is consistent with that of the composition enrichment in the different identities (Fig.3.3). As K increases, the flux evolves from being mostly retrograde at low K (from *trans*-rich toward less mature compartments) to being anterograde at high K (from *cis* to *medial*, and *medial* to *trans*-compartments). In between, the vesicular flux is centripetal toward mixed compartments, leading to a net enrichment in *medial*-identity. The relationship between structure and transport is explained below, and a dissection of these fluxes with respect to the vesicles' composition is shown in Sec.3.3.4. The net flux leaving a particular region of the triangular phase space is proportional to the total mass (number of compartments times their size) with this composition, while the flux arriving at a particular region depends on the number of compartments with that composition. Both quantities are shown on Fig.3.4.

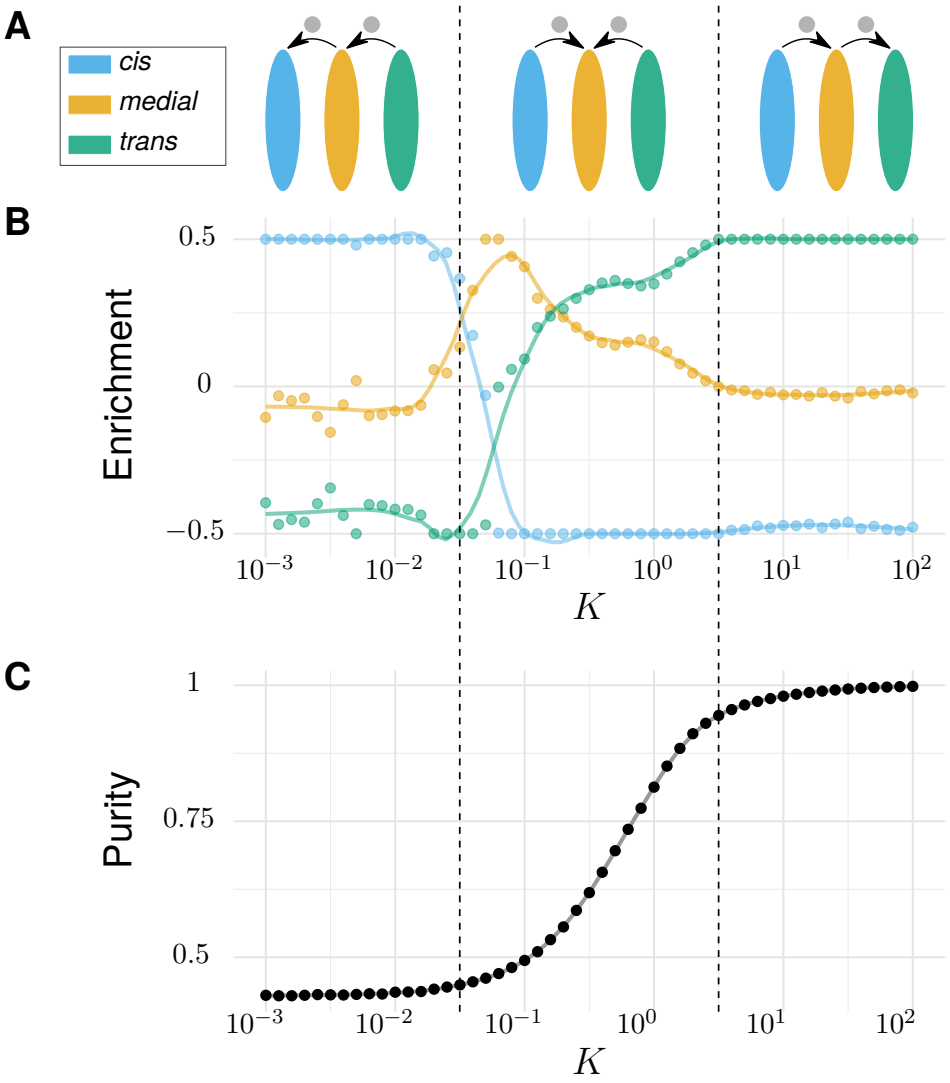

Fig. 3.3: Directionality of vesicular transport, displayed varying the budding rate K for a maturation rate $k_{\mathrm{m}} = 1$ (equal amount of all species in the system). **A-B** steady-state vesicular transport: normalized enrichment (**B**) in *cis* (blue), *medial* (orange) and *trans* (green) identities between the acceptor and donor compartments during vesicular exchange (solid lines are guides for the eyes), and sketches showing the direction of vesicular transport consistent with these data (**A**). See Sec.3.3.4, p.54 for non-normalized fluxes. **C** System purity for the same parameters. Before the purity transition (low values of K - purity ~ 0.5) the vesicular flux is retrograde. After the transition (high values of K - purity ~ 1) the vesicular flux is anterograde. Around the crossover ($K \sim 0.1$), the vesicular flux is centripetal and oriented toward *medial*-compartments. The centripetal flux disappears if inter-compartments fusion is prohibited, see Sec.3.3.6, p.59.

At low budding rate ($K \ll 1$ – top row in Fig.3.4), the system is in the mixed regime, where compartments are large (hundreds of vesicles in size) but mixed (purity $\sim 1/2$). The system is dominated by maturation, and the compartment distribution is spread around a path going from purely *cis* to purely *trans*-compartments, consistent with a dynamics where each compartment maturates independently of the others ($\phi_A = e^{-k_\mathrm{m} t}$, $\phi_B = k_\mathrm{m} t e^{-k_\mathrm{m} t}$ and $\phi_C = 1 - \phi_A - \phi_B$, where t is the typical age of the compartment – see top left panel of Fig.3.4 and Sec.3.3.7). The majority of the transport vesicles are emitted by *trans*-rich compartments, which concentrate most of the system's mass, leading to a retrograde vesicular flux.

At high budding rate ($K \gg 1$ – bottom row in Fig.3.4), the system is in the vesicular regime, where compartments are fairly pure, but rather small, with a size equivalent to a few vesicles. Compartments are exclusively distributed along the *cis/medial* and *medial/trans*-axes of composition, and accumulate at the triangle's apexes. Membrane patches that just underwent maturation bud quickly from the donor compartment and fuse with pure compartments with the appropriate *medial* or *trans*-identity, explaining the clear anterograde vesicular transport. This feature is further reinforced under very high budding rate, where the vesicular flux is dominated by vesicles undergoing maturation *after* budding, which prohibits their back fusion with the donor compartment (see Sec.3.3.4, p.55 for details about the role of vesicles maturation).

In the intermediate regime (middle row in Fig.3.4), the distribution of mixed compartments is more homogeneous along the line describing the maturation of individual compartments – both in terms of mass and number of compartments. *Cis*-rich and *trans*-rich compartments emit comparable amount of transport vesicles, while large *medial*-rich compartments are absent. This leads to a centripetal vesicular flux with an enrichment in *medial* identity (see Fig.3.3). The lack of large *medial*-rich compartment is due to the fact that they can be contaminated by either *cis* or *trans*-species and fuse with *cis*-rich or *trans*-rich compartments. If inter-compartment fusion is prohibited, the enrichment in medial-identity in the intermediate regime is abolished, with a direct transition from anterograde to retrograde vesicular transport upon increasing K (see Sec.3.3.6 and the Conclusion section).

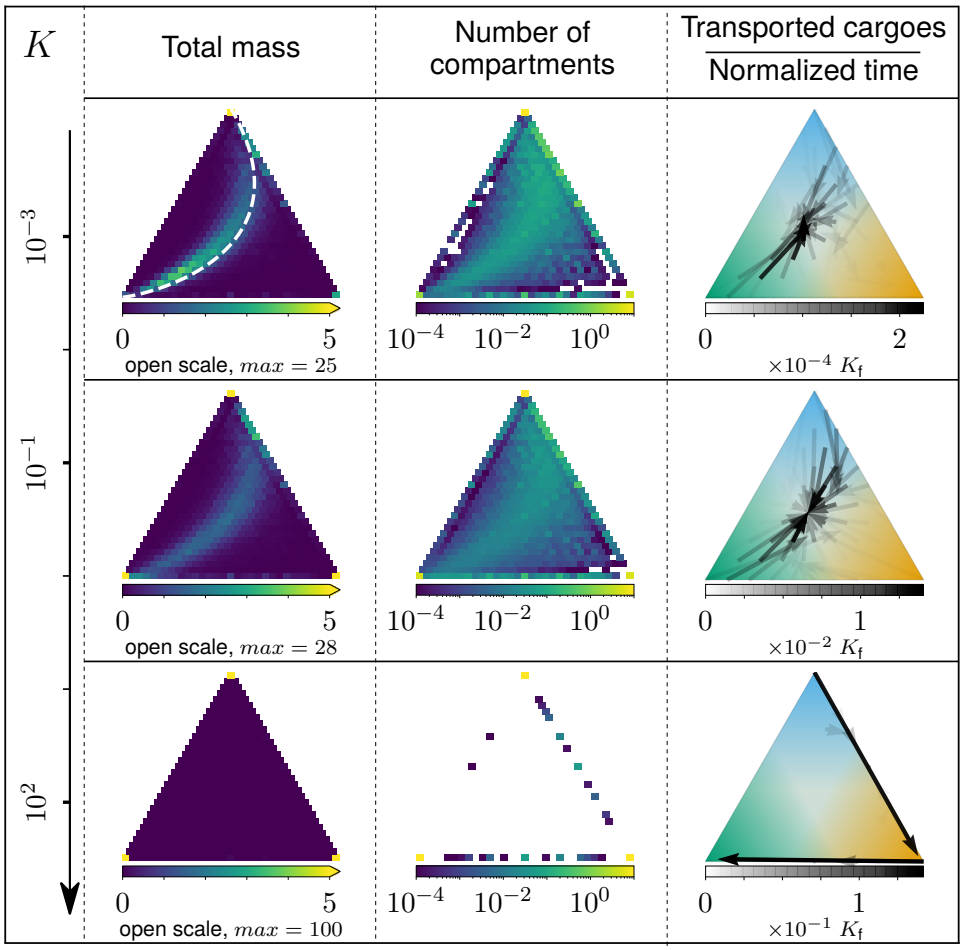

Fig. 3.4: Relationship between the system's structure and the vesicular fluxes. Distribution of the total mass (truncated scale, maximum value in brackets) and number of compartments, and the vesicular flux between them, shown in a triangular composition space. Each point represents a given compartment's composition in *cis* (100% at the top), *medial* (100% at the bottom right) and *trans* (100% at the bottom left) identities. Arrows show the vesicular flux. The base of each arrow is the composition of the donor compartment and the tip is the average composition of receiving compartments (ignoring back fusion). The Arrows' opacity is proportional to the flux of transported cargo going through this path per unit time ($1/K_f$), normalized by the total number of cargo. The dashed line on the top-left triangle is a theoretical prediction discussed in the text. See also Sec.3.3.4 p.52 for further characterizations of the vesicular transport, and Sec.3.3.6 p.59 to discuss the impact of other budding and fusion implementations on the vesicular fluxes.

3.3 Additional analyses and study results

3.3.1 Setting up the simulation

Fixing the steady-state Golgi size

In this section, we check two things on the implementation:

- Is the size of the system large enough to describe a steady-state that does not dramatically depends on the number of interacting elements?

- Is the assumption developed in the previous chapter (Sec.2.8.1) – and used to compute the influx rate from the ER – relevant? For the record, we assumed all identities in the system were perfectly sorted, in order to compute the amount of *cis*, *medial* and *trans*-patches at steady-state. This is possibly not the case in regimes where purity is low, and we have to verify to what extend simulations differ from this simplified picture.

The impact of the system's size on the structure of the Golgi is shown on Fig.3.5A. Increasing the total size increases the number of compartments and hence the total fusion flux between compartments. Consequently, compartments are larger in larger systems, and tend to be (slightly) less pure, as fusion increases mixing. In the Main results section, we restrict ourselves to a system size of $N = 300$. This is suitable for Golgi ministacks whose total area is of the order of $1\mu\mathrm{m}^2$ (the area of a mammalian Golgi ribbon is much larger) [YHW09], corresponding to about a few hundreds of vesicles of diameter $\sim 10 - 50\mathrm{nm}$. But we see that despite this increased fusion rate, the qualitative results are the same that what is discussed in the Main results section.

One should remember that the equation used to predict the system's mass N assumes that compartments are pure (perfectly sorted). Fig.3.5B shows that this assumption fails to predict N for systems where the budding rate is low compared to the fusion rate (highly interacting compartments). In this regime, compartments have a great probability to fuse together, creating hybrid *cis/medial/trans*-structures. This makes *medial*-patches sensitive to the interaction with the ER and the TGN, and creates an exit flux for these patches that is not observed in a pure regime. Such systems exhibit a larger exit flux and thus a lower N. Note this is only true for maturation rates lower than the fusion rate, as the system is saturated with *trans*-patches for high k_m (see previous chapter, Sec.2.8.1).

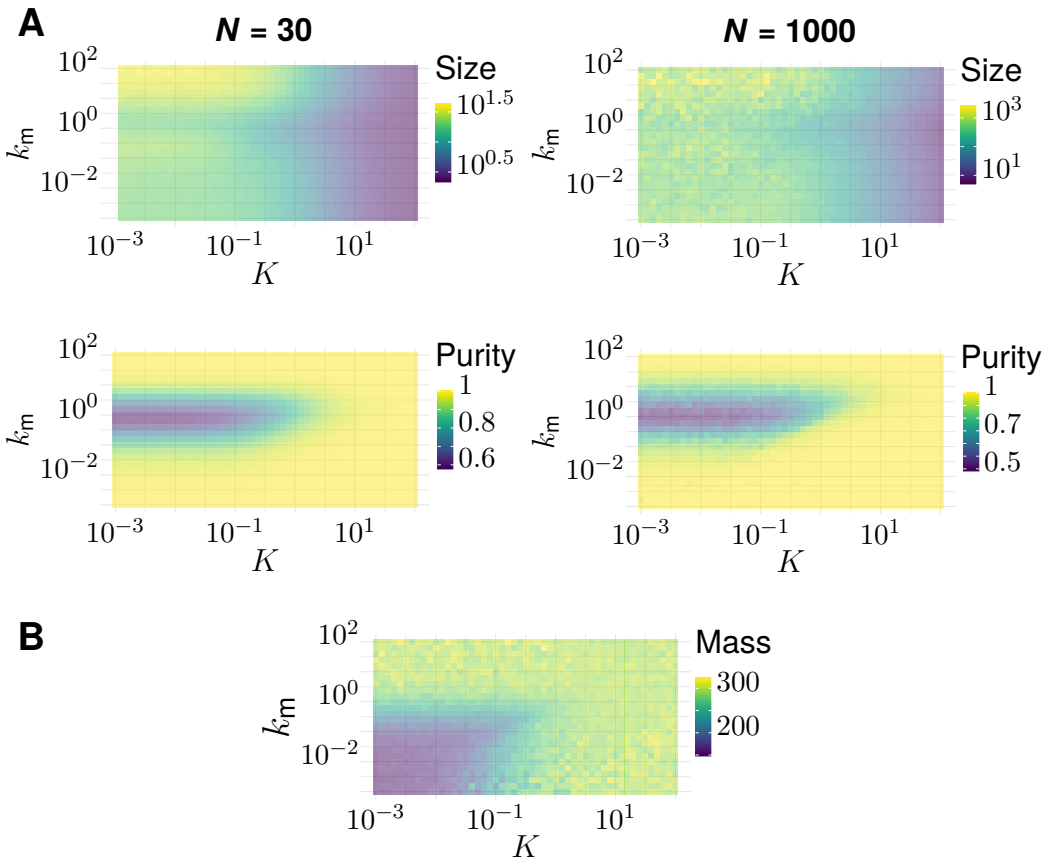

Fig. 3.5: Link between the Golgi's total mass and its steady-state organization. A. Size dependence of the Golgi's steady-state organization (to be compared with Fig.3.2 in the Main results section). We look at two different systems that only differ in term of the average total mass N, that equals 30 or 1000. Typical size of compartments and average system purity are shown as a function of k_m and K. In both cases $\alpha = 1$ (see previous chapter, Sec.2.8.1). **B**. Average steady-state total mass N, as a function of k_m and K, for simulation in which the influx is set to have $N \simeq 300$ (see equation Eq.2.7 of previous Chapter Sec.2.8.1, p.33).

Transport of passive cargo

The direction of vesicular transport is assessed by following the transport of passive cargo injected from the ER as part of incoming *cis*-vesicles. The cargo used in this chapter are passive cargo. These molecules are passive in the sense that their probability of joining a vesicle is insensitive to the vesicle membrane identity: when a compartment of size n buds a vesicle, each cargo in this compartment has a probability $1/n$ to join the budding vesicle. In the simulation, the number of cargo molecules in the system is kept to a fixed number (typically 20) by injecting a new one each time one leaves the system trough fusion with the boundaries.

3.3.2 Quantification to characterize the system

Computation of the purity

The purity of a compartment P is defined such that its value is 0 for a perfectly mixed compartment containing the same amount of *cis*, *medial*, and *trans*-species, and it is equal to 1 for a pure compartment containing a single species. With ϕ_i the fraction of the species i in the compartment, the purity P is defined as:

$$P = \sqrt{\frac{3}{2}\sum_i (\phi_i - 1/3)^2} \tag{3.1}$$

On a triangular composition space where each corner corresponds to a pure compartment, P is the distance from the center of the triangle, see Fig.3.1 – Main results section. When we show snapshots of the system, each compartment is represented as a sphere whose area is proportional to the compartment size (defined as an equivalent number of vesicles). A compartment's composition is represented as a color following the color code shown in Fig.3.1. The system's purity is a global average (over time and over all compartments) of the purity of individual compartments, weighted by their sizes and ignoring vesicles (that are always pure as they are composed of one unique identity).

Computation of the typical size

Among other mechanisms, this theoretical organelle self-organizes by budding and fusion of components. In that sense, it is a scission-aggregation structure which should follow the laws dictating the behavior of this class of systems. As the fusion kernel allows fusion between all compartments, one of these laws is the fact that the size distribution for small compartments should follow a power-law. Because of the scission, compartments cannot grow indefinitely and the power-law ends by an exponential cutoff [TSS05; VTS15]. Thus, the size distribution c_n of compartments of size n should, on a first approximation, follow this general formulation:

$$c_n \sim \text{Const}\; n^{-\beta} \exp\left(-\frac{n}{n_c}\right) \tag{3.2}$$

where n_c is the cut-off size and β is an exponent that has been calculated to be $\beta = 3/2$ in a similar system [TSS05]. There are multiple ways to characterize the average size of the distribution, using ratios of moments $k+1$ over k of the distribution:

$$\langle n \rangle_k \equiv \frac{\sum_{n=1}^{\infty} n^{k+1} c_n}{\sum_{n=1}^{\infty} n^k c_n} \tag{3.3}$$

It turns out that for $n_c \gg 1$, $\sum_{n=1}^{\infty} n^{k-\beta} e^{-n/n_c} \sim 1$ if $1+k-\beta < 0$ and $\sum_{n=1}^{\infty} n^{k-\beta} e^{-n/n_c} \sim n_c^{1+k-\beta}$ if $1+k-\beta > 0$. In order to have $\langle n \rangle_k \sim n_c$, we need to choose the exponent k such that $k > \beta - 1 = 1/2$ in the present case. In the Main results section, we adopt $k = 1$ and define the characteristic size of the distribution as:

$$\langle n \rangle \equiv \frac{\sum_{n=1}^{\infty} n^2 c_n}{\sum_{n=1}^{\infty} n c_n} \xrightarrow[n_c \gg 1]{} \frac{n_c}{2} \tag{3.4}$$

As shown in Fig.3.2A of the Main results section, the calculated average is in good agreement with simulations' data.

Computation of the mean enrichment

To discriminate between the two models of Golgi's dynamics that we can find in the literature, we need to quantify whether the vesicular transport is anterograde or retrograde. Indeed, the "Vesicular transport" model assumes that cargo is transported sequentially from *cis* to *medial* to *trans*-compartments while resident enzymes remain in place, meaning that the vesicular flux is anterograde. On the other hand, "Cisternal maturation" models assume that cargo remain inside cisternae, and resident enzymes are recycled, thus requiring a retrograde vesicular flux. One way to measure this flux in our simulations is to follow passive cargo molecules and quantify whether they move to more or less mature compartments, as they get carried by vesicles. To do so, we record all events that affect cargo molecules. Every time a compartment buds a cargo, we store the composition of this compartment and compare it to the one in which the vesicle later fuses. Both compositions are a vector $\vec{C}$, with three components that are the fraction ϕ_i (i equals *cis*, *medial* and *trans*) of the donor and acceptor compartments. Defining $\vec{C_d}$ the composition of the donor compartment, and $\vec{C_a}$ the composition of the acceptor, we can compute the enrichment $\vec{E}$ as:

$$\vec{E} = \vec{C_a} - \vec{C_d} \tag{3.5}$$

The sum of $\vec{C_a}$ (or $\vec{C_b}$) components equals 1 (as they are fractions of each identity), and the sum of $\vec{E}$ components equals $\vec{0}$, which simply means one cannot gain in fraction of any identity without losing the same amount of the others. We can now compute $\langle \vec{E} \rangle$ to calculate the mean enrichment in *cis*, *medial* and *trans*-species, between a budding event and the next fusion event.

However, and because of back fusion events (fusion into the same compartment that previously budded the vesicle), $\langle \vec{E} \rangle$ components can be close to 0. This is particularly true for pure, sorted systems. In that case, a budded vesicle has the same identity as its donor compartment, and thus has a great probability to fuse

back with the same compartment or one of very similar composition. That is why, non-treated data do not allow discriminating well between an anterograde and a retrograde regime when the purity (and thus K) is high (Fig.3.7A - Sec.3.3.4, p.54). As we are primarily interested in the sign of these vectors' components, we normalize $\vec{E}$ using the L_1 norm ($\sum_i |E_i| = 1$).

Computation of the vesicular flux vector field

The vesicular flux discussed in the previous section can be directly displayed on the triangle of composition we introduced in Fig.3.1. Instead of computing $\langle \vec{E} \rangle$ for all $\vec{E}$, we can bin data with respect to the donor compartment composition (typically triangular bins of size $\Delta\phi = 0.1$) and calculate the average enrichment for each bin of donor compartments. To get rid of back fusion effects in this quantification, we remove the vectors $\vec{E}$ for which all components are smaller (in absolute values) than the binning mesh-grid. For each binned composition we can now compute the mean enrichment vector, and plot this vector on the 2D triangular composition space. To emphasize the dominant fluxes in this vector field, the opacity of vectors is set proportionally to the flux of transported cargo per unit time (normalized by the total amount of cargo in the system). This can be seen on Fig.3.4 – Main results section.

3.3.3 Detailed characterization of the steady-state composition

The fluctuations of the system around its steady-state are characterized by computing the temporal standard deviation of the system's total mass and purity, shown in Fig.3.6A-B. Fluctuations decrease as the budding rate K increases. This makes sense, as compartments are on average smaller for larger budding rate, so that the removal of a compartment by fusion with the boundaries has a smaller impact on the system's state. We note in Fig.3.6A, that the total mass of the system depends on the budding rate K, despite the fact that the influx J is varied according to Eq.2.7 – see Methods chapter – to limit variations of the system's size (model of the compartments' size derived in Sec.3.3.7). This is due to the fact that Eq.2.7 is valid only in the limit of pure compartments (large K). For smaller values of the budding rate, *medial*-compartments contaminated by *cis* and *trans*-species and may thus exit the system by fusing with the boundaries, which decreases the total mass for low K. For the regime we are interested in, namely $k_{\mathrm{m}} \sim \alpha \sim 1$, this phenomenon is practically negligible, but its impact on the average mass is more severe for lower k_{m} (see previous chapter, Sec.2.5.1 and Sec.2.8.1).

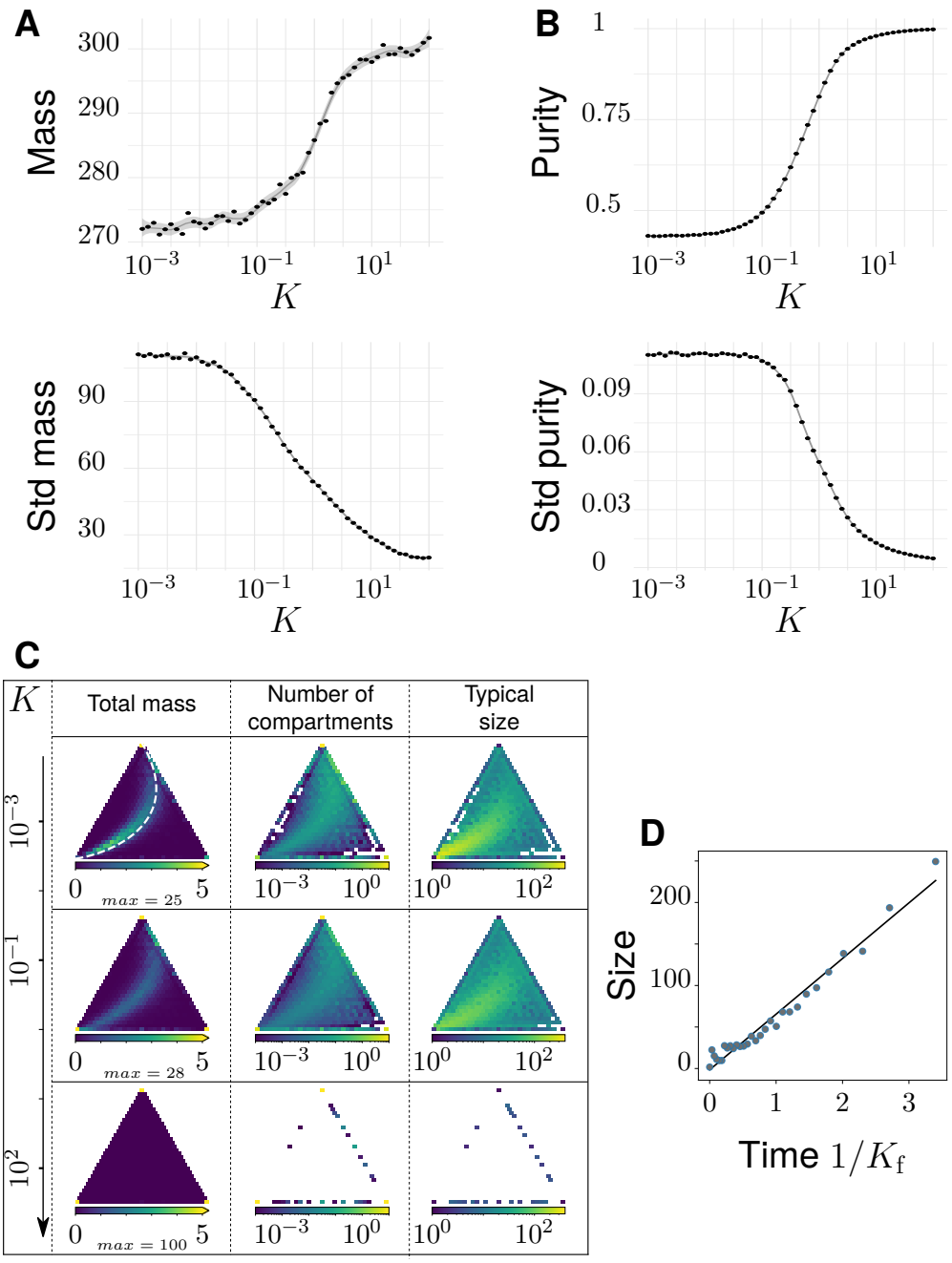

Fig. 3.6: Steady-state composition and fluctuation of compartments. Related to Fig.3.2 - Main results section. **A-B** Characterization of the system's temporal fluctuation as a function of the budding rate K. **A** average values of the system total mass (top panel) and standard deviation of the mass (bottom panel). **B** average values of the system purity (top panel) and standard deviation of the purity (bottom panel). **C** Distribution of the total mass, number of compartments and their average size, as a function of the compartments' composition, shown in a triangle plot (see Sec.3.3.2) for different values of the (normalized) budding rate K. The average size for a given composition is calculated as the average mass divided by the average number of compartments. Plots are shown for four different values of K, with $k_m = \alpha = 1$. The dashed white line on the top, left panel (low K regime) corresponds to the theoretical prediction of Eq.3.21 in Sec.3.3.7, p.67. **D** The evolution of the compartment's size as a function of time, in the low $K = 10^{-3}$ limit, agrees with the linear prediction of Eq.3.19.

We also characterize the variation of the compartments' size and abundance as a function of their composition. In the Main results section (Fig.3.4), variations of the total mass (number of membrane patches) and the number of compartments is shown as a function of their composition, in the composition triangular space defined in Sec.3.3.2, p.39. This is obtained by binning the composition space in such a way that the characterization is both relatively precise and statistically significant (binning ϕ with a mesh of $1/30$). The mass and number of compartments are averaged over the simulation time (once the steady-state is reached) for each composition bin. These results are reproduced in Fig.3.6C, where the average compartment's size, computed as the ratio of average mass over average number of compartments, is also shown.

For low values of the budding rate K, both the mass and the number of compartments follow the theoretical line obtained from the "cisternal maturation" limit (Eq.3.21, derived in Sec.3.3.7, p.67). Compartments also grow linearly in time, in agreement with Eq.3.19. Their sizes are shown in Fig.3.6D, as a function of their theoretical lifetime. The sizes are computed by measuring the average compartment size for each composition bin along the theoretical line. The compositions are then used to estimate the lifetime of compartments using Eq.3.21.

3.3.4 Detailed characterization of vesicular transport

Quantification of the back-fusion

In the Main results section, we discussed the importance of back-fusion when the budding rate K increases. To determine the likelihood of a vesicle to fuse back with the compartment it budded from, or a compartment of similar composition, we analyzed the trajectories of passive cargo.

Back fusion is defined as a vesicular transport event where the donor and acceptor compartments fall within the same composition bin. The fraction of the total vesicular flux leaving a compartment that undergoes back fusion is shown as a function of the compartment's composition in a triangular composition space in Fig.3.7A (top panel). As expected, back-fusion is dominant near the apexes of the composition triangle, where compartments are pure and mostly bud vesicles of identity similar to their own identity. These vesicles are very likely to fuse back with the donor compartment by homotypic fusion. The back fusion flux increases with the budding rate K, going from $\sim [90\%,\ 10\%,\ 20\%]$ for respectively [*cis*, *medial* and *trans*]-compartments when $K = 10^{-2}$, to $\sim 100\%$ when $K = 10^{2}$ for all compartments.

The mean enrichment (composition difference between donor and acceptor compartments) seen by a transport vesicle is plotted in the Main results section in a normalized fashion. Non-normalized enrichment is plotted in Fig.3.7A (bottom panel). The mean enrichment for all three identities vanishes when K is large. This is explained by the contribution of back fusion. When K is large, the compartments are very pure, and vesicles have a high probability to undergo back fusion, leading to a small value of the net enrichment.

Vesicular transport by composition

Fig.3.4 of the Main results section shows the average flux of vesicular transport as a vector field on the triangular composition phase space. The main conclusion is that the vesicular flux is retrograde (toward *cis*-compartments), when the compartments are mixed (low budding rate K), anterograde when the compartments are pure (high K), and centripetal (toward compartments of *medial*-identity) for intermediate budding rates. In the Main results section, only the total flux is described, which is the sum of the fluxes of vesicles of the three different identities. To better understand this net enrichment, the total flux can be dissected into the flux of *cis*, *medial* and *trans*-vesicles. These results are shown in Fig.3.7B.

For low budding rate ($K \ll 1$), compartments are mixed with all three identities, with a composition distributed around a trajectory given by Eq.3.21 (derived in Sec.3.3.7, p.67) and shown in Fig.3.6C. These mixed compartments emit vesicles of all identities. The *cis*-vesicles predominantly fuse with pure *cis*-compartments, which always exist at steady-state, since pure *cis*-vesicles are continuously being injected in the system. On the other hand, *medial* and *trans*-vesicles fuse with *cis/medial* and *cis/trans*-compartments, as pure *medial*-compartments are absent, and pure *trans*-compartments are few and transitory. In this limit, the net enrichment is completely dominated by the retrograde transport of *cis*-vesicles, and is positive in *cis*-identity and negative in *trans*-identity.

For intermediate budding rate ($K \sim 0.1 \to 1$), and as K increases, components can be efficiently sorted as they mature, since the budding and maturation rates are of the same order. Medial compartments are rather unstable, as they can fuse with both *cis*-rich and *trans*-rich compartments. Their reformation involves *medial* vesicles leaving *cis*-rich and *trans*-rich compartments to fuse with each other or small *medial*-rich compartments. Fig.3.7C, shows that this is the main contribution to the overall vesicular flux, thereby defining the centripetal net vesicular flux shown in Fig.3.4 – Main results section. Note that they primarily exit *trans*-compartments

for $K \sim 0.1$, and *cis*-compartments for $K \sim 1$, denoting a transition from retrograde to anterograde vesicular fluxes.

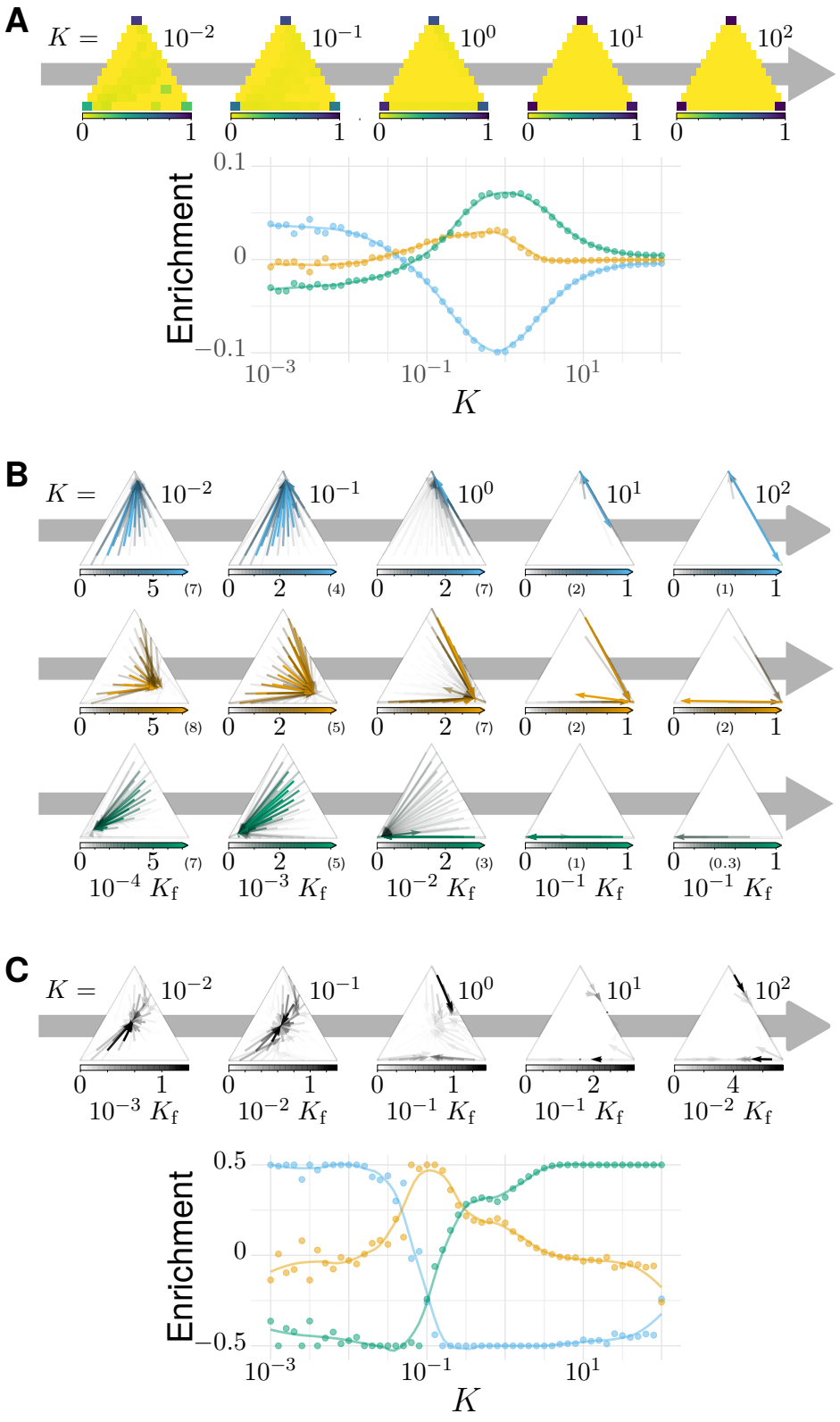

Fig. 3.7: Caption on next page.

Detailed characterizations of the vesicular transport. Related to Fig.3.3-3.4 – Main results section. $\alpha = k_{\mathrm{m}} = 1$ for all panels. **A** Characterization of vesicle back-fusion (fusion of vesicles with the same compartment or with a compartment of comparable composition). Top panel: fraction of vesicular flux undergoing back-fusion, as a function of the composition of the budding compartments, for different values of the budding rate K. Bottom panel: non-normalized enrichment in *cis* (blue), *medial* (orange) and *trans*-species (green) seen by a passive cargo, between a budding and the next fusion event, as a function of K. **B** Vesicular fluxes of *cis* (blue), *medial* (orange) and *trans* (green) vesicles for different values of the budding rate K. The base of each arrow gives the composition of the donor compartment and the tip gives the average composition of receiving compartments - ignoring back-fusion - as in Fig.3.4, Main results section. Arrows' opacity displays the normalized number of cargo (divided by the total number of cargo in the system) transported per unit time (normalized by the fusion rate). Scales are open to allow easier comparisons between species (max value in parenthesis). **C** Net vesicular flux, excluding vesicle maturation, for different values of the budding rate K. Top panel: vesicular flux is represented as a vector field as in Fig.3.4 – Main results section. Bottom panel: vesicular flux is represented as the enrichment between the donor and the acceptor compartment, excluding back-fusion, as in Fig.3.3 – Main results section.

For high budding rate ($K \gg 1$), compartments are very pure, and most budding events lead to vesicle back fusion from the donor compartment (Fig.3.7A). A new phenomenon can be observed, which is the anterograde transport of *cis* and *medial*-vesicles fusing with *medial* and *trans*-compartments, respectively. This is due to vesicle maturation *after* budding, as discussed below.

Role of vesicles maturation

The maturation of vesicles after their budding from an immature compartment has been presented as a mechanism to prevent back fusion with the donor compartment and to promote anterograde vesicular transport (see Discussion of chapter's results – Main results section). This mechanism is naturally included in our model, as vesicles have the same maturation rate than any membrane patch that belong to bigger compartments. One can notice on Fig.3.7B, that there is a major increase of the anterograde *cis*-to-*medial* and *medial*-to-*trans* vesicular fluxes between $K = 10$ and $K = 10^2$. This is due to the maturation of the vesicles *after* their budding. The budding vesicle has the same identity as the donor compartment, but undergoes maturation before undergoing back fusion and fuses with a more mature compartment.

Fig.3.7C, shows the net vesicular flux (for the same simulation as in the Main results section) ignoring the events where vesicles undergo maturation after their budding. The net vesicular flux vanishes in the vector field for high budding rates when these events are removed. We interpret this result considering dimers and trimers are dominant when K is large. Disregarding vesicle maturation, such compartments

emit as many immature vesicles fusing with immature compartments as mature vesicles fusing with mature compartments, yielding a vanishing net vesicular flux. However, this is not true for the net enrichment which still displays an anterograde signature of the vesicular transport. Indeed, the explanation of the vesicular transport considering the minority identity (see Discussion of chapter's results – Main results section) is still relevant in this regime; compartments larger than 3 vesicles can generate anterograde transport by budding patches of membrane that just underwent maturation. Consequently, the net enrichment displays the characteristics of an anterograde vesicular flux even in the absence of vesicle maturation.

3.3.5 Role of boundaries composition

Our system contains two boundaries: the *cis*-face (the ER) and the *trans*-face (the TGN). *cis*-vesicles are injected via the *cis*-face, and compartments may exit the system by fusing with either boundary. The way the different compartments fuse with the boundaries has a strong impact on their lifetime and average size. In the model, this is characterized by the parameter α, which represents the fraction of the boundary composed of species able to elicit homotypic fusion of Golgi's components, *i.e.* the fraction of *cis*-species in the ER and of *trans*-species in the TGN, and might be different for the two boundaries. In the Main results section, we focus on the case $\alpha = 1$ (arguably the maximum possible value) for both *cis* and *trans* boundaries. Here, we discuss the impact of this parameter on the structure of the steady-state, and we compare the results of simulations with the analytical model derived in Sec.3.3.7, p.62.

Decreasing this parameter has two major impacts on the steady-state organization: it decreases the maturation rate for which the steady-state fraction in *cis*, *medial* and *trans*-species are equal and it increases the residence time of compartments in the system. This increases their size, as they have more time to aggregate, and increases the system's fluctuations, as larger compartments have a stronger impact each time they exit or fuse together.

The impact of α on the fraction of *cis*, *medial* and *trans*-species in the system is rather straightforward if compartments are pure (see previous chapter, Sec.2.8.1). In this case, the exit flux can be exactly computed, and Eq.2.6 shows that the different species are in equal amount at steady-state when $k_{\mathrm{m}} = \alpha$. If $k_{\mathrm{m}} \gg \alpha$, the membrane patches have time to undergo maturation before exiting the system, which is then dominated by *trans*-species. The purity of the compartment is high, but this is a rather uninteresting limit as the system is dominated by a single species. If $k_{\mathrm{m}} \ll \alpha$, compartments are recycled out of the system before *trans*-membrane

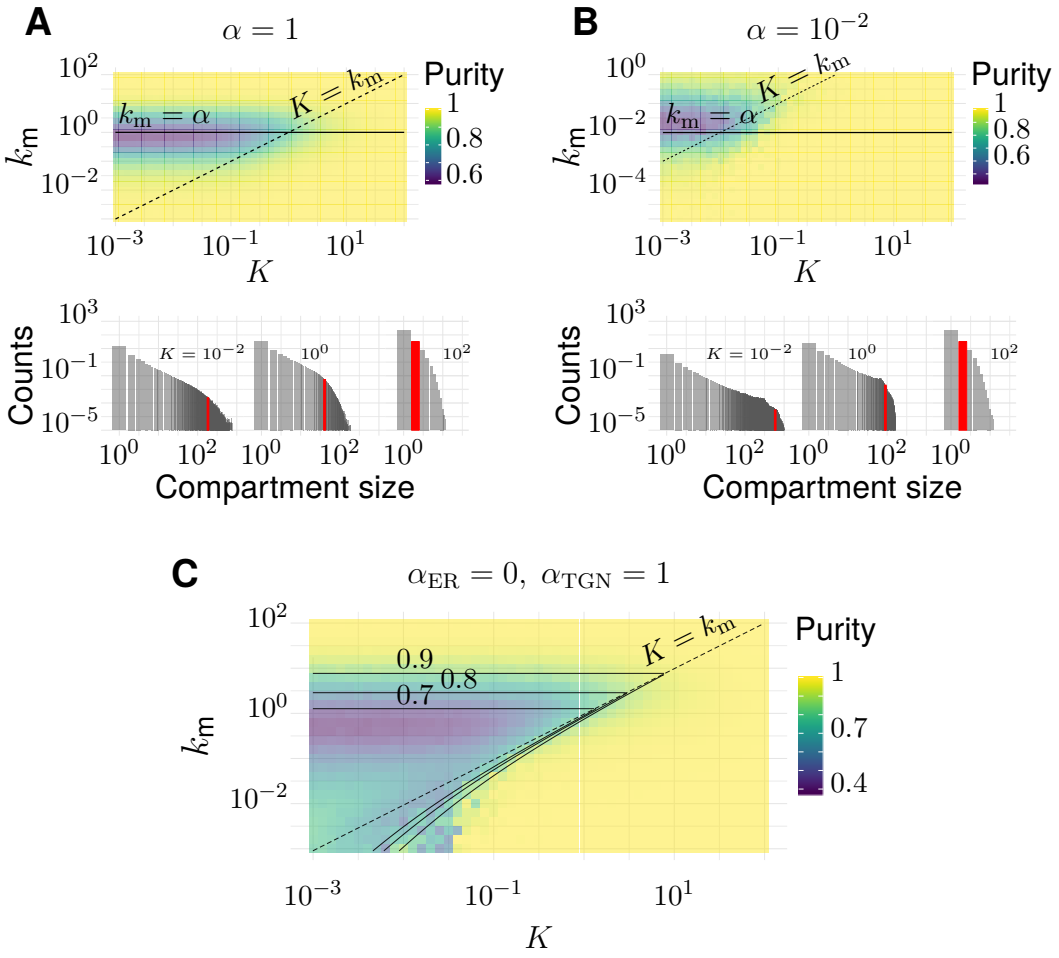

Fig. 3.8: Impact of the composition of the system's boundaries (ER and TGN) on the steady-state organization. Related to Fig.3.2 - Main results section. **A-B** The fraction α of active species driving homotypic fusion with the boundaries are identical for the ER and the TGN. **A** $\alpha = 1$ (same value as in the Main results section) **B** $\alpha = 10^{-2}$. For both cases, the top panel is the purity diagram as a function of the normalized maturation rate k_m and budding rate K. Dashed lines correspond to $k_m = K$ and solid lines to $k_m = \alpha$. For both cases, the bottom panel shows some examples of the size distribution for $k_m = \alpha$ and different values of K. **C** Purity diagram as a function of k_m and K when fusion with the ER is abolished: $\alpha_{ER} = 0$ whereas $\alpha_{TGN} = 1$. Solid lines are the predictions of the analytical model developed in Sec.3.3.7, p.62.

patches appear, and the system is dominated by *cis* and *medial*-species, which are of equal amount at steady state if the system is perfectly sorted.

The same conclusion can be reached in the slow budding regime when compartments are not pure. Let's consider a *cis*-rich compartment of size n contaminated by a fraction $\phi_{\textit{medial}}$ of *medial*-species, and let's disregard, for simplicity, budding and fusion with other compartments. The number of *medial*-patches increases by maturation with a flux $k_{\mathrm{m}} n(1-\phi_{\textit{medial}})$, and decreases by compartment fusion with the boundary, which removes all *medial*-patches with an average flux $\alpha(1-\phi_{\textit{medial}}) \times n\, \phi_{\textit{medial}}$. At steady-state, one thus expects $\phi_{\textit{medial}} \simeq k_{\mathrm{m}}/\alpha$, suggesting that the lowest purity will be observed for $k_{\mathrm{m}} \simeq \alpha$. The results of simulations, shown in Fig.3.8A-B, confirm this prediction.

The transition of purity occurs when sorting mechanisms become more efficient than mixing mechanisms. As a first approximation mixing occurs by maturation and sorting by budding, yielding the prediction that the purity transition occurs when $K \simeq k_{\mathrm{m}}$. Additional mixing mechanisms include the fusion of two slightly impure compartments of different compositions. Such slow events become relevant if compartments remain in the system for a long time, *i.e.* if fusion with the boundaries is slow (small values of α). In this case, the transition of purity occurs for $K > k_{\mathrm{m}}$. Phase diagram of the system's purity for a system where $\alpha = 10^{-2}$ can be found in Fig.3.8B. As expected the diagram is centered around $k_{\mathrm{m}} = \alpha$, with a transition of purity between $K \sim 10^{-2}$ and $K \sim 10^{-1}$ (and thus $K > k_{\mathrm{m}}$).

As it tunes the residing time of compartments in the system, α also impact the average compartment's sizes. Decreasing the value of α increases the residence time and leads to larger compartments, as predicted by Eq.3.7 (derived in Sec.3.3.7, p.62). Note however that for small budding rates, when compartments are mixed and their exit through the boundary is difficult to estimate, the size distribution deviates from the single-component ideal distribution.

The Golgi being a highly polarized organelle, it could be argued that the parameters controlling the fusion with the *cis* face (ER) and the *trans* face (TGN), α_{ER} and α_{TGN} could be different. An obvious way to reduce the retrograde exit of material from the ER is to reduce α_{ER}. To investigate the role of this asymmetry, we use an extreme regime of $\alpha_{\mathrm{ER}} = 0$ and $\alpha_{\mathrm{TGN}} = 1$. This prevents the recycling of impure compartments by fusion with the ER and broadens the low purity region of the parameter space, as shown in Fig.3.8C, and explained by the analytical model presented in Sec.3.3.7, p.62.

3.3.6 Other budding and fusion schemes

Linear budding

To verify whether the assumption of non-linear budding (the form of the budding function $f(\phi)$ presented in the previous chapter 2.4.3) has a strong impact on the results, we performed simulations with a linear budding mechanism ($f(\phi) = \phi$), for which the budding flux for a given identity is linear with the number of patch with this identity ($J_{\mathrm{b},i} = K_{\mathrm{b}} n \phi_i = K_{\mathrm{b}} n_i$). As shown in Fig.3.9A-B, the average compartment size and purity follow the trends discussed in the Main results section for non-linear budding case. However, the purity transition occurs for larger K, since the total budding flux is merely proportional to the compartment's size for linear budding, and is thus smaller than for non-linear budding, where it is proportional to the size times the number of species. Non-linear budding thus appears important to obtain systems that are at the same time well sorted, and with large compartments.

Even though the purity transition is shifted toward higher values of K, the link between purity and vesicular flux is qualitatively conserved (Fig.3.9C). For low purity, the system is retrograde with an enrichment in *cis*-species and a depletion of more mature species, and for high purity it is anterograde. However, the retrograde flux is less marked than with a non-linear budding rate (no clear depletion in *trans*-species). Indeed, efficient sorting relies on the capacity to export the minority component out of a compartment. Within the non-linear budding scheme, the rate of export is proportional to the compartment's size and does not depend on the number of minority components to export. Within the linear budding scheme however, it is proportional to the number of minority components. In the low K regime, *trans*-rich compartments are large. They emit a large vesicular flux of immature components within the non-linear budding scheme, but this flux is much smaller within the linear budding scheme. This explains the qualitative difference between the enrichment curves in the low K regime for the non-linear budding scheme (large depletion in *trans* identity – Fig.3.3 – Main results section) and the linear budding scheme (almost no change in *trans* identity – Fig.3.9C).

Non-fusing compartments

Fusion between compartments is an important ingredient of the model discussed in the Main results section. It could be argued that the fusion of large cisternae with one another could be a much slower process than fusion involving much smaller transport vesicles. We have performed simulations where fusion between compartments is

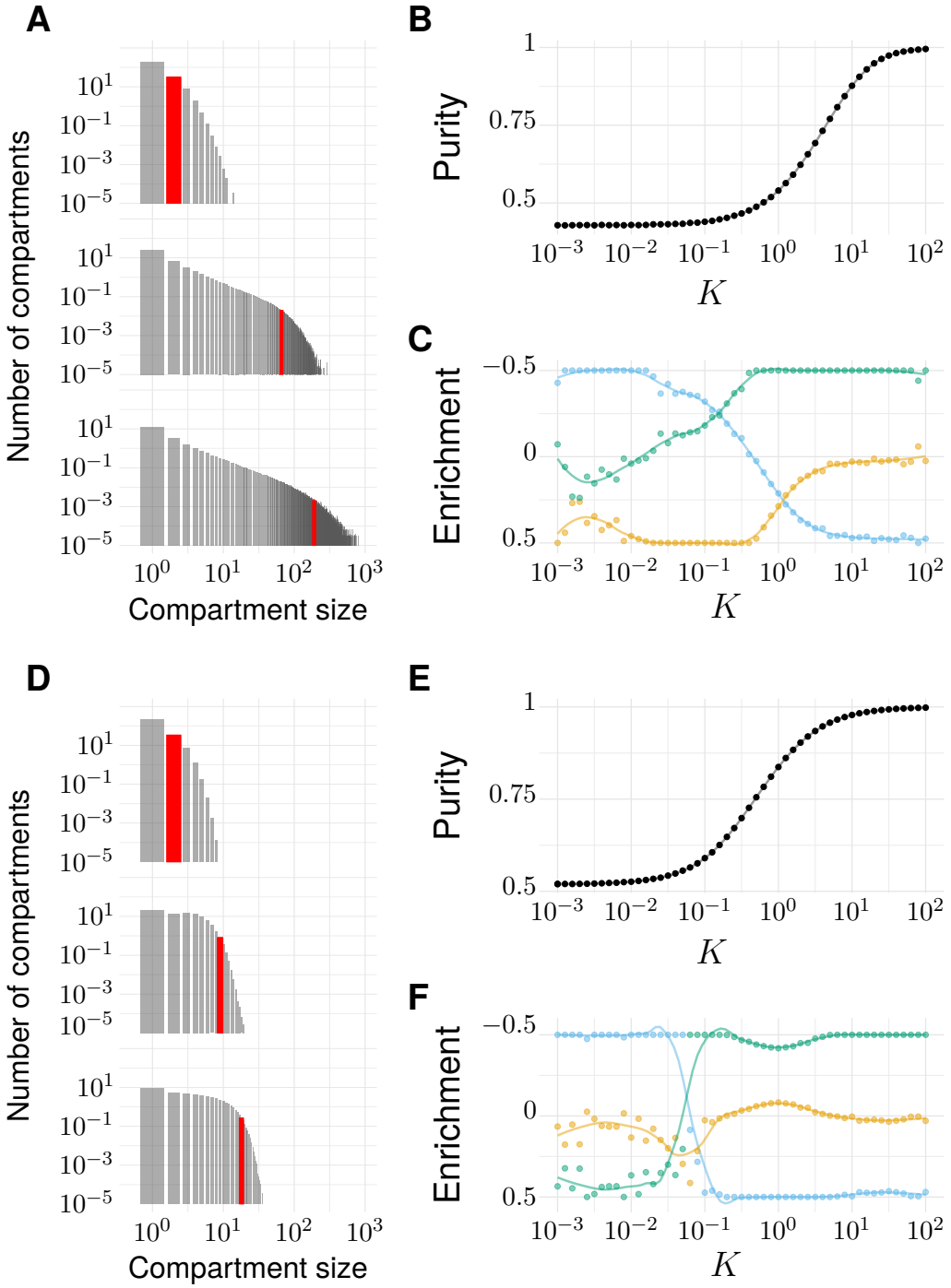

Fig. 3.9: Impact of different budding and fusion kernels on the systems organization and vesicular transport. Related to Fig.3.2-3.3-3.4 – Main results section. $k_{\mathrm{m}} = \alpha = 1$. **A-C** Linear budding scheme. **D-F** Inter-compartment fusion is prohibited. **A**, **D** Size distribution of compartment for K equals 10^{-2} (top), 1 (middle) and 10^{2} (bottom). **B**, **E** Steady-state purity as a function of K. **C**, **F** Enrichments in *cis* (blue), *medial* (orange) and *trans*-species (green) during vesicular transport (details of computations of this enrichment presented in Sec.3.3.2, p.49) as a function of K.

prohibited if both compartments are larger than a vesicle. Note that in the model, such compartments are still able to fuse with the boundaries, so that the system's composition can still be predicted from the results of previous chapter, Sec.2.8.1. The results of this model are shown in Fig.3.9D-F.

The size distribution of non-fusing compartment shows a broad peak, instead of the power-law seen in the case where compartments can fuse. As compartments can only grow by vesicle fusion and not by compartments' fusion, their size is smaller than in the previous case. The compartments size is results from a balance between the rate at which compartments are recycled (fuse with one boundary) and the rate at which they grow by vesicle fusion. Consequently, the size distribution only weakly depends on K, as compartments have very little time to fuse with vesicles before exiting the system (Fig.3.9D). The theoretical size distribution of compartments growing by vesicle fusion can be found in Sec.3.3.7, p.3.3.7.

As expected, and because we remove the possible interactions between compartments, the centripetal flux we observe between the previously described anterograde and retrograde is abolished. This is particularly visible if we plot the (normalized) mean enrichment in *cis*, *medial* and *trans*-species seen by cargo as they are transported via vesicular fluxes (Fig.3.9F). As before, the system goes from a purely retrograde flux, characterized by a depletion in *trans*-species and an enrichment in *cis*-species, to an anterograde flux, characterized by an enrichment in *trans*-species and a depletion in *cis*-species. However, the transitional centripetal regime we previously described, characterized by an enrichment in *medial*-species, vanishes. This suggests this particular regime is indeed resulting from the possible fusion between compartments, as it destabilizes *medial*-compartments that have a great probability to fuse with slightly impure *cis* or *trans*-compartments. Thus, the transport is anterograde as soon as the purity transition occurs (Fig.3.9E).

3.3.7 Analytical Models

The complexity of the system prohibits rigorous analytical calculation. Nevertheless, analytical results can be obtained for a number of interesting quantities provided some simplifying assumptions are made. We present below some of these derivations, that help to make sense of a number of the numerical results.

Typical size of compartments

In this section we derive a simple model to calculate the typical compartments' size as a function of the system's parameters. The goal is to get an indicator that is easy to manipulate, for which we do not need to compute the total size distribution.

Eq.2.6, from previous chapter, allows to calculate the total amount of *cis*, *medial* and *trans*-species in a sorted system. To calculate the typical size of compartments, we assume that there is a single large compartment for each species, of size n, that coexists with a number n_{v} of vesicles of the same identity. The compartment's size satisfies:

$$\frac{\partial n}{\partial t} = n_{\mathrm{v}} - Kn \quad \xrightarrow[\text{steady state}]{} \quad \frac{n}{n+n_{\mathrm{v}}} = \frac{1}{1+K} \tag{3.6}$$

With K the budding rate normalized by the fusion rate. Using Eq.2.7, we can compute the maximum size of compartments of each identity n_{cis}, n_{medial} and n_{trans} as a function of the system's size N:

$$\begin{aligned} n_{cis} &= \frac{N_{cis}}{1+K} = \frac{N}{1+K}\frac{\alpha_{\mathrm{TGN}}}{2\alpha_{\mathrm{TGN}}+k_{\mathrm{m}}} \\ n_{medial} &= \frac{N_{medial}}{1+K} = \frac{N}{1+K}\frac{\alpha_{\mathrm{TGN}}}{2\alpha_{\mathrm{TGN}}+k_{\mathrm{m}}} \\ n_{trans} &= \frac{N_{trans}}{1+K} = \frac{N}{1+K}\frac{k_{\mathrm{m}}}{2\alpha_{\mathrm{TGN}}+k_{\mathrm{m}}} \end{aligned} \tag{3.7}$$

For a given set of parameters, the maximum between n_{cis}, n_{medial} and n_{trans} is a good indicator of the characteristic compartment's size, as can be seen from the fit of the phase diagram in Fig.3.2B – Main results section.

Steady-state purity of compartments

We want to build a simple model to explain how the system's purity is affected by the parameters. This is challenging as all events (budding, fusion and maturation) influence the purity of a compartment. We seek to determine the purity transition, namely the values of K and k_{m} for which a pure system becomes impure.

We make the following approximations, based on the assumption that the system is almost pure: *(i) trans*-compartments are pure as they cannot be contaminated by maturation. *(ii) cis* and *medial*-compartments share the same purity. *(iii)* The total amount of the different species N_{cis}, N_{medial} and N_{trans} follows the steady-state repartition of *cis*, *medial* and *trans*-species in a pure limit, given by Eq.2.6. Most of this mass is within compartments.

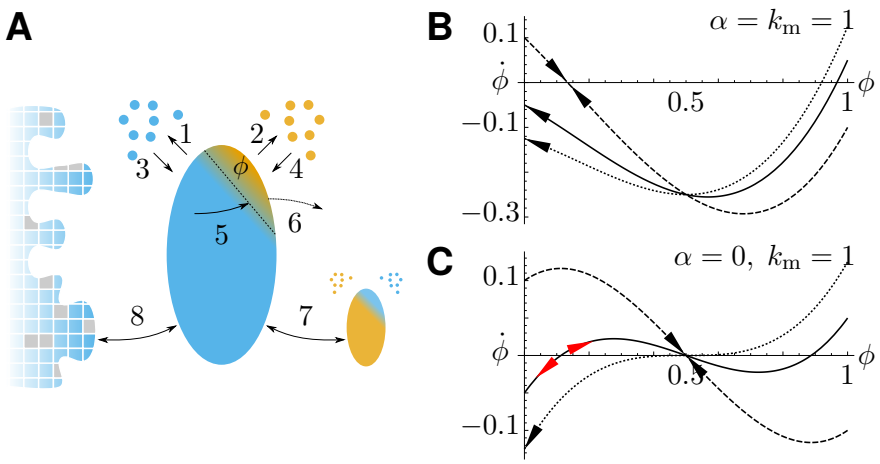

Fig. 3.10: Analytical description of the *cis*-compartment purity. Related to Fig.3.2 - Main results section. **A**. Analytical model of the steady-state contamination by a *medial*-species (orange) of a *cis*-compartment (blue). The fraction occupied by the *medial*-species is named ϕ. The eight events ((1)-(8)) impacting ϕ are listed in the text. **B-C**. Time variation $\dot{\phi}$ as a function of ϕ, with $k_m = 1$ and for different K (0.9 dashed line, 1.05 plain line, and $1 + 1/8$ doted line). ϕ has a stable value when $\partial_\phi \dot{\phi} < 0$ and $\dot{\phi} = 0$ or $\dot{\phi}|_{\phi=0} < 0$ (black arrows). It is potentially unstable when $\partial_\phi \dot{\phi} > 0$ and $\dot{\phi}_{\phi\sim 0} = 0$ (red arrows). **B**. For $\boldsymbol{\alpha = 1}$: $K = 0.9$ (dashed) exhibits a stable fixed-point for $\phi > 0$ but with $\phi < 1/2$ as $\alpha > 0$; $K = 1.05$ (plain) and $K = 1 + 1/8$ (dotted) exhibit a stable concentration for $\phi = 0$. **C**. For $\boldsymbol{\alpha = 0}$: $K = 0.9$ (dashed) exhibits a stable fixed-point for $\phi = 1/2$; $K = 1.05$ (plain) exhibits an unstable fixed-point near $\phi = 0$; $K = 1 + 1/8$ (dotted) does not display this unstable fixed-point as $K \geq k_m + 1/8$ (see text).

The purity of a compartment – defined in the Main results section – is:

$$P = \sqrt{\left(3/2 \sum_i (\phi_i - 1/3)^2\right)}$$

We consider that *cis*-compartments (*medial*-compartments) are contaminated by an average fraction $\langle\phi\rangle \ll 1$ of *medial*-patches (*trans*-patches), while *trans*-compartments are pure. The purity of *cis* and *medial*-compartments is thus:

$$P_{\textit{cis, medial}} = \sqrt{1 - 3\langle\phi\rangle(1 - \langle\phi\rangle)} \text{ and } P_{\textit{trans}} = 1$$

Weighting these with the fraction of the different species in the system (from Eq.2.6) gives

$$\langle P\rangle = \frac{2\alpha_{\mathrm{TGN}}\sqrt{1 - 3\langle\phi\rangle(1 - \langle\phi\rangle)} + k_m}{2\alpha_{\mathrm{TGN}} + k_m} \tag{3.8}$$

To compute the average contamination $\langle\phi\rangle$, we consider the different events that affect the purity of a *cis*-compartment of size n contaminated by a fraction ϕ of *medial*-patches, surrounded by a number n_v of *cis*-vesicles, and a number n'_v of *medial*-vesicles. These events are sketched in Fig.3.10 and listed below:

1. Budding of *cis*-patches (increases ϕ)
2. Budding of *medial*-patches (decreases ϕ)
3. Fusion of *cis*-vesicles (decreases ϕ)
4. Fusion of *medial*-vesicles (increases ϕ)
5. Maturation of *cis*-patches (increases ϕ)
6. Maturation of *medial*-patches (decreases ϕ)
7. Fusion with a *medial*-compartment ($\phi \to \frac{1}{2}$)
8. Fusion with the ER ($\phi \to 0$)

The rate $p(i)$ (normalized by the fusion rate) for each mechanism, and the extent $\delta\phi$ to which it affects ϕ, are:

$$p(1) = nK\ , \qquad \delta\phi(1) = \frac{n\phi}{n-1} - \phi\ ; \qquad p(2) = nK\ , \qquad \delta\phi(2) = \frac{n\phi - 1}{n-1} - \phi$$
$$p(3) = n_{\rm v}(1-\phi)\ , \qquad \delta\phi(3) = \frac{n\phi}{n+1} - \phi\ ; \qquad p(4) = n'_{\rm v}\phi\ , \qquad \delta\phi(4) = \frac{n\phi + 1}{n+1} - \phi$$
$$p(5) = n(1-\phi)k_{\rm m}\ , \qquad \delta\phi(5) = \frac{1}{n}\ ; \qquad p(6) = n\phi k_{\rm m}\ , \qquad \delta\phi(6) = -\frac{1}{n}$$
$$p(7) = \phi(1-\phi)\ , \qquad \delta\phi(7) = \frac{1}{2} - \phi\ ; \qquad p(8) = \alpha(1-\phi)\ , \qquad \delta\phi(8) = -\phi$$

We can now compute the temporal variation of ϕ: $\dot{\phi} = \sum p(i)\delta\phi(i)$. We concentrate on the limit of large compartments: $n \gg 1$. For simplicity, we also assume that $n \gg (n_{\rm v} - n'_{\rm v})$, so that the net contribution of vesicle fusion to the purity variation, which scales like $(n'_{\rm v} - n_{\rm v})/n$, is negligible. Neglecting stochastic fluctuations, the mean-field evolution of the fraction of contaminating species is:

$$\dot{\phi} = (k_{\rm m} - K)(1 - 2\phi) + \phi(1-\phi)(1/2 - \phi - \alpha) \tag{3.9}$$

Below, we discuss separately the case where $\alpha = 1$ (fast fusion with the ER boundary – discussed in the Main results section), and the case where $\alpha = 0$ (no exit through the ER – discussed in Sec.3.3.5, p.56).

• $\alpha = 1$. A pure compartment; $\phi = 0$, is stable ($\dot{\phi}|_{\phi=0} < 0$) when $k_{\rm m} < K$. If $k_{\rm m} > K$, the compartment is contaminated by a stable fraction of *medial*-patches given by the single stable root of Eq.3.9 (see Fig.3.10B). The purity transition lines shown in Fig.3.2C of the Main results section are obtained by inserting this root in Eq.3.8.

• $\alpha = 0$. If $K < k_{\rm m}$, the single root of Eq.3.9 is for $\phi = 1/2$ and is stable. The system is always impure with mixed *cis-medial* compartments. If $K > k_{\rm m}$, pure compartments ($\phi = 0$) are stable at the mean-field level, but there exist an unstable fixed point for small values of ϕ. Stochastic fluctuations may bring the system passed the unstable fixed point toward the stable mixed solution $\phi = 1/2$. For $K > k_{\rm m} + \frac{1}{8}$,

$\phi = 1/2$ is an unstable fixed point and the only stable solution is for $\phi = 0$ (see Fig.3.10C). The purity transition is thus with the range $k_{\rm m} < K < k_{\rm m} + \frac{1}{8}$.

A more precise characterization of the transition in the case $K > k_{\rm m}$ requires including stochastic effects. The different stochastic events are associated to very different fluctuations amplitudes. Budding and fusion of vesicles and maturation of membrane patches represent small fluctuations for a large compartment, while fusion between compartments and with the boundaries represent a very large alteration of the purity. In what follows, we propose a simplified treatment of this process, focusing on the case $\alpha = 0$ for simplicity, and neglecting the contribution of vesicle fusion as discussed above. For a compartment of size n contaminated by $n_{\textit{medial}}$ patches, we identify 2 types of mechanisms (depending on their amplitude). First, a smooth drift in the contamination due to maturation (with a rate $k_{\rm m}(n - n_{\textit{medial}})$) and budding (with a rate Kn). Second, a jump in the contamination due to fusion with the neighbor compartment (rate $n_{\textit{medial}}(n - n_{\textit{medial}})/n^2$). We compute below the mean contamination, assuming that the *cis*-compartment spends a time $\tau_{\rm conta}$ undergoing small fluctuations $\delta\phi \simeq 0$ close to the pure state, before fusing with a *medial*-compartment of composition $1 - \delta\phi$. The resulting compartment with $\phi \simeq 1/2$ then spends a time $\tau_{\rm deconta}$ undergoing a decontamination process, which depends on the balance between budding and maturation.

We first calculate the average value $\delta\phi$ of the contamination around $\phi = 0$ due to maturation and budding, disregarding inter-compartment fusion. The probability $\mathbb{P}(n_{\textit{medial}})$ of finding $n_{\textit{medial}}$ in the cisterna satisfies:

$$\begin{aligned}\dot{\mathbb{P}}(n_{\textit{medial}}) = &- \mathbb{P}(n_{\textit{medial}})(k_{\rm m}(n - n_{\textit{medial}}) + K \times n) \\ &+ \mathbb{P}(n_{\textit{medial}} - 1)\ k_{\rm m}(n - n_{\textit{medial}} + 1) \\ &+ \mathbb{P}(n_{\textit{medial}} + 1)K \times n\end{aligned} \tag{3.10}$$

In the limit $n \gg n_{\textit{medial}}$, this becomes:

$$\dot{\mathbb{P}}(n_{\textit{medial}})/n = -\mathbb{P}(n_{\textit{medial}})(k_{\rm m} + K) + \mathbb{P}(n_{\textit{medial}} - 1)k_{\rm m} + \mathbb{P}(n_{\textit{medial}} + 1)K \tag{3.11}$$

The steady-state solution is

$$\mathbb{P}(n_{\textit{medial}}) = (k_{\rm m}/K)^{(n_{\textit{medial}})} / \sum_{i=0}^{n/2} (k_{\rm m}/K)^i = \frac{(K - k_{\rm m})(k_{\rm m}/K)^{(n_{\textit{medial}})}}{K - k_{\rm m}(k_{\rm m}/K)^{n/2}} \tag{3.12}$$

and the average contamination $\delta\phi$ due to budding and maturation is:

$$\delta\phi = \sum_{i=0}^{n/2} \frac{i}{n} \times \mathbb{P}(i) \simeq \frac{k_{\rm m}}{n(K - k_{\rm m})}, \text{ (for } K > k_{\rm m}) \tag{3.13}$$

These fluctuations in composition allow fusion between compartments, at a rate $\delta\phi(1-\delta\phi) \simeq \delta\phi$ (for $\delta\phi \ll 1$). The average waiting time for an inter-compartment fusion event is thus $\tau_{\text{conta}} = 1/\delta\phi$.

After inter-compartment fusion, the compartment is at $\phi = 1/2$, which is an unstable fixed point according to Eq.3.9. Any small fluctuation in composition leads to a smooth decontamination that satisfies $\dot{\phi} = (k_{\text{m}} - K)(1-2\phi)$, disregarding inter-compartment fusion. The decontamination time τ_{deconta} and the average contamination during the process $\langle\phi\rangle_{\text{deconta}}$, can be estimated by integrating $\dot{\phi}$, from $\phi = 1/2 - 1/n$ to $\phi = 0$:

$$\tau_{\text{deconta}} = \frac{\log(n/2)}{2(K-k_{\text{m}})}, \quad \langle\phi\rangle_{\text{deconta}} = \frac{2 + n\left[\log(n/2) - 1\right]}{2n\log(n/2)} \tag{3.14}$$

We can now calculate $\langle\phi\rangle$ as a temporal average of ϕ:

$$\langle\phi\rangle = \frac{\tau_{\text{conta}} \times \delta\phi + \tau_{\text{deconta}} \times \langle\phi\rangle_{\text{deconta}}}{\tau_{\text{conta}} + \tau_{\text{deconta}}} \tag{3.15}$$

When $\log(n/2)$ is close to 1 (typically true for the range of n that is interesting here, $n \sim 100$), $\langle\phi\rangle$ can be simplified to:

$$\langle\phi\rangle \simeq \frac{k_{\text{m}} + 2k_{\text{m}}(K-k_{\text{m}})}{2k_{\text{m}} + 2n(K-k_{\text{m}})^2} \tag{3.16}$$

Injecting this result into Eq.3.8 gives the approximate purity boundary for $\alpha_{ER} = 0$:

$$\langle P\rangle \simeq 1 - \frac{3\alpha_{\text{TGN}}}{2\alpha_{\text{TGN}} + k_{\text{m}}} \frac{k_{\text{m}} + 2k_{\text{m}}(K-k_{\text{m}})}{2k_{\text{m}} + 2n(K-k_{\text{m}})^2} \tag{3.17}$$

Despite numerous simplifications, the model gives good predictions on the purity, both for $\alpha_{\text{ER}} = \alpha_{\text{TGN}} = 1$ (Fig.3.2 - Main results section) and for $\alpha_{\text{ER}} = 0$, $\alpha_{\text{TGN}} = 1$ (Fig.3.8 – Sec.3.3.5, p.57). Depending on the normalized maturation rate k_{m}, we can discriminate three regions in the purity phase diagram:

- $k_{\text{m}} \gg 1$, the system is saturated in *trans*-species and is thus always pure.
- $k_{\text{m}} \sim 1$, compartment's contamination occurs by maturation, matured species are sorted by budding. The purity transition occurs for $K \simeq k_{\text{m}}$ (impure system if $K < k_m$).
- $k_{\text{m}} \ll 1$, the system is saturated by *cis* and *medial*-compartments, and the transition of purity occurs for $K \ll 1$: the fusion rate is dominant in this regime. Thus, interaction with the boundaries or other compartments are crucial to understand the transition of purity. For $\alpha_{\text{ER}} = 1$, fusion with the ER decontaminates the system, thus the transition occurs for $K < k_{\text{m}}$. The

transition becomes independent of K for very small maturation rates, where the system is saturated in *cis*-species. For $\alpha_{\mathrm{ER}} = 0$, purifying the system by recycling compartments is not possible, and inter-compartment fusion decreases the purity, thus the transition of purity requires large values of the budding rate $K > k_{\mathrm{m}}$, as given by Eq.3.17.

Compartments composition in the "cisternal maturation" regime

For low values of the budding rate K, the system is in the "cisternal maturation" regime and vesicular transport is retrograde. The compartment distribution is spread around a path going from purely *cis* to purely *trans*-compartments in the triangular composition phase space (see top-left panel of Fig.3.4 in the Main results section or Fig.3.6C – Sec.3.3.3). To make sense of this distribution, we consider a simple system where a compartment, undergoing biochemical maturation, grows by fusion from a constant pool of vesicles containing the same number n_{v} of vesicle for all three identities. Calling $n_{cis}(t)$, $n_{medial}(t)$ and $n_{trans}(t)$ the amount of components of the three identities in the compartment (of total size $n(t) = \sum n_i$, for i equals *cis*, *medial*, *trans*), and neglecting vesicle budding (small budding rate) the mean-field equation satisfied by these quantities are:

$$\begin{aligned}
\partial_t n_{cis} &= n_{\mathrm{v}} \frac{n_{cis}}{n} - k_{\mathrm{m}} n_{cis} \\
\partial_t n_{medial} &= n_{\mathrm{v}} \frac{n_{medial}}{n} + k_{\mathrm{m}} (n_{cis} - n_{medial}) \\
\partial_t n_{trans} &= n_{\mathrm{v}} \frac{n_{trans}}{n} + k_{\mathrm{m}} n_{medial}
\end{aligned} \tag{3.18}$$

starting with a vesicle of *cis* for $t = 0$: $n_{cis}(0) = 1$, $n_{medial}(0) = n_{trans}(0) = 0$. The compartment's size evolves linearly with time:

$$n(t) = 1 + n_{\mathrm{v}} t \tag{3.19}$$

and the composition of each species satisfies:

$$\begin{aligned}
n_{cis}(t) &= (1 + n_{\mathrm{v}} t) e^{-k_{\mathrm{m}} t} \\
n_{medial}(t) &= (1 + n_{\mathrm{v}} t) k_{\mathrm{m}} t \; e^{-k_{\mathrm{m}} t} \\
n_{trans}(t) &= (1 + n_{\mathrm{v}} t) \left(1 - (1 + k_{\mathrm{m}} t) e^{-k_{\mathrm{m}} t} \right)
\end{aligned} \tag{3.20}$$

The fraction of each species in the compartment is thus independent on n_{v}, and reads:

$$\phi_{cis}(t) = e^{-k_{\mathrm{m}} t} \; , \; \phi_{medial}(t) = k_{\mathrm{m}} t \; e^{-k_{\mathrm{m}} t} \; , \; \phi_{trans}(t) = \left(1 - (1 + k_{\mathrm{m}} t) e^{-k_{\mathrm{m}} t} \right) \tag{3.21}$$

The trajectory followed by such compartments in the composition phase space is in very good agreement with the distribution shown in Fig.3.4 of the Main results section (see also Fig.3.6D – Sec.3.3.3, p.51, where the average compartment size along this trajectory is shown to agree with Eq.3.19).

Size distribution of non fusing compartments

In Sec.3.3.6, we propose another kernel of fusion in which compartments cannot fuse together. The assumption used otherwise, is that everything can fuse with everything, and only local interactions based on compartments' composition tune this mechanism. But, one can argue that the fusion rate between large structures is much smaller than the one between compartments and vesicles. That is why we check in Sec.3.3.6 this assumption does not qualitatively change our understanding of the system. Better, it helps us in understanding the centripetal flux, we observed in the Main results section.

We however saw that the size distribution is dramatically changed in this regime of non-fusing compartments. To better understand why the power law – one could expect from a scission aggregation system – is abolished, we propose here a computation of this size distribution.

We consider compartment of a single identity, defined by their size i. We count n_i compartments of size i. Each compartment can fuse with a vesicle with a rate K_f – one unique identity. Each compartment of size $i \geqslant 2$ can bud a vesicle with a rate $i \times K_\mathrm{b}$. New vesicles are added with a rate K_i. Each vesicle can exit the system with a rate $\alpha \times K_\mathrm{f}$. Note that compartments cannot fuse with the exit, which is an important difference from the current implementation and results presented in Sec.3.3.6. We normalize the time by the fusion rate, leading to the same dimensionless rates K for budding, and J for influx we introduced in the Methods chapter.

For compartments of size 1, the number of these compartments n_1 follows:

$$\frac{\mathrm{d}n_1}{\mathrm{d}t} = J + 4Kn_2 + K\sum_{i=3}^{\infty} in_i - n_1(n_1-1) - \alpha n_1 - n_1\sum_{i=2}^{\infty} n_i \tag{3.22}$$

For compartments of size 2, n_2 follows:

$$\frac{\mathrm{d}n_2}{\mathrm{d}t} = \frac{n_1(n_1-1)}{2} + 3Kn_3 - 2Kn_2 - n_1n_2 \tag{3.23}$$

For compartments of size $i > 2$, n_i follows:

$$\frac{\mathrm{d}n_i}{\mathrm{d}t} = K(i+1)n_{i+1} + n_1 n_{i-1} - Kin_i - n_1 n_i \tag{3.24}$$

We use the method of generating functions [Wil14], and define $G(x)$:

$$G(x) = \sum_{i=1}^{\infty} n_i x^i \tag{3.25}$$

Which derivatives with respect to x is:

$$G'(x) = \frac{\mathrm{d}G(x)}{\mathrm{d}x} = \sum_{i=1}^{\infty} i n_i x^{i-1} \tag{3.26}$$

Which allows us to compute:

$$\begin{aligned}\sum_{i=1}^{\infty} \frac{\mathrm{d}n_i}{\mathrm{d}t} x^i = {} & G'(x)[K - Kx] + G(x)[n_1 x - n_1] \\ & + G'(1)Kx - G(1)n_1 x \\ & - x^2 \frac{n_1^2 + n_1}{2} \\ & + x\left(n_1 + n_1^2 + J - \alpha n_1\right) \\ & - Kn_1 = 0\end{aligned} \tag{3.27}$$

Which is true $\forall\ x,\ 0 \leqslant x \leqslant 1$. For $x = 1$ we get:

$$KG'(1) - n_1 G(1) = \frac{n_1 + n_1^2}{2} + \alpha n_1 - n_1 - J - n_1^2 + Kn_1 \tag{3.28}$$

Which allows us to compute $G(1)$:

$$G(1) = \frac{2KG'(1) + n_1^2 + n_1 - 2\alpha n_1 + 2J - 2Kn_1}{2n_1} \tag{3.29}$$

That we can now inject in the previous equation:

$$\begin{aligned}\sum_{i=1}^{\infty} \frac{\mathrm{d}n_i}{\mathrm{d}t} x^i = {} & G'(x)[K - Kx] + G(x)[n_1 x - n_1] \\ & - x^2 \frac{n_1^2 + n_1}{2} \\ & + x\left(n_1 K + n_1/2 + n_1^2/2\right) \\ & - Kn_1 \\ = {} & (1-x)\left(KG'(x) - n_1 G(x) + \frac{n_1 x}{2}(n_1 + 1) - Kn_1\right)\end{aligned} \tag{3.30}$$

For consistency, the results will need to obey the following constraints:

- We lost the dependency in J and α. Defining the system total mass N, we will have to verify the mass conservation:

$$\begin{aligned} \frac{\mathrm{d}N}{\mathrm{d}t} &= J - \alpha n_1 = 0 \\ \Rightarrow n_1 &= J/\alpha \end{aligned} \tag{3.31}$$

- We will also have to verify that the limit $x \to 1$ of the solution $G(x)$ satisfying Eq.3.30, will agree with the relationship Eq.3.29 between $G(1)$ and $G(1)$.

Solving Eq.3.30 for $x \neq 1$, and at steady-state $\sum_{i=1}^{\infty} \frac{\mathrm{d}n_i}{\mathrm{d}t} x^i = 0$ we get:

$$G(x) = C \exp\left(\frac{n_1 x}{K}\right) + \frac{K(n_1 - 1) + x n_1(n_1 + 1)}{2n_1} \tag{3.32}$$

As $G(0) = 0$, we compute:

$$C = \frac{K(n_1 - 1)}{2n_1} \tag{3.33}$$

And thus:

$$G(x) = \frac{\left(\exp\left(\frac{n_1 x}{K}\right) - 1\right) K(n_1 - 1) + x n_1(n_1 + 1)}{2n_1} \tag{3.34}$$

If we come back to the 2 problems we had, we can compute the limit of $G(x)$ and $G'(x)$ when $x = 1$:

$$G(1) = \frac{\left(\exp\left(\frac{n_1}{K}\right) - 1\right) K(n_1 - 1) + n_1(n_1 + 1)}{2n_1} \tag{3.35}$$

$$G'(1) = \frac{\exp\left(\frac{n_1}{K}\right) n_1(n_1 - 1) + n_1(n_1 + 1)}{2n_1} \tag{3.36}$$

Injected back in Eq.3.29, we find $n_1 = J/\alpha$: everything is consistent at this point.

We can now decompose the sum of $G(x)$ by order of i, remarking that $\exp(ax) = \sum_{i=0}^{\infty} \frac{(ax)^i}{i!}$. At the first order $i = 1$, we get $n_1 x = n_1 x$: n_1 will be our constant in the system. For higher orders, we get:

$$\begin{aligned} n_i &= \frac{(n_1 - 1)}{2} \frac{(n_1/K)^{i-1}}{i!} \\ &= \left(\frac{J}{\alpha K}\right)^{i-1} \frac{J/\alpha - 1}{2 \times i!} \end{aligned} \tag{3.37}$$

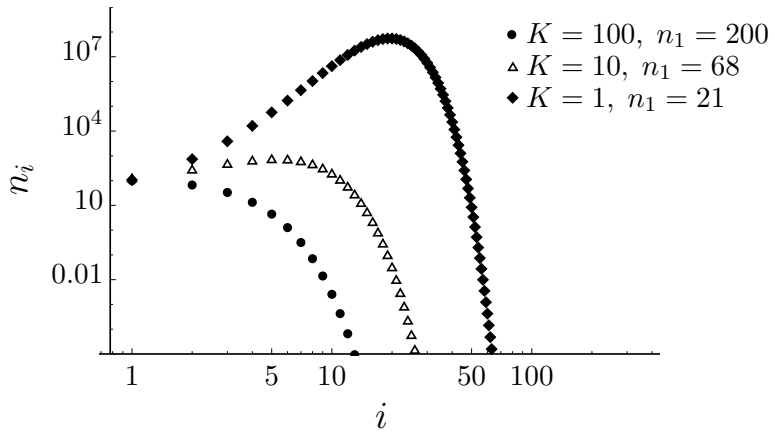

Fig. 3.11: Analytical size distribution in a non-fusing compartment kernel. The number of compartments n_i is plotted as a function of their size i, for different values of K larger than 1. Values of n_1 where taken from the simulation data.

One should bear in mind that this computation is not what we simulated in Sec.3.3.6. And big differences are expected, mainly because compartments can exit the system in the simulation, and not in this computation. Part of the mass in compartments never buds out these compartments, thus $n_1 = J/\alpha$ is expected not to be satisfied in all regimes:

- It should be satisfied in large K regimes (as everything is vesicular), and we indeed observe that $n_1 = 200$ for $K = 100$ and a total mass $N = 300$ – see Fig.3.9.

- It should not be satisfied in regimes of low K values, as other compartments can fuse with the boundaries, and thus the mass conservation does not simply rely on the entry and exit of vesicles. In this regime, n_1 should be smaller than J/α, which is the case in the simulations. Note however that we predict $n_i > 0,\ \forall i > 1$ only if $n_1 > 1$, which is observed in the simulations.

For very low K, we expect $(n_1/K)^{i-1}$ to grow faster that $i!$, that will then become larger for large i, and scale in i^i – Stirling's approximation. We thus expect a peak for $K < n_1$. This peak is not observed when compartments can fuse with the exit (Fig.3.9D) because compartments leave the system before getting big enough.

Allowing compartments to exit the system complicates a lot computations. As the aim of the current section was to verify results in Fig.3.9 were consistent with the fusion kernel change, we qualitatively compare this solution with simulation data. Plots of Eq.3.37 can be found in Fig.3.11. We see a qualitative resemblance with the size distribution of Fig.3.9D, despite the fact the current model does not describe the exact same system.

3.4 Discussion of chapter's results

The genesis and maintenance of complex membrane-bound organelles such as the Golgi apparatus rely on self-organization principles that are yet to be understood. The minimal model we presented in the Methods chapter allows a steady-state in which Golgi-like structures spontaneously emerge from the interplay between three basic mechanisms: the biochemical maturation of membrane components, the composition-dependent vesicular budding, and inter-compartment fusion. As our model does not include space, we do not refer to the spatial structure of a stacked Golgi, but rather to the self-organization of Golgi components into compartments of distinct identities undergoing vesicular exchange. Despite the absence of spatial information, we observe the emergence of directional vesicular exchanges between compartments of different identities. This suggests that spatial information is less crucial than biochemical ones, and is in line with observations that modifying the spatial structure of the Golgi preserves its functionality [Dun+17]. Our main result is that the steady-state organization of the organelle, in terms of size and composition of its compartments, is intimately linked to the directionality of vesicular exchange between compartments through the mechanism of homotypic fusion. Both aspects are controlled by a kinetic competition between vesicular exchange and biochemical maturation.

The results presented in Fig.3.2 can be used to explain a number of experimental observations. The predicted role of the budding and fusion rates is in agreement with the phenotype observed upon deletion of Arf1 (a protein involved in vesicle budding), which decreases the number of compartments and increases their size, particularly that of *trans*-compartments which seem to aggregate into one major cisterna [Bha+14]. A comparable phenotype has been observed upon mutation of NSF (a fusion protein), which produces extremely large, but transient, *trans*-compartments [Tan+18], thereby increasing the system's stochasticity (see Sec.3.3.3, p.51 for a quantification of the fluctuations in our model). This is consistent with an increase of the fusion rate according to our model. Furthermore, the predicted correlation between compartments' size and purity is in agreement with the observation that decreasing the budding rate by altering the activity of COPI (a budding protein) leads to larger and less sorted compartments [Pap+15]. Modifying the expression of *VPS74* (yeast homolog of *GOLPH3*) leads to an altered Golgi organization, comparable to the *ARF1* deletion phenotype [Iye+18]. Both Δ*arf1* and Δ*vps74* present an enlargement of the Golgi cisternae and a disruption of molecular gradients in the system, which we interpret, in the limits of our system, as a lower purity due to slower sorting kinetics following an impairment of the budding dynamics.

The directionality of vesicular transport is intimately linked to the steady-state organization of the organelle; vesicular transport is anterograde when compartments are pure, and it is retrograde when they are mixed. This can be intuitively understood with the notion of "contaminating species". If a compartment enriched in a particular molecular identity emits a vesicle of that identity, the vesicle will likely fuse back with the emitting compartment by homotypic fusion, yielding no vesicular exchange. On the other hand, an emitted vesicle that contains a minority (contaminating) identity will homotypically fuse with another compartment. If budding is faster than maturation, the contaminating species is the one that just underwent maturation, and its budding and fusion with more mature compartment leads to anterograde transport. In such systems, compartments are rather small and pure. If maturation is faster than budding, the contaminating species is the less mature one, leading to retrograde transport. Such systems are rather mixed with large compartments. Thus, the directionality of vesicular exchange is an emergent property intimately linked to the compartments' purity. The *medial*-rich compartments are special in that regard: for intermediate values of the purity ($K \sim k_{\mathrm{m}}$), they may be contaminated both by yet to be matured *cis*-species and already matured *trans*-species and can fuse both with *cis*-rich and *trans*-rich compartments. If inter-compartment fusion is allowed, large *medial*-rich compartments are relatively scarce, and emit few vesicles. On the other hand, *medial*-vesicles emitted by *cis/medial* and *medial/trans*-compartments may fuse together to form (small) *medial*-rich compartments. For intermediate values of the budding rates, this vesicular flux dominates vesicular exchange and leads to a centripetal vesicular flux towards *medial*-compartments (details in Sec.3.3.4, p.54). If inter-compartment fusion is prohibited, which for instance corresponds to a situation where Golgi cisternae are immobilized [Dun+17], *medial*-rich compartments are present at steady-state, the centripetal vesicular flux is less intense, and the purity transition is accompanied by a direct transition from retrograde to anterograde vesicular flux (Sec.3.3.6, p.59).

Regardless of the model's details, we find that systems showing a well-defined polarity with well sorted cisternae exhibit anterograde vesicular fluxes, whereas systems with mixed compartments exhibit retrograde fluxes. The former dynamics is expected when biochemical maturation is the slowest kinetic process and compartments are long-lived, while the latter is expected when vesicular exchange is slow and the system is composed of transient compartments undergoing individual maturation. One can relate this prediction to the difference in organization and dynamics between the Golgi of S. cerevisiae and the more organized Golgi of higher organisms such as vertebrates. Maturation of Golgi cisternae has been directly observed in S. cerevisiae [Los+06], with colocalization of different identity markers within single cisternae (low purity) during maturation, whereas vesicular transport phenotypes have been indirectly observed [Dun+17] or inferred through modeling [DRS13] in mammalian cells. Consistent with our predictions, Golgi dynamics is one to two

orders of magnitude faster in S. cerevisiae Golgi cisternae (maturation rate $\sim 1/\mathrm{min}.$ [Los+06; Mat+06]) than in mammalian cells (export rate $\sim 1/30\mathrm{min}.$ [Bon+98]). At this point, one may speculate a link between structure and function through kinetics. A well sorted and polarized Golgi is presumably required to accurately process complex cargo. The glycosylation of secreted cargo is key to the interaction of a vertebrate cell with its organism's immune system [RC12], and glycans appear to be more diverse in higher eukaryotes – which also possess a highly organized Golgi – than in unicellular eukaryotes like yeast [Wan+17]. The Golgi organization in S. cerevisiae could thus be the result of an adaptation that has favored fast transport over robustness of processing, leading to a less organized Golgi characterized by cisternal maturation and retrograde vesicular transport. Remarkably, the slowing down of Golgi transport when S. cerevisiae is starved in a glucose-free environment coincides with the Golgi becoming more polarized [Lev+10], strengthening the proposal derived from our model of a strong connection between transport kinetics and steady-state Golgi structure.

In summary, we have analyzed a model of self-organization and transport in cellular organelles based on a limited number of kinetic steps allowing for the generation and biochemical maturation of compartments, and vesicular exchange between them. Although we kept the complexity of individual steps to a minimum, our model gives rise to a rich diversity of phenotypes depending on the parameter values, and reproduces the effect of a number of specific protein mutations. We identify the concomitance of a structural transition (from large and mixed to small and pure sub-compartments) and a dynamical transition (from retrograde to anterograde vesicular exchange).

4 Cargo transport and sorting in a self-organized Golgi apparatus

Contents for this chapter

4.1 Chapter's abstract

In previous chapter, we propose a simple model of how eukaryotic cells control self-organization and dynamics of membrane-bound organelles, such as the Golgi

apparatus. We gave some insights on how vesicular transport spontaneously emerges from this self-organized steady-state, and show that purely anterograde or retrograde vesicular transports are asymptotic behaviors of a much richer dynamical system. But how cargo-proteins are getting transported in such structure remains an open question. This is particularly true for cargo that interact with their surrounding environment, and exhibit affinity to some membrane identities and not others – cargo which transport in the system is not solely the result of passive fluxes we described in previous chapter. Here, we address these issues implementing direct interactions of cargo proteins with their local membrane environment. We mostly discuss a two-identity system (with only *cis* and *trans* identities), but also give results for the full, three-identity (*cis*, *medial* and *trans*) system. We show that different types of cargo can undergo different routes of vesicular transport within the same organelle. These parallel pathways sort cargo in different compartments at steady-state and affect their traveling time through the organelle.

4.2 Model adaptation

To facilitate understanding and analytical modeling (derived in Sec.4.4.6), we consider a simpler modeling approach, implementing only 2 membrane identities: *cis* and *trans*-species (Fig.4.1A). In previous implementations, *medial*-species was different from the 2 others, as purity of *medial*-compartments tune how these compartments interact with the ER and the TGN. In a pure regime, *medial*-compartments cannot fuse homotypically with the boundaries, that are composed of *cis* and *trans*-patches. But in low purity regime, the same compartments get contaminated by *cis* and *trans*-patches, and thus become sensitive to the boundaries. Because of that, the existence of three identities complicates a lot the analytical developments. That is why, in models of the previous chapters, we either assumed a pure regime, or created models for 2-species and extrapolated results for a 3-species system.

In the two-species implementation, steady-state composition is easier to compute. For a compartment containing a fraction ϕ of the *cis*-identity, and $1-\phi$ of the *trans*-identity, the compartment's exit rate $\phi\alpha + (1-\phi)\alpha = \alpha$. In other words, in the limit $\alpha_{\mathrm{ER}} = \alpha_{\mathrm{TGN}} = \alpha$, compartments' exit rate does not depend on their composition, and the development introduced in Sec.2.8.1 becomes:

$$\begin{aligned} N_{\textit{cis}} &= \frac{J}{\alpha + k_{\mathrm{m}}} \\ N_{\textit{trans}} &= N_{\textit{cis}} \frac{k_{\mathrm{m}}}{\alpha} \\ \text{and thus: } N &= J/\alpha \end{aligned} \tag{4.1}$$

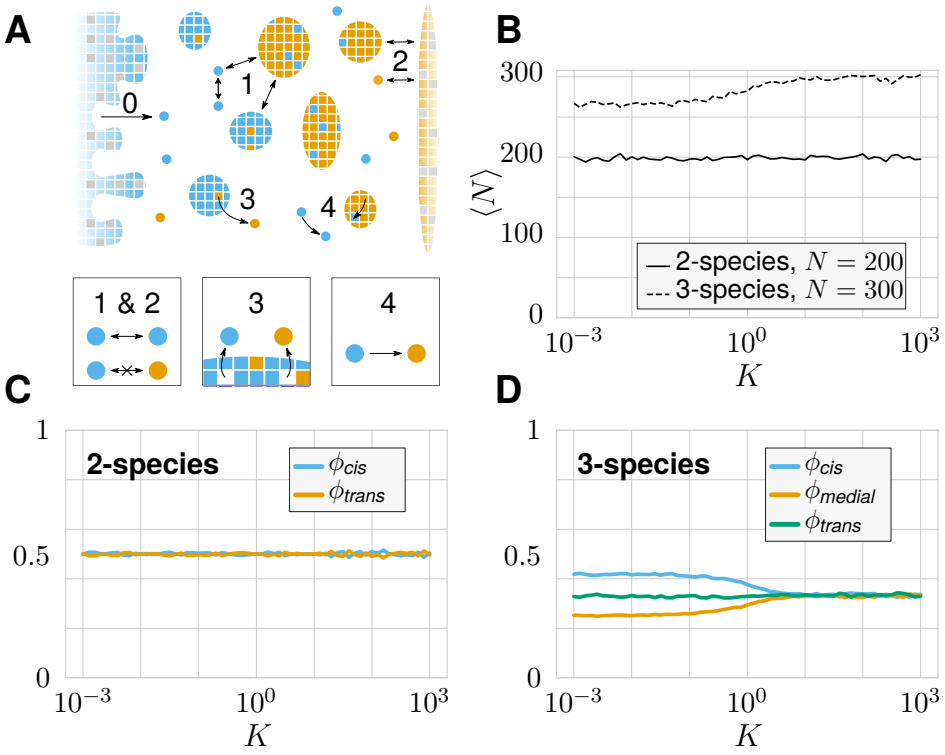

Fig. 4.1: Two-species model of a self-organized Golgi apparatus. A Model adaptation of Fig.2.1, p.27. The system includes two membrane identities (*cis*: blue, *trans*: orange). Everything is kept unchanged otherwise. **B** Steady-state mass in the Golgi $\langle N \rangle$, as a function of K, $k_{\mathrm{m}} = \alpha = 1$ and $J = 200$. **C-D** Steady-state composition (average fraction ϕ in each species) as a function of K in a 2-species (**C**) and 3-species (**D**) system. $k_{\mathrm{m}} = \alpha = 1$ and $J = 200$. Note that the color of *trans*-species has been changed from green to orange, for the sake of contrast for color-blind readers.

These equations remain true independently of system's purity. Both Golgi's mass (Fig.4.1B) and composition (Fig.4.1C-D) are easier to predict from these equations, and thus to fix in simulations. In this chapter, we focus on the case preferably studied in the previous chapter: $\alpha = k_{\mathrm{m}} = 1$ – same amount of each species at steady-state. We keep the same normalized injection rate J, so that the average mass in the system N is fixed to $200 - 100$ patches per species.

4.3 Main results

4.3.1 Vesicular transport biased by cargo-membrane interactions

In previous chapter, we characterized vesicular transport comparing the average composition of donor compartments, with the average composition of acceptor compartments. This led us to a quantification, called enrichment: $\vec{E}$. This vector

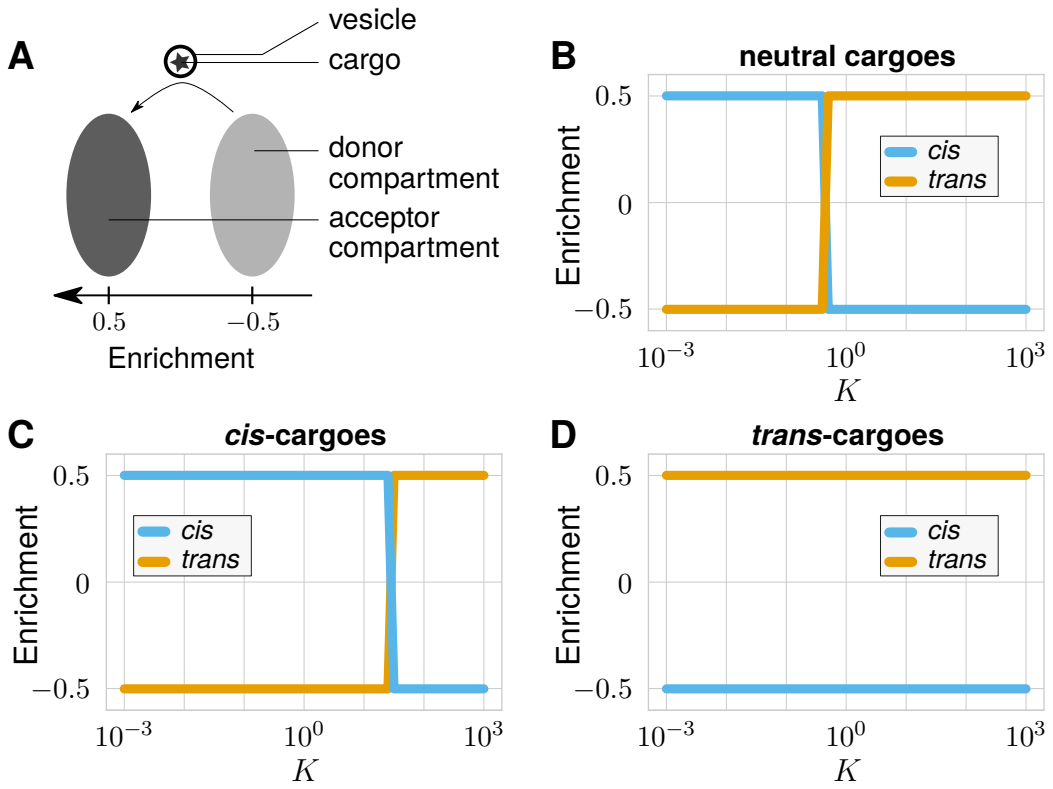

Fig. 4.2: Directionality of vesicular transport, following cargo-proteins with different affinities, varying the budding rate K. $k_{\mathrm{m}} = \alpha = 1$. **A** Schematic representation on how to interpret enrichment's data: majority species in the donor compartment has a -0.5 enrichment, and 0.5 for the majority species in the acceptor compartment (see text). **B-D** Computed enrichment for neutral (**B**), *cis* (**C**) and *trans* (**D**) cargo. *cis* component of enrichment $\vec{E}$ is displayed in blue, and orange for *trans* component. See Fig.4.10 p.93 for non-normalized data and Fig.4.11 p.95 for results in a 3-species system.

has a component for each membrane-species, components which sign gives the directionality of vesicular transport. Transport is anterograde when enrichment in *trans*-species is positive and negative for *cis*-species, and it is retrograde when positive for *cis* and negative for *trans*-species.

Enrichment data are easier to interpret in a 2-species system. Indeed, when traveling from one compartment to another, decreasing the fraction in one identity results in a gain in the other. The two components of $\vec{E}$ thus have the same absolute values, but with different signs. Once normalized by the l_1 norm, one component is 0.5, and the other -0.5. The positive value corresponds to the species that is gained during vesicular transport, identity of the acceptor compartment, and the other the identity that is lost, identity of the budding compartment (Fig.4.2A).

When following neutral cargo-proteins – cargo that do not have a particular affinity for any membrane identity – vesicular transport shows a transition in its directionality, going from a retrograde one at low K, to an anterograde one at large K (Fig.4.2B). This transition occurs for $0.1 < K < 1$, the value of K that marks a transition from a centripetal to an anterograde vesicular flux in 3-component systems. (Fig.3.3 – Main results section).

For cargo that do have an affinity for a defined membrane identity, we focus on the asymptotic situation of a strong affinity, introduced in the Methods chapter (Sec.2.6). Cargo-proteins have a $\xi = 1$ affinity for one species, and 0 for the other. In current chapter, we refer to *cis*-cargo (*trans*-cargo) as cargo having a 1 affinity for *cis*-species (*trans*-species) and 0 for the other.

In mixed compartments, *cis* and *trans*-cargo only interact with species for which they have a strong affinity. This affects the probability for these cargo to be packaged into a budding vesicle: instead of being $1/n$ for a neutral cargo (n the compartment's size), it is ξ_i/n_i, for any patch of identity i, where n_i is the number of patch of that identity in the compartment, for which the cargo has a strong affinity. If a cargo is trapped in a compartment with no affinity interaction ($n_i = 0$), it behaves like passive one.

Figure 4.2C shows that *cis*-cargo follow a retrograde route of vesicular transport, in systems for which $K < 1$. This is expected as the overall vesicular transport is retrograde for this range of parameters. More interestingly, *cis*-cargo keep a retrograde route in the Golgi when budding rate $1 < K < 10$, whereas such systems exhibit anterograde vesicular transport for neutral cargo. On the other hand, Fig.4.2D shows that *trans*-cargo always follow an anterograde vesicular route in the Golgi independently of the values of K. For the sake of completeness, non-normalized enrichments can be found in Sec.4.4.4, p.93. The same quantification for a 3-species

system can be found in Sec.4.4.5 for comparison: introduction of *medial*-species does not qualitatively change the results.

4.3.2 Steady-state sorting of cargo in compartments

Different cargo-proteins experience different routes in the Golgi. Because of that, one could expect these cargo are addressed to different compartments at steady-state: *cis*-cargo in *cis*-compartments, and *trans*-cargo in *trans*-compartments. We propose a quantifier, the sorting of cargo S, to account for the system's capacity to do so (see Sec.4.4.2 p.4.4.2 for details about the quantification). It equals 1 when cargo are in compartments only of the proper identity (the one they have a strong affinity for), and 0 when they are in compartments of the opposite identity. For mixed compartments, and in the limit of cargo with strong affinities, it equals the fraction of species in the compartment for which the cargo has a strong affinity.

Sorting values are averaged over all cargo-proteins of the same affinity, and presented in Fig.4.3. We follow 3 of them – *cis*, *trans* and neutral. We also plot the average sorting of *cis* and *trans*-cargo combined.

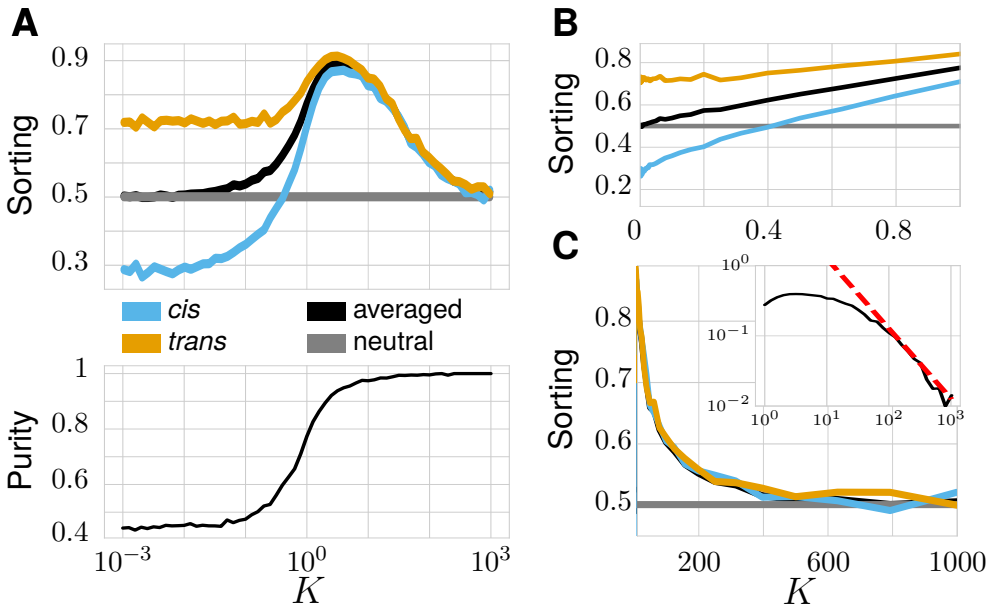

Fig. 4.3: Cargo sorting in the Golgi, varying their affinity for membrane identities, as a function of K and computed for *cis* (blue) *trans* (orange) and neutral (grey) cargo. $k_{\mathrm{m}} = \alpha = 1$. **A** Sorting of cargo-proteins (top panel) as a function of K and its link to the steady-state purity (bottom panel). **B** Sorting for small values of K – plotted in a linear scale. **C** Sorting for large values of K, dotted red line is a fit in Const$/K$ predicted by the analytical model presented in Sec.4.4.6 p.100. See Fig.4.12 for data in the 3-species implementation.

By construction, sorting of neutral cargo always equals $1/2$, which is the standard for other quantifications. As the system is tuned so that the amount of *cis*-species equals the amount of *trans*-species, the probability to be in contact with one or the other species is 50%. For cargo of extreme affinities – that are *cis* and *trans*-cargo – this quantifier gives the average fraction of *cis* (*trans*) patches, seen by a *cis* (*trans*) cargo (see Sec.4.4.2 p.4.4.2).

Fig.4.3 shows 3 different regimes depending on the values of K:

$K \gg 1$. For infinite K, the system is vesicular: transport between compartments is irrelevant and cargo are trapped in vesicles. Before exiting the Golgi, vesicles assume *cis* and *trans*-identity for the same amount of time (see Sec.4.4.6, p.100). Sorting in a vesicular regime is thus $1/2$. For large, but finite values of the budding rate, sorting varies as $1/K$. This can be understood considering the following. Sorting depends on the probability to find compartments that can address different cargo in different vesicles. The smallest compartment that is able to do so is a dimer composed of one *cis* and one *trans*-patch. By scission, it creates two vesicles, on that sends back *cis*-cargo in *cis*-compartments, and one that addresses *trans*-cargo in *trans*-compartments. The probability to find such hetero-dimers scales in $1/K^2$ and thus the budding flux out of these compartments $K \times 1/K^2 = 1/K$ (fit in Fig.4.3C). Complete model can be found in Sec.4.4.6, p.100, short description in the box below.

> We consider a pool of vesicles aggregating to form dimers, dimers that separate again with a rate K. The amount of dimers thus scales in $1/K$. Once assembled, these dimers have two possibilities: either they disassemble with rate K, or they mature with a rate k_m, and form heterodimers we are interested in. The fraction of dimers creating heterodimers thus scales in $\frac{k_\mathrm{m}}{k_\mathrm{m}+K}$. Multiplied by the fraction of vesicles that formed dimers in the first place, it gives $\frac{1}{K}\frac{k_\mathrm{m}}{k_\mathrm{m}+K}$. In our system, $k_\mathrm{m} = 1$ and $K \gg 1$, this the probability to find such hetero-dimers scales in $1/K^2$.

$K \ll 1$. For very low budding rates, one could expect a comparable low sorting regime, as cargo-proteins are trapped in compartments that cannot bud vesicles efficiently. And indeed, cargo exhibit a 0.5 sorting value on average (Fig. 4.3A). However, sorting is smaller than 0.5 for *cis*-cargo and larger for *trans*-cargo. This asymmetry between cargo types is explained by the behavior of compartments themselves. In the low K regime, compartments keep aggregating mass over time, because budding is inefficient to compensate fusion fluxes.

In the same time, compartments mature from a *cis* to a *trans*-identity. These effects combined make *trans*-compartments bigger than *cis*-ones. But the bigger the compartments, the more the cargo-proteins in them, yielding a better sorting of *trans*-cargo. A model of this phenomenon can be found in Sec.4.4.6, p.98. Fig.4.3B shows that sorting grows linearly with K. This is consistent with the fact that sorting relies on vesicular transport to segregate identities.

$K \sim 1$. Between these extreme regimes of low sorting, Fig.4.3A shows an optimum at $1 < K < 10$, which corresponds to the end of the purity transition. In this regime, cargo are in compartments that assume up to 90% of the identity of good affinity.

Comparison with a 3-species system can be found in Sec.4.4.5: reintroduction of *medial*-species does not qualitatively change the results.

4.3.3 Kinetics of cargo transport in a RUSH-like implementation

The residence time of cargo in the system may be tuned by their sorting in different compartments. Kinetics of cargo-proteins is particularly interesting to investigate, as it can be compared to existing biological data. To our knowledge, the first experiment that directly observes kinetics of cargo getting transported through the Golgi is [Bon+12]. By genetically manipulating the expression of cargo, they retain them in the ER *via* interaction with a hook (streptavidin – streptavidin-binding peptide). The injection of a chemical (biotin) lifts this restriction and releases cargo in the Golgi. By tracking the fluorescence of cargo, they follow the kinetics of arrival and departure of cargo, to and from the Golgi (Fig.4.4B). Different cargo have different residing times in the system, from being quickly addressed to the TGN (like TNF-α), to being sequestered in the Golgi (ManII).

In our framework, we can simulate such experiments by slightly modifying how cargo-proteins are created in the ER (see Sec.4.4.1, p.87). Instead of being produced continuously, a large amount of cargo-proteins is put in the ER before being released after Golgi reaches steady-state. We follow 4 types of cargo: *cis*, *trans*, neutral, and cisternal cargo that cannot be packaged in a budding vesicle. The latter cargo simulates large proteins like procollagen that are thought not to be carried by usual transport vesicles [Bon+98].

Figure 4.4A shows that the system's capacity to exhibit different transport kinetics, strongly relies on the Golgi's capacity to sort its components. The difference of

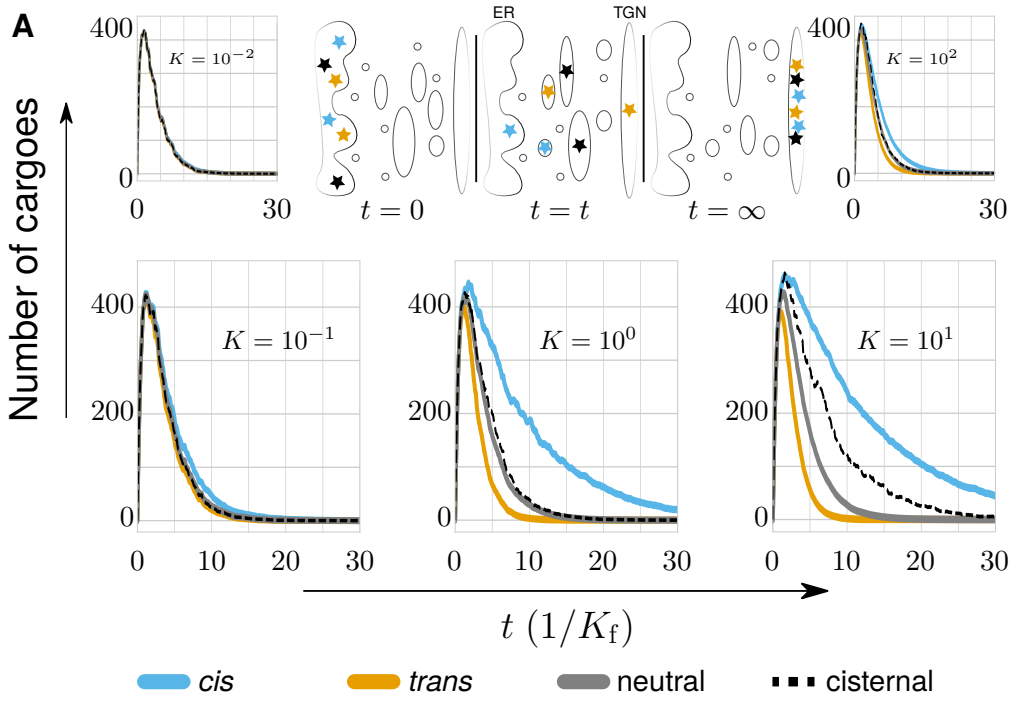

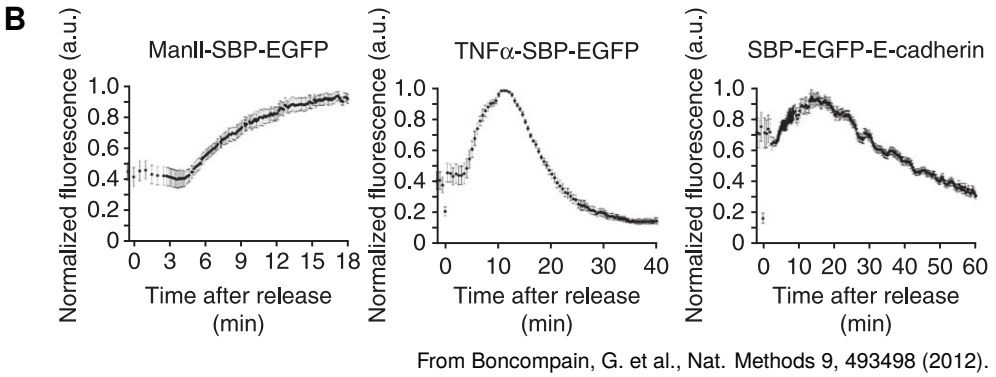

From Boncompain, G. et al., Nat. Methods 9, 493498 (2012).

Fig. 4.4: RUSH-like simulation and real RUSH data of cargo transported in the Golgi. **A** Number of cargo in the system as a function of time K_f^{-1} (normalized by the fusion rate) and computed for *cis* (blue) *trans* (orange), neutral (grey) and cisternal (dashed) cargo. $k_m = \alpha = 1$. Initially, 1000 cargo of each identity are placed in the ER, and released at $t = 0$. Sketch of the simulation is shown on the top-middle panel. **B** *In vivo* RUSH data from [Bon+12]. Fluorescence of different cargo (related to their amount in the Golgi) is tracked over time: ManII – a Golgi enzyme, TNF-α – a cytokin, and E-cadherin – a trans-membrane protein responsible for cellular adhesion. See Sec.4.4.1, p.87 for details about the RUSH-like simulation. To be compared with the 3-species implementation, Fig.4.13, p.98.

kinetics between different types of cargo is maximum for $1 < K < 10$, budding rates for which sorting is maximum. Cargo residing time in the Golgi depends on the vesicular transport they follow. Cargo experimenting a retrograde transport – *cis*-cargo – stay longer in the system than the others. On the contrary, cargo getting quickly addressed to more mature compartments – *trans*-cargo – stay very briefly in the system. Interestingly, for $1 < K < 10$, cisternal cargo stay longer in the system than neutral ones, which is expected as the overall vesicular transport is anterograde. For completeness, RUSH-like simulation performed on a 3-species Golgi can be found in Fig.4.13 Sec.4.4.5 p.98.

The results shown in Fig.4.4 are relevant to probe the residence dynamics of different proteins at the scale of the entire Golgi apparatus. But they do not inform us on the dynamics at the scale of individual compartments, which is accessible in our numerical simulations. Time evolution of compartments is a relevant phenomenon to follow when compartments do evolve over time, and thus mature. This means we investigate regimes in which maturation is faster than budding of newly matured membrane patches, regime of low purity. That is why, we focus on cases where $K \leq 0.1$. One should however bear in mind that the following quantifications are preliminary results. Data are obtained after non-trivial normalizations, and we encourage the reader to see Sec.4.4.2, p.88 and p.90, to have a clear overview of limitations of these quantifications. In our simulation, it is difficult to follow a given compartment over time. In the low budding regime, we have shown that the size of a compartment is a good proxy for its age (Fig.3.6 – previous chapter and verified in Sec.4.4.2); older compartment are correspondingly larger.

In a low budding rate regime, $K \leq 0.1$, compartments undergo maturation from *cis* to *trans* identity, as they are aging (Fig.4.5A-B left panels). This dynamics of maturation is in agreement with analytical results presented in Sec.4.14. The amount of cargo-proteins (normalized per the amount of cisternal cargo) in cisternae, is not constant over time in regime of low but non-negligible budding rate: $K = 0.1$. In small – and therefore new *cis*-compartments – cargo-proteins experiencing a retrograde vesicular transport (*cis*-cargoes) are more numerous than cisternal ones (Fig.4.5A top right panel). This amount decreases over time as compartments grow and mature to a *trans*-identity. This is consistent with the fact that these cargo leave *trans*-compartments (from which they get depleted) to reach *cis*-ones (in which they get enriched) because of retrograde vesicular transport. For the moment, statistics are not sufficient to conclude for neutral and *trans*-cargo. But we however get a glimpse on the fact *trans*-cargo are depleted in early compartments, and that neutral cargo concentration is decreasing as compartments are aging. This phenotype is abolished by severely disrupting budding mechanisms (Fig.4.5B top right panel).

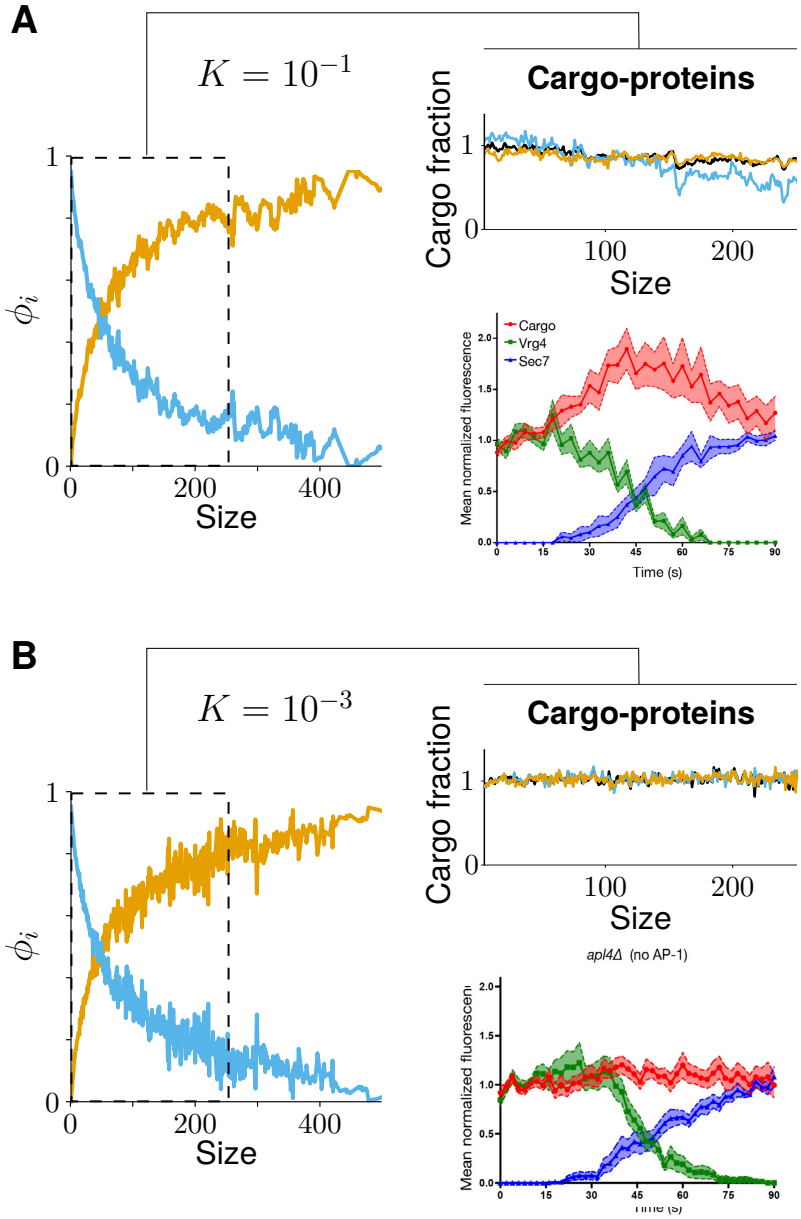

Fig. 4.5: Link between compartment composition dynamics and concentration of cargo-proteins, in a low budding rate regime, $k_{\mathrm{m}} = \alpha = 1$, $K = 0.1$ (**A**) or $K = 10^{-3}$ (**B**). For both **A-B** Left panel: fraction ϕ in the i-species (*cis* blue, *trans* orange) as a function of compartments' age, inferred from their size (see Sec.4.4.2, p.88) – Top right panel: normalized amount (see Sec.4.4.2, p.90) of *cis* (blue), *trans* (orange) and neutral (black) cargoes as a function of compartment's age – Bottom right panel: *In vivo* data from [Cas+19], amount of cargo-proteins in cisternae (red) as they mature from a *cis* (green) to a *trans* (blue) identity, over time.

Experimentally, such quantification can be performed in Yeast, where cisternae are dispersed in the cytoplasm. Recent experiments have succeeded in correlating cargo dynamics to compartments' maturation in this cellular system [Cas+19]. While compartments exhibit maturation from a *cis* to a *trans*-identity, the fluorescence intensity of cargo peaks then decreases. This was taken as an indication of antero-grade vesicular transport, that takes cargo from *trans*-cisternae to address them in *cis*-ones (Fig.4.5A – bottom right panel). This phenotype disappears when altering budding, after which cargo amounts remain constant over compartments' aging, as expected in a purely cisternal maturation model (Fig.4.5A – bottom right panel). These are interesting results as they show that systems dominated by maturation of cisternae still exhibit vesicular transport, particularly for cargo-proteins undergoing a retrograde route in the Golgi. This is entirely consistent with the vision of Golgi dynamics emerging from our model, which sees this dynamics as resulting from the interplay between the kinetics of vesicular transport and biochemical maturation.

All these data comfort results of our model, as they show the same overall phenotypes. A notable difference is that maturation follows a simple exponential transition in our simulation, whereas it occurs in a sigmoidal fashion in living cells (Fig.4.5A-B bottom right panels). This can affect the time during which cargo accumulate in compartments, and explain why we do not observe a peak at the transition from *cis* to *trans* in our simulation. Adding some cooperativity in membrane maturation could tackle this issue and yield quantitative agreement with biological data. We discuss in depth the latter adjustment and others in Discussion chapter.

4.4 Additional analyses and study results

4.4.1 Setting up the simulation

Cargo released in a steady-state Golgi

In physiological conditions, cargo are continuously created in the ER before being addressed to the Golgi. To model this, one should implement two quantities: the cargo synthesis rate inside the ER, and their injection rate in the Golgi.

All cargo in the ER are treated like neutral ones, and one must define the ER size n_{ER} to compute the probability for cargo to be packaged in vesicles, probability that scales in $1/n_{\mathrm{ER}}$. *In vivo*, ER exit sites (ERES) have a diameter $0.5\mu m$ [BS09], and a surface of $0.2\mu m^2$. For small Golgis (around $1\mu m^2$) we count between 4 and 5

ERES, meaning a same surface area $\sim 1\mu m^2$ for both Golgi and ERES. We thus take $n_{\mathrm{ER}} = N$ (N the Golgi's total area).

The injection rate per cargo is thus J/n_{ER}. As cargo-proteins are not interacting with one another in our model, we consider a dilute regime for cargo in the ER. We choose an arbitrary concentration of 1 cargo per 100 membrane patches. The synthesis rate of cargo is thus $2K_{\mathrm{f}}$. Note that if cargo are taken back to the ER from the Golgi, they are not destroyed and can be injected back to the Golgi, the same way as newly synthesized cargo.

Cargo released in a RUSH-like system

To simulate RUSH experiments, we need a large amount of cargo-proteins in the ER before release, amount we call n_{cargo}. The larger this amount the better the statistics. One could want the fluctuations of cargo counts in the ER to be consistent with *in vivo* observations, and fix the average number of cargo per vesicle accordingly. The maximum amount of cargo per vesicle is observed at $t = 0$, when it is $J * n_{\mathrm{cargo}}/n_{\mathrm{ER}}$. We set n_{cargo} so that the concentration per vesicle is consistent with biological data.

In cells, concentration of cargo-proteins varies a lot between vesicles, but also between cargo types. It can potentially be of few thousands proteins [MR19], but has been observed to be much less for some of them [Tak+06] – in synaptic vesicles. Around 15 RABs have been counted, but only 1 SNAP-29 (fusion proteins). We thus consider a relatively low concentration of cargo per vesicles, that is 5 per membrane patches, and thus $n_{\mathrm{cargo}} = 1000$ in the ER at $t = 0$.

We wait for the Golgi to reach steady-state before releasing cargo, and stop simulation when all of them are in the TGN. Multiple RUSH-like simulations are performed and averaged: typically 100 of them for each parameters set.

4.4.2 Quantification to characterize the system

Computation of cargo-proteins sorting at steady-state

We propose to quantify the sorting of cargo in compartments of different identities as follows. It equals 1 when all membrane patches surrounding the cargo are of the identity with which it has a strong affinity. It equals 0 when the cargo is trapped in a compartment for which it does not have any affinity. It is kept constant for neutral

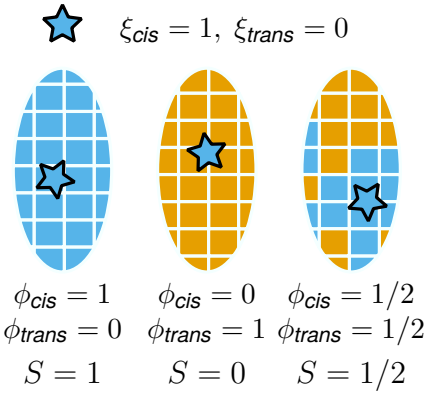

Fig. 4.6: Three examples of cargo's sorting S, for a *cis*-cargo in 3 different compartments. Compartments are defined by their composition ϕ in *cis* and *trans*-identities.

cargo. The sorting $S(\vec{\xi}, \vec{C})$, for a cargo of affinity $\vec{\xi} = (\xi_{cis}, \xi_{trans})$, in a compartment of composition $\vec{C} = (\phi_{cis}, \phi_{trans})$, follows:

$$S(\vec{\xi}, \vec{C}) = \frac{\sum_i \phi_i \times \xi_i}{\sum_i \phi_i \times \sum_i \xi_i} = \vec{C} \cdot \vec{\xi} \tag{4.2}$$

Schemes of some sorting values can be found in Fig.4.6.

One notices that it always equals $1/2$ for neutral cargo: $\xi_i = 1/2,\ \forall i$. For cargo of strong affinities ($\xi_i = 1$ for one identity and 0 for the other) it equals ϕ_i with i the identity for which the cargo has a strong affinity. This quantification is computed for each cargo over time and averaged for all cargo of the same type.

Tracking composition of individual compartments over time

The aim of current section is to propose a quantification that records temporal evolution of compartments in simulations. The incentive for such quantification is twofold: to verify our modeling approach in Sec.4.14 is correct (does maturation occur in an exponential fashion, and are compartments growing linearly over time), and to compare simulation results with biological ones of [Cas+19]. In the publication we focus on, systems exhibit maturation of cisternae over time, and are thus inferred to be in a low K regime. That is why we focus on cases where $K \leq 0.1$. For consistency with the latter publication in which they track cargo kinetics in the Golgi, we adopt a RUSH-like implementation of simulations.

The present implementation allows us to introduce cargo-proteins that cannot be packaged and budded out from compartments: cisternal cargo. Because they cannot undergo vesicular transport, following the journey of such cargo is comparable with

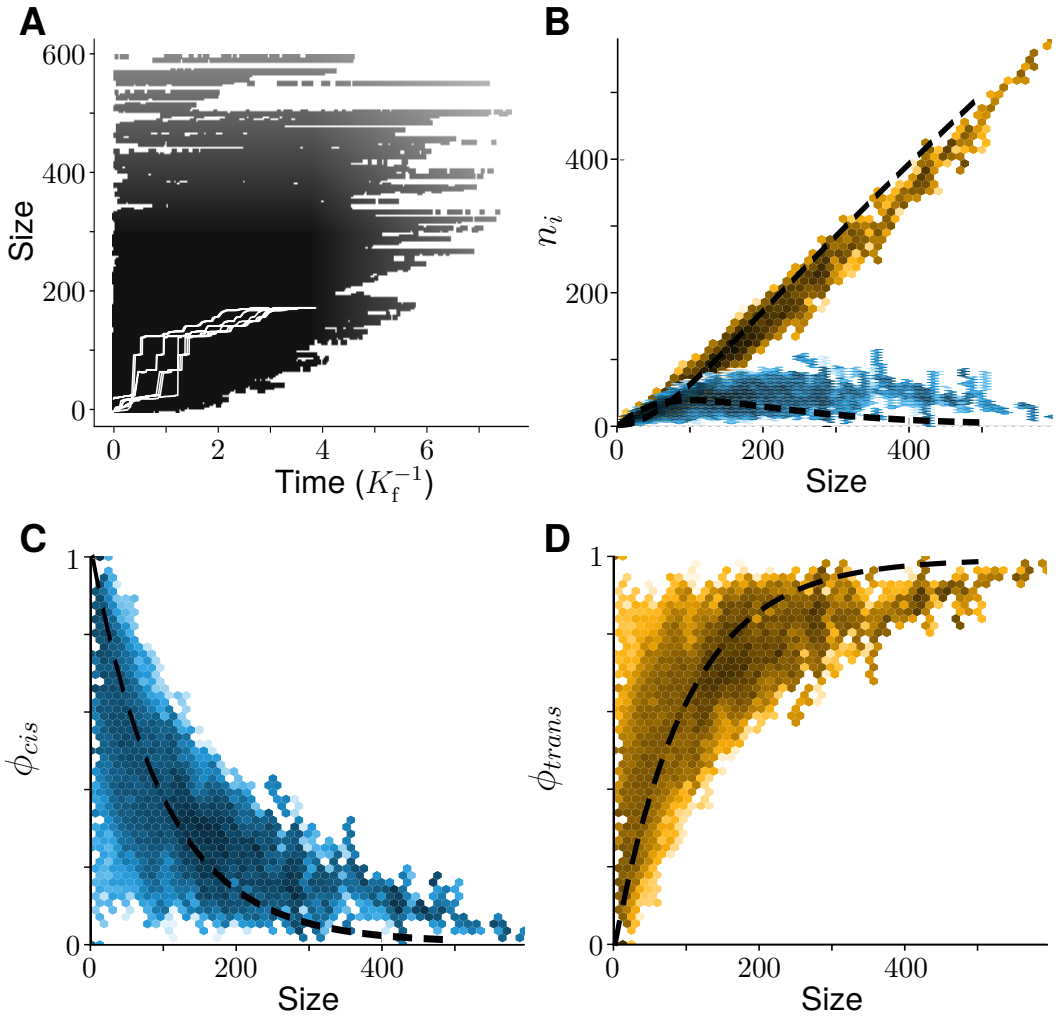

Fig. 4.7: **Tracking composition of individual compartments over time**, and over compartments' size. $K = 10^{-3}$, $k_m = \alpha = 1$, 2-D histogram: the darker the more numerous (arbitrary units). Dashed lines: model prediction from Sec.4.14, p.99, transposing time dependency into size dependency by assuming compartments' size scales as $j \times t$, $j \sim J/2$ as discussed in the modeling section. **A** Amount of compartments containing cisternal cargo as a function of their size, and the time after cargo release from the ER. White line: trajectories of individual compartments. **B** Number of patches N of identity i (*cis* in blue, *trans* in orange) as a function of compartments' size. **C-D** Fraction in *cis* (**C**) and *trans*-patches (**D**) in compartments as a function of their size.

following compartments themselves. We thus record compartments' composition in which cisternal cargo are trapped. Because we are interested in compartment having followed a complete journey in the Golgi, we only consider the ones fusing with TGN (not the ones fusing back to the ER). And because we do not want to consider vesicles that have just underwent few maturation and fusion events before exiting, we only consider compartments that exit with a size larger than 75% of the system's total mass N.

Even with these criteria, it is challenging to synchronize the individual trajectories of each cargo. As shown if Fig.4.7A, large jumps in compartments' size can be observed, corresponding to fusion of two compartments. We however see that the overall trend followed by compartments over time is a linear increase of their mass, with a growing factor of $\sim 100 K_{\mathrm{f}}$. This is consistent with predictions of our mean-filed modeling approach (Sec.4.14) – compartments linearly growing with a rate $\sim J/2$. Following compartments' composition as a function of their mass is thus a satisfactory alternative approach to following their composition with time.

With this alternative representation of compartments' aging, both compartment composition in term of number (Fig.4.7B) and fraction of *cis* and *trans*-patches (Fig.4.7C-D) are in good agreement with analytical developments (Fig.4.14). The amount of *cis*-patches increases linearly before decreasing, whereas the amount of *trans*-patches grows linearly with the size of compartments, and thus their age. The fraction of *cis*-patches follows an exponential decay, whereas the fraction of *trans*-species in compartment grows exponentially.

Tracking cargo in compartments over time

The aim of current section is to propose a quantification of cargo-proteins amounts in compartments, and display it over time. As discussed in previous section, it is challenging to follow compartments over time because of asynchronicity of the different trajectories. To tackle this issue, age of compartments is inferred from their size.

When following the total amount of cargo-protein in compartments as a function of compartments' size, multiple problems arise (Fig.4.8A). Despite the fact we see slight differences between cargo types, all cargo follow the same trend: their amount increases linearly with the compartments' size, before decreasing and showing large fluctuations. The first trend is expected, as the larger the compartment the greater the probability to find a cargo in it. But this is so dominant that it hides other phenomena in this regime. The other trend comes from the fact compartments can

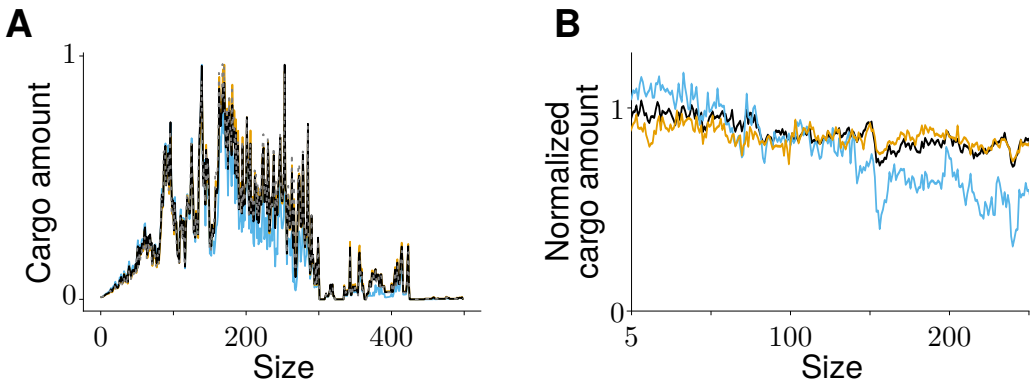

Fig. 4.8: **Quantification of the amount of cargo-proteins as compartments are aging**, correlated with compartments' size. $K = 0.1$, $k_{\mathrm{m}} = \alpha = 1$. **A** Total amount of cargo-proteins in compartments of a given size. *cis*-cargo are plotted in blue, *trans* in orange, neutral in black and cisternal in dashed grey. **B** Normalized amount of *cis*, *trans* and neutral cargo (divided by the amount of cisternal ones) as a function of compartments' size. *cis*-cargo are plotted in blue, *trans* in orange and neutral in black.

exit the system at any time. Cargo-proteins initially injected from the ER continuously leave the system through the TGN. As compartments aggregate mass over time, large compartments, meaning compartments that had the time to aggregate, have fewer remaining cargo to encapsulate.

One way to tackle this issue is to normalize the amount of cargo-proteins per the amount of cisternal cargo in compartments. As these cargo cannot undergo vesicular transport, variations in this normalized amount reflect how the others are affected by vesicular transport. We however have to introduce two cut-off in this normalization: we do not consider compartments larger than 250 as we currently do not have enough statistical power to resolve this regime; we do not consider vesicles or group of fused vesicles (arbitrary size of ≤ 5) as cisternal cargo cannot enter such compartments. Results of this normalization are shown in Fig.4.8B and Fig.4.5A – Main results section.

The other way to tackle this issue is to consider a steady-state regime with cargo-proteins being injected continuously over time, instead of implementing a RUSH-like system. This would eliminate the second trend in simulations, where the amount of cargo decreases over time and provide us better statistical power to resolve regimes of large compartments. This quantification has not been performed yet, but is our very next step to better characterize vesicular transport experienced by single cisternae.

4.4.3 Detailed characterization of the composition

Steady-state composition

In the Main results section, we did not characterize the steady-state organization and assumed the 2-species system implementation follows the same trends as the 3-species one. For the sake of completeness, we characterize this steady-state and show here the typical size of compartments and their purity as a function of K (Fig.4.9).

We need to introduce an extended version of the purity, as compared to the 3-species case. For a compartment containing n_{id} possible different identities, the purity P of the compartment follows:

$$P = \sqrt{\frac{n_{\mathrm{id}}}{n_{\mathrm{id}} - 1} \sum_i (\phi_i - \frac{1}{n_{\mathrm{id}}})^2} \tag{4.3}$$

with i the different possible identities (either *cis*/*trans* or *cis*/*medial*/*trans*), and ϕ_i the fraction of the i-identity in the compartment.

We see that the 2-species system exhibits the same behavior as the 3-species one: low K gives a low purity / big compartments regime, high K gives high purity / vesicular compartments. Around $K \sim 1$, compartments are rather big and pure. The three steady-state we introduced in the previous chapter, namely the "mixed", "sorted" and "vesicular" regimes are still relevant to describe the 2-species implementation.

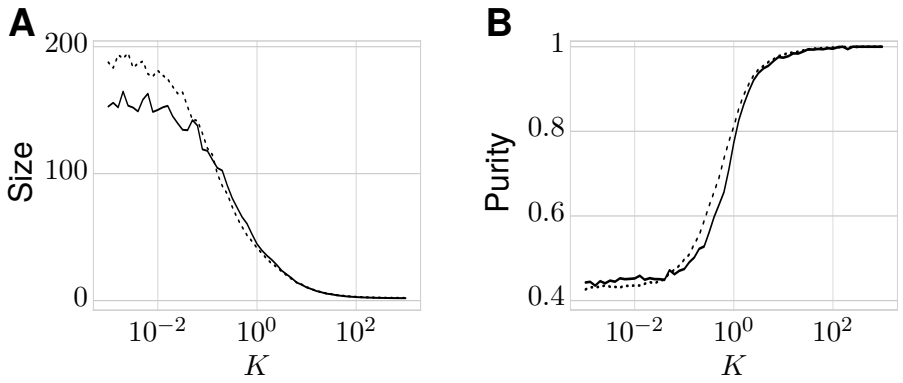

Fig. 4.9: Steady-state organization in a 2-species system, $\alpha = k_{\mathrm{m}} = 1$ and $J = 200$. **A** Typical size (same quantification than the one used in previous chapter, Sec.3.3.2, p.48) as a function of K, plain lines are data for a 2-species system, dotted lines are data for a three species system. **B** Average purity (see text) as a function of K, plain line are data for a 2-species system, dotted line are data for a three species system.

Small differences are however present. As the total mass is lower in the 2-species than the 3-species system, compartment's size is lower in the 2-species for $K \ll 1$. However, it becomes the same as soon as Golgi gets pure, and thus the number of species becomes irrelevant to define the size of compartments. For $K \lessapprox 1$, the 2-species system shows slightly larger compartments, as the very non-linear budding scheme scales with the number of different identities. For the same reason, sorting mechanisms are stronger in a three species system, and purity is slightly higher when $K \lessapprox 1$ in the 3-species one. The extreme regimes of $K \gg 1$ and $K \ll 1$ show comparable values of purity in both implementations.

4.4.4 Detailed characterization of the vesicular transport

Mean enrichment (composition difference between donor and acceptor compartments) seen by a transport vesicle is shown in Main results section in a normalized fashion – $\vec{E}$ is divided by its l_1 norm. Non-normalized data are presented here in Fig.4.10. It is the same quantification as the one in Fig.3.7A (bottom panel) of previous chapter, but considering only two biochemical species (instead of three), and following cargo of different affinities.

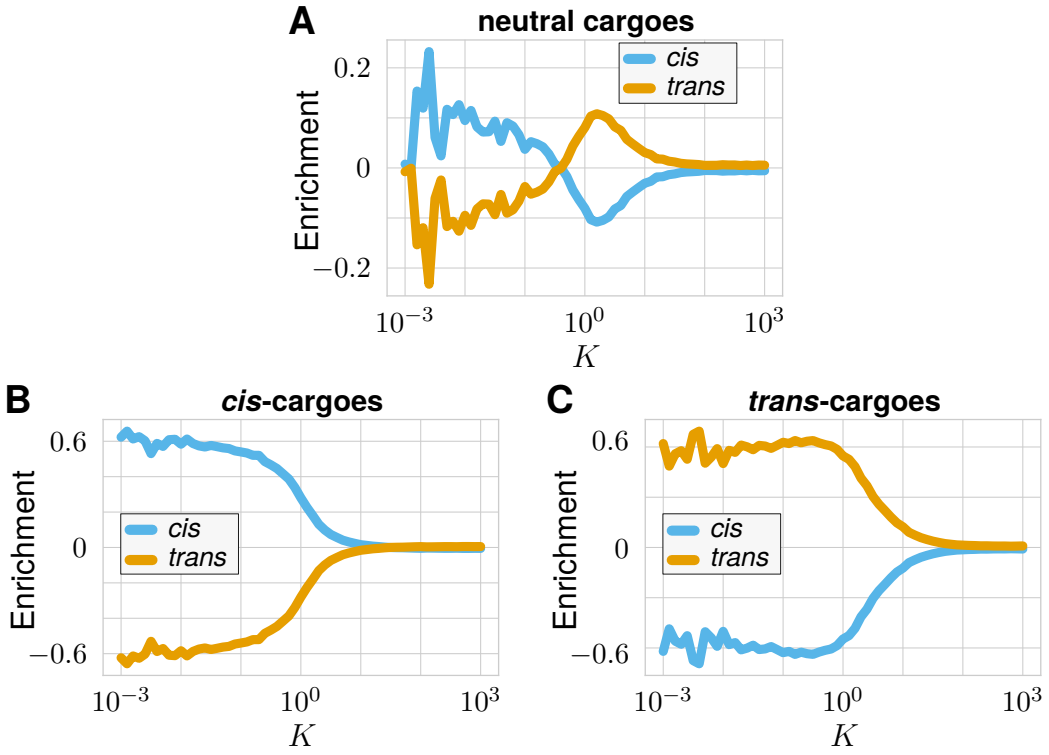

Fig. 4.10: Non-normalized enrichments in a 2-identity system, following cargo with different affinities, varying the budding rate K. Related to Fig.4.2 – Main results section. $k_{\mathrm{m}} = \alpha = 1$. **A-C** Non-normalized (average per vesicle) enrichment for neutral (**A**), *cis* (**B**) and *trans* (**C**) cargo. $\vec{E}$ *cis* component is plotted in blue, and in orange for the *trans* component.

Results for neutral cargo in Fig.4.10A are very close to the ones in Fig.3.7A (bottom panel) of previous chapter. Vesicular transport assumes retrograde directionality for low K – enrichment in *cis* and depletion in *trans*-species; and a retrograde one for intermediate values of K – enrichment in *trans* and depletion in *cis*-species. As before, enrichment vanishes for $K \gg 1$, because back fusion with the donor compartment or a compartment of similar composition dominates this high purity regime.

Results in Fig.4.10B-C show that *trans*-cargo always follow an anterograde route, whereas *cis*-cargo undergo retrograde vesicular transport through the Golgi up the high values of the budding rate ($K \sim 1 - 10$). For very large K, both collapse because of back-fusion. Note that the average enrichment for *cis*-cargo collapses for lower values of K than neutral and *trans*-cargo. As the budding rate becomes large, the "natural" tendency of *cis*-cargo to undergo retrograde transport in *cis*-vesicles is reduced by a forced anterograde flux, governed by maturation of vesicles.

4.4.5 Cargo transport and sorting in a 3-species system

In Main results section, we characterized both vesicular transport and cargo sorting in a 2-species system. We now verify that the 3-species implementation – that is a biologically more accepted picture of the Golgi – exhibits the same trends. In brief, enrichment (Fig.4.11) and sorting (Fig.4.12) are comparable between implementations. As the simulation used here is different from the one used in previous chapters, Fig.4.11A reproduce results of Fig.3.3 for comparisons.

Figure 4.11B shows *cis*-cargo follow a retrograde path in vesicular transport for $K < 1$, and keep a retrograde route in the Golgi for $1 < K < 10$. However, for $1 < K < 10$, enrichment becomes negative for the *medial*-component, meaning donor compartments are *medial* and not *trans*-compartments. As the Golgi is pure in this range of budding rates, only *medial*-compartments are still contaminated by *cis*-patches, and thus only *medial*-compartment can promote retrograde vesicular transport toward *cis*-compartments. For larger values of K, the system is dominated by maturation of transport vesicles, and exhibits an anterograde flux for *cis*-cargo.

For $K < 10$ *medial*-cargo undergo a centripetal vesicular transport, exiting both *cis* and *trans*-compartments to fuse with *medial*-ones (Fig.4.11C). For larger values of K we observe an anterograde flux because of vesicles maturation. Finally, Fig.4.2D shows that *trans*-cargo always follow an anterograde vesicular transport, independently of the budding rate values.

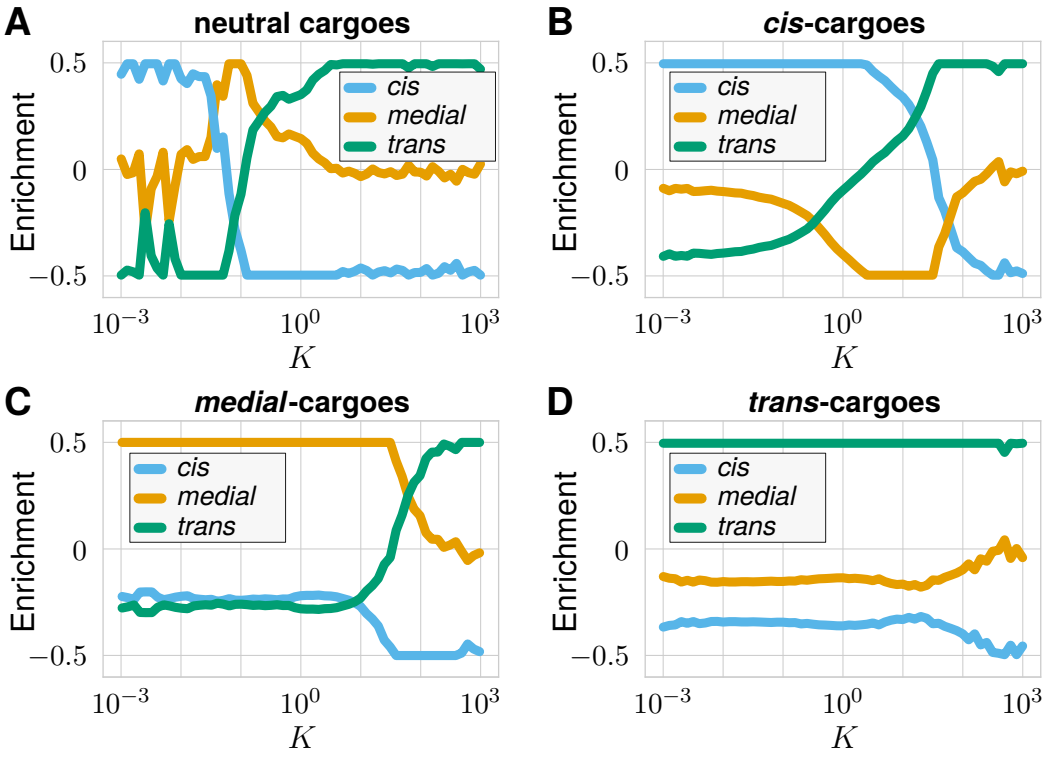

Fig. 4.11: Directionality of vesicular transport in a 3-identity system, following cargo with different affinities, varying the budding rate K. $k_{\mathrm{m}} = \alpha = 1$. Related to Fig.4.2 (2-species) – Main results section. **A-D** Computed enrichment for neutral (**A**), *cis* (**B**) *medial* (C) and *trans* (**D**) cargo. $\vec{E}$ *cis* component is plotted in blue, and in orange for the *trans* component.

As shown in Fig.4.12, sorting is governed by the same rules as the ones presented in Main results section. Depending on the value of the budding rate K, one can distinguish 3 different regimes:

- For $K \gg 1$, the Golgi is vesicular and sorting is low. As there are now 3 species instead of 2, vesicles spend one third of their time (instead of half) in each identity. Minimum sorting value is thus $1/3$ when K tends to infinity. For large but finite budding rate, sorting scales in $1/K$ as observed in a 2-species implementation (fit in Fig.4.12C, analytical model in Sec.4.4.6, p.100).

- For $K \ll 1$, the Golgi exhibits low sorting. On average, it equals $1/3$ for *cis*, *medial* and *trans*-cargo combined (Fig.4.12A). As for a 2-species system, sorting is smaller than 0.5 for cargo with great affinity for immature (*cis* and *medial*) identities, and larger for *trans*-cargo.

- Between these extreme regimes of low sorting, Fig.4.12A shows an optimum at $1 < K < 10$, which corresponds to the end of the purity transition. In this regime, cargo-proteins are in compartments composed of 80% of the identity for which they have a good identity.

In Fig.4.4 – Main results section, we discussed how cargo kinetics can be affected by Golgi's steady-state organization, and cargo affinities. The 3-species implementation is governed by the same rules as the 2-species one as shown in Fig.4.13. The difference between kinetics of different cargo-proteins is maximum when $1 < K < 10$. In this regime, cargo experimenting a retrograde transport – *cis*-cargo – stay longer in the system than the others. On the contrary, cargo getting quickly addressed to more mature compartments – *trans*-cargo – stay very briefly in the system. As $1 < K < 10$, cisternal cargo stay longer in the system than neutral ones because of the overall anterograde vesicular transport.

New phenotypes are however observed, and *medial*-cargo do not follow the same kinetics as neither *cis* nor *trans*-ones. Indeed, whereas *medial*-cargo hardly interact with boundaries when $K > 1$, *cis* and *trans*-cargo do: *cis*-cargo continuously recycle between ER and Golgi, and *trans*-cargo are quickly addressed to the TGN. Because of that, these two never reach great concentration in the Golgi (between 400 and 500 cargo at $t = 2$). On the contrary, and because they aggregate in *medial*-compartments that hardly interact with the boundaries, the amount of *medial*-cargo peak at much larger values (more than 600 at $t = 2.5$, $K = 10$).

We also observe that all kinetics are delayed, and that the amounts of all cargo peak to higher values. This can be understood considering two cases of cargo transport through the Golgi: either cargo tend to reach TGN quickly (*trans*-cargo),

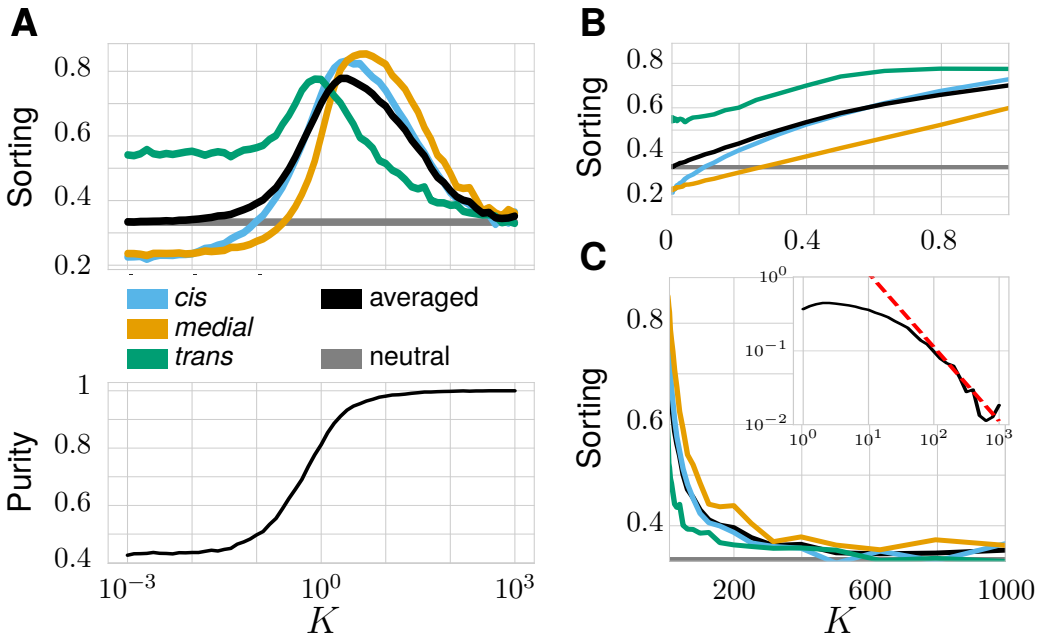

Fig. 4.12: Cargo-proteins sorting in the Golgi, varying their affinity for membrane identities, as a function of K and computed for *cis* (blue) *medial* (orange) *trans* (green) and neutral (grey) cargo. Related to Fig.4.3 – Main results section. $k_{\mathrm{m}} = \alpha = 1$. **A** Sorting of cargo (top panel) as a function of K and its link to the steady-state purity (bottom panel). **B** Sorting for small values of K – plotted in a linear scale. **C** Sorting for large values of K, dotted red line is a fit in Const$/K$ predicted by the analytical model presented in Sec.4.4.6 p.100.

or they randomly follow maturation events before reaching the TGN (*cis* and *medial* cargo in *trans*-compartments). In the first case, the probability to find a *trans*-patch in a immature compartment is low, as an intermediate *medial*-identity delays the formation of *trans*-patches in *cis*-compartments. Thus, *trans*-cargo have to reach a medial compartment, before their affinity becomes efficient in sorting them toward *trans*-compartments. In the second case, cargo have to be surrounded by some *trans*-patches to reach the TGN: patches of membrane surrounding them have to undergo 2 maturation steps (instead of 1) before reaching *trans*-identity, thus delaying their exit to the TGN. In both cases, the dynamics of exit is slowed down, whereas dynamics of injection in the Golgi is not affected: the amounts of all cargo peak to high values.

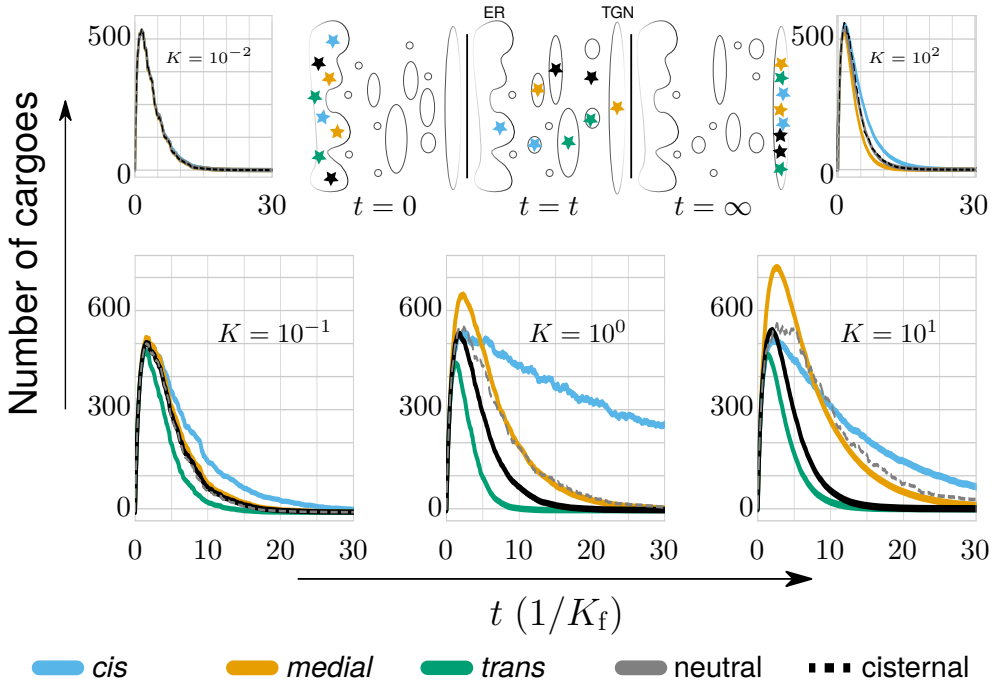

Fig. 4.13: RUSH-like simulation of cargo-proteins transported in a 3-species Golgi, related to Fig.4.4 – Main results section. Number of cargo in the system as a function of time K_{f}^{-1} (normalized by the fusion rate) and computed for *cis* (blue) *medial* (orange), *trans* (green), neutral (grey) and cisternal (dashed) cargo. $k_{\mathrm{m}} = \alpha = 1$. Initially, 1000 cargo of each identity are placed in the ER, and released at $t = 0$. Sketch of the simulation is shown on the top-middle panel.

4.4.6 Analytical models

Compartment composition and cargo sorting in a low K regime (extension of the model introduced in Sec.3.3.3)

In the low budding rate regime, the vesicular transport between compartments is inefficient and system's dynamics can be understood from the dynamics of a single compartment. This is a relevant kinetics to investigate as it defines what biochemical environment is seen by cargo over time. We already know how the overall Golgi mass reaches a steady-state from Eq.4.1, but this mean-field equation does not account for the dynamics of a compartment aggregating mass and maturing. This section presents a simple model of this phenomenon, in the limit $K = 0$ – no budding.

We consider a compartment composed of n_{cis} *cis* and n_{trans} *trans*-patches. The overall mass of the compartment is $n = n_{cis} + n_{trans}$. The compartment aggregates mass over time by homotypically fusion with vesicles at a rate j. The flux j is decomposed in a fraction $\frac{n_{cis}(t)}{n(t)}$ of *cis*-vesicles, and $\frac{n_{trans}(t)}{n(t)}$ of *trans*-vesicles – to satisfy homotypic fusion. Note that j is not strictly identical to J (the injection rate

of *cis*-vesicle in the Golgi), but j is assumed to be proportional to J. Indeed, as a first approximation, a newly injected vesicle can undergo two events: fusing back to the ER with a rate α, or fusing with the compartment (before or after maturation of the vesicle) with an overall rate 1. In this approximation, j scales as $J/(1+\alpha)$. Compartment's *cis*-patches mature with a rate k_{m}.

We assume the compartment starts as a vesicle of *cis*-identity at $t = 0$. The temporal evolution of n, $\dot{n}$ satisfies:

$$\dot{n} = j \Rightarrow n(t) = 1 + j\ t \tag{4.4}$$

The temporal evolution of n_{cis} and n_{trans}, respectively $\dot{n_{cis}}$ and $\dot{n_{trans}}$ satisfy:

$$\dot{n_{cis}} = j \times \frac{n_{cis}(t)}{n(t)} - k_{\mathrm{m}} n_{cis}(t) \Rightarrow n_{cis}(t) = (1 + j\ t)\exp\left(-k_{\mathrm{m}} t\right) \tag{4.5}$$

$$\dot{n_{trans}} = j \times \frac{n_{trans}(t)}{n(t)} + k_{\mathrm{m}} n_{cis}(t) \Rightarrow n_{trans}(t) = (1 + j\ t)(1 - \exp\left(-k_{\mathrm{m}} t\right)) \tag{4.6}$$

Plots of $n_{cis}(t)$ and $n_{trans}(t)$ can be found in Fig.4.14A. The corresponding fraction ϕ_{cis} in *cis* and ϕ_{trans} in *trans*-species in the compartment, as a function of time, is shown in Fig.4.14B. Note this is consistent with simulation data of Sec.4.4.2, p.88.

From now, we did not consider compartment's fusion with the boundaries. This can occur at any time with a rate $\alpha\left(\frac{n_{cis}(t)}{n(t)} + \frac{n_{trans}(t)}{n(t)}\right) = \alpha$. The survival probability $p(t)$, for a compartment created at $t = 0$, to be present in the system at $t = t$ satisfies:

$$p(t + dt) = p(t)(1 - \alpha dt) \Rightarrow p(t) = \exp\left(-\alpha\ t\right) \tag{4.7}$$

We can now compute sorting of *cis* and *trans*-cargo in this compartment. Here, sorting corresponds to the averaged fraction in *cis* (*trans*) species seen by a *cis*

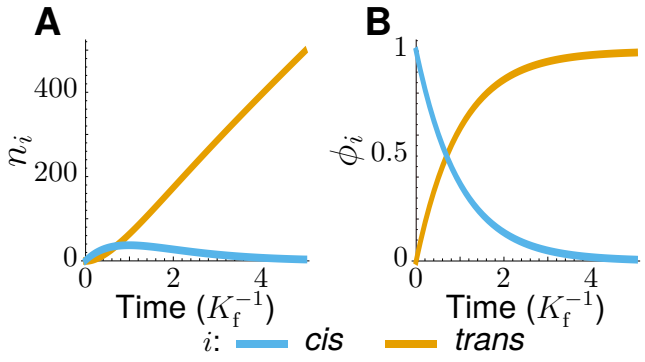

Fig. 4.14: Analytical temporal evolution of compartment's composition in a zero budding rate regime – $K = 0$. **A** Number of i-patches in the compartment as a function of time (normalized by the fusion rate). **B** Fraction of i-patches in the compartment as a function of time. i can be either *cis* (blue) or *trans* (orange).

(*trans*) cargo over time (See Sec.4.4.2, p.87). For a unique i-cargo, sorting is proportional to $\int dt\ p(t)\phi_i(t)$. But one should remember that the amount of cargo increases over time, as cargo can be injected at any time between the creation of the compartment and its exit. The amount of cargo scales linearly with compartment's mass: as sorting is inefficient they all behave like passive cargo. The average sorting values S_{cis} (S_{trans}) for *cis* (*trans*) cargo is thus:

$$S_{cis} = \frac{\int_0^\infty dt\ n_{cis}(t)p(t)}{\int_0^\infty dt\ n(t)p(t)} = \frac{\alpha^2(j + k_\mathrm{m} + \alpha)}{(j + \alpha)(k_\mathrm{m} + \alpha)^2} \tag{4.8}$$

$$S_{trans} = \frac{\int_0^\infty dt\ n_{trans}(t)p(t)}{\int_0^\infty dt\ n(t)p(t)} = \frac{k_\mathrm{m}(\alpha(k_\mathrm{m} + \alpha) + j(k_\mathrm{m} + 2\alpha))}{(j + \alpha)(k_\mathrm{m} + \alpha)^2} \tag{4.9}$$

$k_\mathrm{m} = \alpha = 1$, and $j \sim 10^2$. Previous equation can be simplified in a $k_\mathrm{m} \sim \alpha \ll J$ limit:

$$S_{cis} = \frac{\alpha^2}{(k_\mathrm{m} + \alpha)^2} \tag{4.10}$$

$$S_{trans} = \frac{k_\mathrm{m}^2 + 2\alpha k_\mathrm{m}}{(k_\mathrm{m} + \alpha)^2} \tag{4.11}$$

For $k_\mathrm{m} = \alpha = 1$, this gives a 25% sorting for *cis*-cargo and 75% for *trans*-cargo, which is in good agreement with results in Fig.4.3 – Main results section.

Compartment composition and cargo sorting in a large K regime

In systems with a very high value of K, compartments are mostly vesicular. To better understand this regime, we propose a model to compute the time-average composition of vesicles, and link it to sorting of cargo trapped in them. Then we study a model of compartments' aggregation and dissociation in a high K regime. The aim is to compute the probability to find *cis-trans* dimers in the system, the smallest (hence the most abundant for high budding rate) compartments capable of sorting cargo-proteins in vesicles of different identities.

We consider a *cis*-vesicle injected in the system at time $t = 0$. We name $p_{cis}(t)$ the probability for this vesicle to remain in the system with a *cis*-identity, and $p_{trans}(t)$ the probability this vesicle is still in the system but with a *trans*-identity. This vesicle

can undergo two events: exiting the system with a rate α, or, when it is a *cis*-vesicle, maturing its identity to *trans*. The time variation of p_i, $\dot{p_i}$ ($i =$ *cis* or *trans*) satisfies:

$$\dot{p_{cis}}(t) = -p_{cis}(t)(\alpha + k_{\mathrm{m}}) \Rightarrow p_{cis}(t) = \exp\left[-(k_{\mathrm{m}} + \alpha)t\right] \tag{4.12}$$

$$\dot{p_{trans}}(t) = -p_{trans}(t)\alpha + p_{cis}(t)k_{\mathrm{m}} \Rightarrow p_{trans}(t) = \exp\left[-\alpha t\right] - \exp\left[-(k_{\mathrm{m}} + \alpha)t\right] \tag{4.13}$$

We can now compute sorting of *cis* and *trans*-cargo in this vesicle. Here, sorting corresponds to the averaged fraction in *cis* (*trans*) species seen by a *cis* (*trans*) cargo over time (See Sec.4.4.2, p.87). For a unique i-cargo, sorting is proportional to $\int dt\ p_i(t)$. The average sorting values S_{cis} (S_{trans}) for *cis* (*trans*) cargo is thus:

$$S_{cis} = \frac{\int_0^\infty dt\ p_{cis}(t)}{\int_0^\infty dt\ p_{cis}(t) + p_{trans}(t)} = \frac{1}{k_{\mathrm{m}} + \alpha} \tag{4.14}$$

$$S_{trans} = \frac{\int_0^\infty dt\ p_{trans}(t)}{\int_0^\infty dt\ p_{cis}(t) + p_{trans}(t)} = \frac{k_{\mathrm{m}}}{\alpha(k_{\mathrm{m}} + \alpha)} \tag{4.15}$$

In our simulation, $\alpha = k_{\mathrm{m}} = 1$, and thus both sorting values equal $1/2$.

We now consider a system with a large but finite value of K. We assume each i-species can be either in a vesicle with concentration c_1^i or in a dimer with a concentration c_2^i. We want to compute the average number of heterodimers c_2^* (containing 2 species) that can be formed by maturing a *cis*-dimer. Dimers are formed by homotypic fusion of two identical vesicles, with a rate proportional to the number of possible pairs of the said vesicles. They disassemble with a rate K, multiplied by their size (2) and the number of identities in them (non-linear budding). New *cis*-vesicles are injected in the system with a rate J. All *cis*-patches mature with a rate k_{m}. We assume $c_1^i \gg 1,\ \forall i$. At steady-state, the temporal evolution of the number of *cis*-vesicles c_1^{cis}, *trans*-vesicles c_1^{trans}, *cis*-dimers c_2^{cis}, *trans*-dimers c_2^{trans} and heterodimers c_2^* satisfy:

$$\begin{aligned}
d_t c_1^{cis} = 0 =& J - (c_1^{cis})^2 + 4K(c_2^{cis} + c_2^*) - (\alpha + k_{\mathrm{m}})c_1^{cis} \\
d_t c_2^{cis} = 0 =& \frac{(c_1^{cis})^2}{2} - 2Kc_2^{cis} - (\alpha + 2k_{\mathrm{m}})c_2^{cis} \\
d_t c_1^{trans} = 0 =& -(c_1^{trans})^2 + 4K(c_2^{trans} + c_1^*) - \alpha c_1^{trans} + k_{\mathrm{m}} c_1^{cis} \\
d_t c_2^{trans} = 0 =& \frac{(c_1^{trans})^2}{2} - 2Kc_2^{trans} - \alpha c_2^{trans} + k_{\mathrm{m}} c_2^* \\
d_t c_2^* = 0 =& -4Kc_2^* - (\alpha + k_{\mathrm{m}})c_2^* + 2k_{\mathrm{m}} c_2^{cis}
\end{aligned} \tag{4.16}$$

This system of equations is solvable but gives a complicated analytical result. However, some quantities simplify. The total mass in the system is:

$$c_1^{cis} + 2c_2^{cis} + c_1^{trans} + 2c_2^{trans} + 2c_2^* = J/\alpha$$

The mass of *cis*-elements N_{cis} is:

$$N_{cis} = c_1^{cis} + 2c_2^{cis} + c_2^* = J/(\alpha + k_{\mathrm{m}})$$

The mass of *trans*-elements N_{trans} is:

$$N_{trans} = c_1^{trans} + 2c_2^{trans} + c_2^* = \frac{J\ k_{\mathrm{m}}}{\alpha(\alpha + k_{\mathrm{m}})}$$

All these quantities are consistent with previous analytical developments presented in Sec.2.8.1 and Sec.4.1.

The quantity that is interesting us, c_2^*, does not simplify and gives analytical complicated results. We give its expression at lowest order. For $K \to \infty$, we find:

$$c_2^* = \frac{J^2\ k_{\mathrm{m}}}{8\ (k_{\mathrm{m}} + \alpha)^2\ K^2} + o(1/K^3) = \frac{N_{cis}^2\ k_{\mathrm{m}}}{8\ K^2} + o(1/K^3) \tag{4.17}$$

The budding flux from heterodimers is thus proportional to $\frac{N_{cis}^2\ k_{\mathrm{m}}}{8\ K}$. As steady-state composition and maturation rates are fixed, the only left dependency is the budding rate one, which scales like $1/K$.

4.5 Discussion of chapter's results

It is well-established that variation in local membrane properties can lead to the segregation of proteins. Fundamental properties of biological membranes such as their thickness can affect localization of trans-membrane proteins [SSM10]. More recently, it has been shown that trans-membrane proteins require a direct interaction with budding proteins to maintain their localization, and prevent them from escaping the Golgi to other subcellular compartments [LDK18]. These coatomers also interact with RABs and SNAREs (see Introduction chapter) and it has been shown that altering RABs can alter the sorting of cargo-proteins in the Golgi [CKW16]. Taken together, these results strongly suggest that the dynamics of cargo transport across the Golgi is strongly correlated with the dynamics of the membrane biochemical identity. In this chapter, we propose a theoretical model for how such correlation might take place.

Our philosophy throughout this manuscript, is that large-scale order and temporal correlation at the scale of the entire organelle must emerge from the interplay between different types of local interactions at the scale of molecules. We follow the same approach here, and introduce an affinity of cargo for a specific local membrane identity. In other words, cargo-proteins stick to a membrane of the preferred identity. This impacts how they may leave a compartment by budding: the smaller the fraction of the preferred identity in the compartment, the higher the probability to leave the compartment when preferred identity is budded out. Our main results is that affinity is sufficient to bias vesicular fluxes, sort cargo and change their transport kinetics through the organelle. It results in an anterograde vesicular flux for some cargo, in a system for which the overall transport is retrograde, and reciprocally (Fig.4.2). Such interaction is sufficient to sort different types of cargo in compartments of different compositions (Fig.4.3). And this affects the kinetics of cargo transport through the Golgi (Fig.4.4 and 4.5).

The results presented in Fig.4.2 show that both anterograde and retrograde routes coexist in the same self-organized structure. Any local interaction that alter the effective – coarse-grained – cargo affinity, dramatically bias the vesicular route taken by the said cargo. This idea is not new, as it has been proposed nearly two decades ago by [Orc+00], after publications in which they show COP-I vesicles can be classified in different categories depending on the type of cargo they transport [Orc+97]. In our modelling, these sub-populations are *cis*-vesicles carrying *cis*-cargo that fuse homotypically with immature compartments, and thus in a retrograde fashion – and reciprocally for *trans* vesicles and cargo in anterograde transport. Note that this is not possible for very high budding rates regime, governed by vesicle maturation: cargo are packaged vesicles that mature before fusing with another compartment and vesicular transport is always anterograde.

We also show that these local interactions are sufficient to sort different components in different compartments (Fig.4.3). This echoes the fact that disrupting interactions between Golgi's enzymes and membrane components can dramatically relocalize them [BTT18; Sch+19]. This is true for enzymes but also for other cargo-proteins as shown in [CKW16; FCB14]. Our model predicts that such efficient sorting is only possible in intermediate regimes of purity. Indeed, sorting requires high purity, because in a low purity regime, compartments do not have a well-defined identity and sorting is thus ill-defined. But it requires some mixing for the cargo to exercise its preference for some membrane patches. If cargo is trapped in pure compartment of low affinity, no patch of contaminating species can be found for the cargo to be packaged in, budded and transported to another compartment. The optimal value of budding is thus $K \sim 1$, which corresponds to the end of the purity transition. This also corresponds to a regime in which vesicular transport is anterograde. On the other hand, sorting in "Cisternal maturation" like regimes ($K \lesssim 0.1$) is less effective.

We already speculated in previous chapter (Sec.3.4) that presumably low purity systems like Yeasts' Golgi have different glycozylation patterns [Wan+17] partly because of their purity. The difficulty for these systems to sort enzymes in different compartments can be a key to understand this phenotype.

Finally, these local interactions are sufficient to tune kinetics of cargo transport in the Golgi. Despite the fact that model adjustments seem necessary to reach a quantitative agreement with biological data, these results qualitatively reproduce signatures of *in vivo* processes and bring conceptual tools to interpret them. We show that different cargo-proteins undergo different kinetics of transport through the Golgi, whether considering the whole organelle (Fig.4.4) or individual cisternae (Fig.4.5). This depends on the affinity of cargo-proteins for membrane identity, but steady-state organization also plays a crucial role. For example, we show that changing the affinity of cargo from *cis* to neutral accelerate their kinetics of transport through the Golgi, but it is not the only way of achieving such phenotype: disrupting Golgi's organization, by decreasing budding rate brings the exact same result. New data-bases are currently being built to screen drugs with regard to their effects on cargo transport through the Golgi [Zha+18]. In these studies, they distinguish kinetics alterations that do not alter Golgi structure, to the ones that modify the organelle organization. One next step would be to quantify such drugs following the kinetics of different types of cargo-proteins in the same Golgi, at the same time. Indeed, we predict that drugs that affect Golgi's organization, decrease the differences of kinetics between cargo of different affinities. Some cargo-proteins are already known to be fast cargo (TNF-α), and other quite slow ones (cadherin), and could be used for this purpose.

5 Discussion

The ability of organelles to achieve robustness in their structure and dynamics is particularly intriguing. These structures manage to stabilize a steady-state organization while being constantly mixed by passive and energy consuming mechanisms. Quite remarkably, actors tuning organelles properties are much smaller than compartments constituting them, compartments that however organize and act on large scales in cells. Two proteins in different Golgi cisternae cannot dialog with one another, but their respective roles are well integrated into the overall organelle's function. And it is even more impressive when considering the fact that each organelle is not dedicated to one but multiple interplaying functions, and that cells keep control on organelles and can drastically modify their structures and functions if needed.

One could expect the amount of actors required to organize, stabilize and control these organelles to be enormous. It is difficult to say what is a large number of different types of proteins in a biological system and what is not. But considering all the different functions interplaying in the Golgi, less than one thousand different proteins is little [Atl], without even considering that $3/4$ of them are redundant and locate in other compartments as well. One would probably have a lot of difficulties to build a biochemical network fulfilling all Golgi's functions in one unique compartments, in a robust and controlled fashion. That is why we are convinced that structure itself is a support for information, which can be used to decrease the amount of actors interplaying to build organelles and tune their dynamics.

This is the general idea we adopted in the present manuscript, in which we drastically limit the number of mechanisms acting on organelles. Our modeling shows that structures spontaneously emerge from the interplay between three basic mechanisms: the biochemical maturation of membrane identities, the vesicular budding, and inter-compartment fusion. Although these mechanisms only act locally on Golgi membranes, the rate at which they modify organelles is tuned by the system's composition. Steady-state thus results from a continuous feedback between mechanisms creating the organization and the organization tuning the rates of each mechanism.

Chapter 3 shows that our model gives rise to a rich diversity of Golgi structures, depending on the mechanisms' kinetics. The first result is that steady-states can

exhibit either large or small compartments depending on the ratio of budding to fusion rate. But this is not the only effect of budding mechanism. Indeed, vesicular budding is also a sorting mechanism, as it allows the removal of contaminating species in compartments by budding them out. This sorting mechanism competes with mixing mechanisms occurring in the Golgi. Biochemical maturation is one mixing mechanism of great importance: it stochastically changes identity of membrane patches in compartments so that pure compartments containing only one species are never a stable configuration. At steady-state, two regimes of purity can be described: an impure regime if mixing is faster than sorting in compartments, and reciprocally a pure regime when sorting is faster than mixing. Combining compartments' sizes and their purity, we describe three typical steady-state organization:

- A mixed regime, where mixing mechanisms are faster than sorting mechanisms. Budding rate is low in such regimes, thus compartments are large. Maturation is fast and thus cisternae undergo maturation of their identities over time.

- A vesicular regime, where sorting mechanisms are much faster than mixing ones. Budding rate is high in this regime and compartments dissociate into small but pure vesicles.

- A sorted regime where mixing and sorting mechanisms are of the same kinetics. This intermediate regime exhibit a steady-state in which compartments are rather big and rather pure.

The directionality of vesicular transport spontaneously emerges from this steady-state, and is affected by the exact same mechanisms that the ones defining Golgi's structures. It is intimately linked to the Golgi's structure and relies on what mechanism is the fastest between mixing and sorting. Indeed, it relies on the general concept of contaminating species in compartments, that can be understood as follows. In a compartment coexist two types of species, one that is the majority species, one that is minority. If the first one buds out, there is a high probability for it to homotypically fuse back into the same compartment, yielding no vesicular transport. If the second one buds out, it has to fuse into a compartment of different identity than the budding one, creating a vesicular flux. Depending on whether sorting is faster or slower than mixing mechanisms, two cases can be predicted:

- If sorting is faster, contaminating species in compartments are the ones that just underwent maturation. If budded in a vesicle, the vesicle is of a more mature identity than the average identity of the budding compartment, and fuses homotypically with a more mature compartment: vesicular transport is anterograde.

- If mixing is faster, contaminating species in compartments are the ones that have not undergone maturation yet. If budded in a vesicle, the vesicle is of a less mature identity than the average identity of the budding compartment, and fuses homotypically with a less mature compartment: vesicular transport is retrograde.

We identify the concomitance of a structural transition (from mixed to pure compartments) and a dynamical transition (from retrograde to anterograde vesicular exchange). We think this is a very general rule, which subsumes the two classical models of Golgi apparatus that are the “Vesicular exchange” (fixed cisternae and anterograde vesicular flux) and “Cisternal maturation” models (maturing cisternae and retrograde flux of vesicles).

In details, some adaptations of current implementations could however be discussed:

- Within our model, anterograde vesicular transport is accompanied by many spurious events of vesicle back-fusion into the same compartment. This comes from the fact that contaminating species and majority identities have the same budding flux out of compartments. Although back fusion could certainly take place in the Golgi, it could be argued that it constitutes a waste of energy, and that processes could have evolved to limit its importance. From a meddling point of view, this could be achieved by more complicated budding kernels that prevent budding of the majority species. What biochemical mechanism could drive such phenomenon is an open question, but phase separation of different identities with preferred location of the contaminating one toward the rim of cisternae (where budding occurs *in vivo*), could be a candidate.

- For very high budding rates, compartments are very pure and anterograde transport is dominated by vesicles undergoing maturation *after* budding. In our model, such vesicle maturation events, which have been described in the secretory pathway as a way to direct vesicular traffic and to prevent vesicles back-fusion [Lor+11], only occur when compartments are very small (high budding rate). But one could argue vesicular maturation exists within the Golgi at all budding rates, considering un-coating of vesicles as a maturation process.

- We do not consider spatial or mechanical dependencies, that could, for example, prevent fusion between very large structures. Modeling the proteic matrix that tunes the spatial and mechanical environment around the Golgi, and how it affects mixing and sorting mechanism is probably an important step to reach quantitative agreement with biological data. Cisternal stabilizers like GRASP

or vesicles careers like Golgins, known to already be present in the ancestor of eukaryotes [Bar+18], are obvious candidates.

Although more complex models, and in particular the inclusion of spatial dependencies, are surely relevant to organelle's dynamics, the fundamental relationship between kinetics, structure and transport highlighted by our model is a universal feature of the interplay between biochemical maturation and vesicular exchange in cellular organelles.

Chapter 4 shows that the routes of vesicular transport within the Golgi are very flexible. Local interactions between cargo-proteins and compartments' membrane identities are sufficient to bias vesicular transport. Cargo with strong affinity for immature membrane species have a natural tendency to follow a retrograde transport, whereas cargo with strong affinity for mature membranes undergo anterograde transport. Both routes coexist within the same structure, and thus independently of the overall vesicular transport. This result however raises the following question: *in vivo* can we track transport directionality in the Golgi, following cargo? Indeed, all interactions that can be coarse-grained into an effective affinity, can alter vesicular transport. We think it is more relevant to consider these systems as natively supporting bi-directionality of inter compartment exchanges, as proposed in [Orc+00]. One notable counter-argument would be to show that vesicles themselves undergo maturation *after* budding. In such case, vesicular transport is always anterograde, independently of affinity.

Parallel routes of vesicular transport can sort cargo-proteins in different compartments at steady-state. On average, cargo reside in compartments for which they have a strong affinity. This is however organization-dependent and not all types of Golgi exhibit an efficient sorting of cargo. One important conclusion of our study is that sorting is most efficient for intermediate values of the budding rate, when compartment are fairly pure, but not perfectly pure. It requires some purity, because when mixing mechanisms of compartments are faster than sorting ones, compartments' identity is ill-defined and so is cargo sorting. But cargo sorting also relies on some mixing: for a cargo to make use of its affinity, it must be exposed to at least 2 different identities of membrane, one for which it has a strong affinity, and a low one for the other. Without some mixing, cargo are trapped in compartments of pure composition. The optimum in cargo sorting corresponds to regimes in which sorting mechanisms of membrane patches are slightly faster than mixing ones. We show this is a regime of anterograde vesicular transport on average, with cisternae of fixed identities. Note that sorting is not totally abolished for in systems characterized by cisternal maturation, but it is less efficient.

Following cargo-proteins is a crucial point to investigate within our model, as it allows direct comparisons with biological data. We show that kinetics of cargo transport through the Golgi emerge from both the steady-state structure and local interactions between cargo and membrane identities. The system's capacity to exhibit different residing times for different cargo, strongly correlates with its capacity to sort them in different compartments. When cargo sorting is efficient, cargo with strong affinity for immature compartments stay longer in the Golgi than cargo with affinity for mature membranes.

As it allows us to directly compare our results with real measurements, it also brings interesting information on the model limitations, and what should be modified to reach a quantitative agreement with biological data:

- From now, there is no cooperativity in maturation mechanisms, and membrane patches mature with the same rate independently of the surrounding environment. But we observe it is not the case *in vivo* [Mat+06; Los+06; Cas+19]. Implementing cooperativity in maturation would delay the process for pure compartments, and accelerate it during the transition from one identity to the next. This would let time for individual cisternae to reach large sizes before starting maturing, and exhibit a burst of retrograde vesicles during the transition of identity, which is suggested by recent experiments [Cas+19].

- We show that the number of identities in the Golgi does not dramatically alter the different results we present here. However, it does have an impact on the residing time of cargo with strong affinity for immature compartments. The more identities, the more their exit to the TGN is delayed. In the present implementation, cargo-proteins cannot be retained for arbitrary long time in the system. Adding more Golgi identities would be one way to tackle this issue. Another way to achieve the same goal would be to modify the fusion mechanism between different compartments: current implementation is very permissive and allows fusion of large compartments together or even with the exit. Removing this system's feature would prevent major leaks of cargoes toward the exits, without modifying the number of Golgi identities that can be constrained otherwise. For example, we can imagine that the Golgi needs a strict number of different compartments for the cargo to experience a strict amount of steps in their glycozylation process: the number of different identities required has been inferred to be 3 [JT18].

There is thus a lot to be done to fully understand the organization and dynamics of intracellular organelles. But we strongly believe that this work represents a substantial step toward a quantitative understanding of the structure and dynamics of the Golgi apparatus, with far-reaching implications for cellular organelles in general.

Probably the most important message, is that the Golgi displays an optimum in structural organization, cargo sorting and vesicular transport flexibility, when mixing and sorting mechanisms are of the same magnitude. It is conceptually interesting as it highlights the fact that all mechanisms are equally important within organelles, and none of them should be neglected when modelling these systems. But it also has practical implications: it is very close to a pure-impure, anterograde-retrograde vesicular transport transition. If biological systems reside in this optimum, with the exact same mechanisms, even slight modifications of the rates could alter their phenotype in a major way, and explain all the diversity and controversies surrounding the Golgi apparatus.

Bibliography

[ABW90] Kathy R. Albe, Margaret H. Butler, and Barbara E. Wright. „Cellular concentrations of enzymes and their substrates“. In: *Journal of Theoretical Biology* 143.2 (Mar. 1990), pp. 163–195. DOI: 10.1016/S0022-5193(05)80266-8 (cit. on p. 3).

[Ant+00] W. Antonin, C. Holroyd, R. Tikkanen, S. Höning, and R. Jahn. „The R-SNARE endobrevin/VAMP-8 mediates homotypic fusion of early endosomes and late endosomes“. eng. In: *Molecular Biology of the Cell* 11.10 (Oct. 2000), pp. 3289–3298 (cit. on p. 26).

[Atl] The Human Protein Atlas. *The human cell in golgi apparatus - The Human Protein Atlas* (cit. on p. 105).

[Bar+18] Lael D. Barlow, Eva Nývltová, Maria Aguilar, Jan Tachezy, and Joel B. Dacks. „A sophisticated, differentiated Golgi in the ancestor of eukaryotes“. In: *BMC Biology* 16 (Mar. 2018), p. 27. DOI: 10.1186/s12915-018-0492-9 (cit. on pp. 17, 108).

[Bev+02] Brooke J. Bevis, Adam T. Hammond, Catherine A. Reinke, and Benjamin S. Glick. „De novo formation of transitional ER sites and Golgi structures in Pichia pastoris“. en. In: *Nature Cell Biology* 4.10 (Oct. 2002), pp. 750–756. DOI: 10.1038/ncb852 (cit. on p. 5).

[BG04] Juan S. Bonifacino and Benjamin S. Glick. „The mechanisms of vesicle budding and fusion“. eng. In: *Cell* 116.2 (Jan. 2004), pp. 153–166 (cit. on pp. 26, 29).

[Bha+14] Madhura Bhave, Effrosyni Papanikou, Prasanna Iyer, et al. „Golgi enlargement in Arf-depleted yeast cells is due to altered dynamics of cisternal maturation“. eng. In: *Journal of Cell Science* 127.Pt 1 (Jan. 2014), pp. 250–257. DOI: 10.1242/jcs.140996 (cit. on pp. 26, 72).

[Bin+09] Bernd Binder, Andrean Goede, Nikolaus Berndt, and Hermann-Georg Holzhütter. „A conceptual mathematical model of the dynamic self-organisation of distinct cellular organelles“. eng. In: *PloS One* 4.12 (Dec. 2009), e8295. DOI: 10.1371/journal.pone.0008295 (cit. on pp. 20, 24).

[Bon+12] Gaelle Boncompain, Severine Divoux, Nelly Gareil, et al. „Synchronization of secretory protein traffic in populations of cells“. eng. In: *Nature Methods* 9.5 (Mar. 2012), pp. 493–498. DOI: 10.1038/nmeth.1928 (cit. on pp. 82, 83).

[Bon+98] L. Bonfanti, A. A. Mironov, J. A. Martínez-Menárguez, et al. „Procollagen traverses the Golgi stack without leaving the lumen of cisternae: evidence for cisternal maturation“. eng. In: *Cell* 95.7 (Dec. 1998), pp. 993–1003 (cit. on pp. 74, 82).

[BP13] Gaelle Boncompain and Franck Perez. „The many routes of Golgi-dependent trafficking“. eng. In: *Histochemistry and Cell Biology* 140.3 (Sept. 2013), pp. 251–260. DOI: 10.1007/s00418-013-1124-7 (cit. on pp. 24, 30).

[BPM18] Yinon M. Bar-On, Rob Phillips, and Ron Milo. „The biomass distribution on Earth“. en. In: *Proceedings of the National Academy of Sciences* 115.25 (June 2018), pp. 6506–6511. DOI: 10.1073/pnas.1711842115 (cit. on p. 2).

[BS09] Annika Budnik and David J. Stephens. „ER exit sites–localization and control of COPII vesicle formation“. eng. In: *FEBS letters* 583.23 (Dec. 2009), pp. 3796–3803. DOI: 10.1016/j.febslet.2009.10.038 (cit. on p. 86).

[BS13] Mariana G. Bexiga and Jeremy C. Simpson. „Human diseases associated with form and function of the Golgi complex“. eng. In: *International Journal of Molecular Sciences* 14.9 (Sept. 2013), pp. 18670–18681. DOI: 10.3390/ijms140918670 (cit. on p. 14).

[BTT18] Jessica L. Becker, Duy T. Tran, and Lawrence A. Tabak. „Members of the GalNAc-T family of enzymes utilize distinct Golgi localization mechanisms“. eng. In: *Glycobiology* 28.11 (2018), pp. 841–848. DOI: 10.1093/glycob/cwy071 (cit. on p. 103).

[Buc+00] C. Bucci, P. Thomsen, P. Nicoziani, J. McCarthy, and B. van Deurs. „Rab7: a key to lysosome biogenesis“. eng. In: *Molecular Biology of the Cell* 11.2 (Feb. 2000), pp. 467–480. DOI: 10.1091/mbc.11.2.467 (cit. on p. 8).

[Cas+19] Jason C. Casler, Effrosyni Papanikou, Juan J. Barrero, and Benjamin S. Glick. „Maturation-driven transport and AP-1dependent recycling of a secretory cargo in the Golgi“. en. In: *The Journal of Cell Biology* 218.5 (May 2019), pp. 1582–1601. DOI: 10.1083/jcb.201807195 (cit. on pp. 85, 86, 88, 109).

[CGO10] Joseph R. Casey, Sergio Grinstein, and John Orlowski. „Sensors and regulators of intracellular pH“. en. In: *Nature Reviews Molecular Cell Biology* 11.1 (Jan. 2010), pp. 50–61. DOI: 10.1038/nrm2820 (cit. on p. 13).

[CKW16] John V. Cox, Rita Kansal, and Michael A. Whitt. „Rab43 regulates the sorting of a subset of membrane protein cargo through the medial Golgi“. eng. In: *Molecular Biology of the Cell* 27.11 (2016), pp. 1834–1844. DOI: 10.1091/mbc.E15-03-0123 (cit. on pp. 102, 103).

[CRF07] Huaqing Cai, Karin Reinisch, and Susan Ferro-Novick. „Coats, tethers, Rabs, and SNAREs work together to mediate the intracellular destination of a transport vesicle“. eng. In: *Developmental Cell* 12.5 (May 2007), pp. 671–682. DOI: 10.1016/j.devcel.2007.04.005 (cit. on pp. 9, 26, 28).

[CS13] Dean Clift and Melina Schuh. „Re-starting life: Fertilization and the transition from meiosis to mitosis“. In: *Nature reviews. Molecular cell biology* 14.9 (Sept. 2013), pp. 549–562. DOI: 10.1038/nrm3643 (cit. on p. 2).

[De +09] Pablo M. De Biase, Damián Alvarez Paggi, Fabio Doctorovich, et al. „Molecular Basis for the Electric Field Modulation of Cytochrome c Structure and Function“. In: *Journal of the American Chemical Society* 131.44 (Nov. 2009), pp. 16248–16256. DOI: 10.1021/ja906726n (cit. on p. 7).

[Del+08] Perla Del Conte-Zerial, Lutz Brusch, Jochen C. Rink, et al. „Membrane identity and GTPase cascades regulated by toggle and cut-out switches“. eng. In: *Molecular Systems Biology* 4 (2008), p. 206. DOI: 10.1038/msb.2008.45 (cit. on p. 9).

[DRS13] Serge Dmitrieff, Madan Rao, and Pierre Sens. „Quantitative analysis of intra-Golgi transport shows intercisternal exchange for all cargo“. eng. In: *Proceedings of the National Academy of Sciences of the United States of America* 110.39 (Sept. 2013), pp. 15692–15697. DOI: 10.1073/pnas.1303358110 (cit. on pp. 17, 20, 73).

[DS11] S. Dmitrieff and P. Sens. „Cooperative protein transport in cellular organelles“. eng. In: *Physical Review. E, Statistical, Nonlinear, and Soft Matter Physics* 83.4 Pt 1 (Apr. 2011), p. 041923. DOI: 10.1103/PhysRevE.83.041923 (cit. on pp. 20, 26, 29, 33).

[DSG13] Kasey J. Day, L. Andrew Staehelin, and Benjamin S. Glick. „A Three-Stage Model of Golgi Structure and Function“. In: *Histochemistry and cell biology* 140.3 (Sept. 2013), pp. 239–249. DOI: 10.1007/s00418-013-1128-3 (cit. on p. 28).

[Dun+17] Myun Hwa Dunlop, Andreas M. Ernst, Lena K. Schroeder, et al. „Land-locked mammalian Golgi reveals cargo transport between stable cisternae“. eng. In: *Nature Communications* 8.1 (2017), p. 432. DOI: 10.1038/s41467-017-00570-z (cit. on pp. vii, ix, 17, 72, 73).

[ES81] L. Ernster and G. Schatz. „Mitochondria: a historical review.“ en. In: *The Journal of Cell Biology* 91.3 (Dec. 1981), 227s–255s. DOI: 10.1083/jcb.91.3.227s (cit. on p. 2).

[FCB14] Matteo Fossati, Sara F. Colombo, and Nica Borgese. „A positive signal prevents secretory membrane cargo from recycling between the Golgi and the ER“. eng. In: *The EMBO journal* 33.18 (Sept. 2014), pp. 2080–2097. DOI: 10.15252/embj.201488367 (cit. on p. 103).

[Fes+94] Riccardo Fesce, Fabio Grohovaz, Flavia Valtorta, and Jacopo Meldolesi. „Neurotransmitter release: fusion or kiss-and-run?“ In: *Trends in Cell Biology* 4.1 (Jan. 1994), pp. 1–4. DOI: 10.1016/0962-8924(94)90025-6 (cit. on p. 9).

[Gil77] Daniel T. Gillespie. „Exact stochastic simulation of coupled chemical reactions“. In: *The Journal of Physical Chemistry* 81.25 (Dec. 1977), pp. 2340–2361. DOI: 10.1021/j100540a008 (cit. on pp. 27, 32).

[GL11] Benjamin S. Glick and Alberto Luini. „Models for Golgi Traffic: A Critical Assessment“. In: *Cold Spring Harbor Perspectives in Biology* 3.11 (Nov. 2011). DOI: 10.1101/cshperspect.a005215 (cit. on pp. 15, 26, 29).

[Gli02] Benjamin S. Glick. „Can the Golgi form de novo?“ en. In: *Nature Reviews Molecular Cell Biology* 3.8 (Aug. 2002), pp. 615–619. DOI: 10.1038/nrm877 (cit. on pp. 5, 15).

[Gon+10] Haijun Gong, Yusong Guo, Adam Linstedt, and Russell Schwartz. „Discrete, continuous, and stochastic models of protein sorting in the Golgi apparatus“. eng. In: *Physical Review. E, Statistical, Nonlinear, and Soft Matter Physics* 81.1 Pt 1 (Jan. 2010), p. 011914. DOI: 10.1103/PhysRevE.81.011914 (cit. on pp. 20, 24).

[GON06] Bianka L. Grosshans, Darinel Ortiz, and Peter Novick. „Rabs and their effectors: Achieving specificity in membrane traffic“. en. In: *Proceedings of the National Academy of Sciences* 103.32 (Aug. 2006), pp. 11821–11827. DOI: 10.1073/pnas.0601617103 (cit. on pp. vii, 8, 9, 26).

[GS86] G. Griffiths and K. Simons. „The trans Golgi network: sorting at the exit site of the Golgi complex“. en. In: *Science* 234.4775 (Oct. 1986), pp. 438–443. DOI: 10.1126/science.2945253 (cit. on p. 12).

[HC14] Rebecca Heald and Orna Cohen-Fix. „Morphology and function of membrane-bound organelles“. eng. In: *Current Opinion in Cell Biology* 26 (Feb. 2014), pp. 79–86. DOI: 10.1016/j.ceb.2013.10.006 (cit. on p. 23).

[Hir+98] Koret Hirschberg, Chad M. Miller, Jan Ellenberg, et al. „Kinetic Analysis of Secretory Protein Traffic and Characterization of Golgi to Plasma Membrane Transport Intermediates in Living Cells“. en. In: *The Journal of Cell Biology* 143.6 (Dec. 1998), pp. 1485–1503. DOI: 10.1083/jcb.143.6.1485 (cit. on p. 29).

[Hoe+14] Marion C Hoepflinger, Christina Hametner, Takashi Ueda, and Ilse Foissner. „Vesicular trafficking in characean green algae and the possible involvement of a VAMP72-family protein“. In: *Plant Signaling & Behavior* 9 (Mar. 2014). DOI: 10.4161/psb.28466 (cit. on p. 10).

[IM13] Iaroslav Ispolatov and Anne Müsch. „A model for the self-organization of vesicular flux and protein distributions in the Golgi apparatus“. eng. In: *PLoS computational biology* 9.7 (2013), e1003125. DOI: 10.1371/journal.pcbi.1003125 (cit. on pp. 20, 24).

[Iye+18] Prasanna Iyer, Madhura Bhave, Bhawik Kumar Jain, Sudeshna RoyChowdhury, and Dibyendu Bhattacharyya. „Vps74p controls Golgi size in an Arf1-dependent manner“. eng. In: *FEBS letters* (Oct. 2018). DOI: 10.1002/1873-3468.13266 (cit. on p. 72).

[JT18] Anjali Jaiman and Mukund Thattai. „Algorithmic biosynthesis of eukaryotic glycans“. en. In: *bioRxiv* (Oct. 2018), p. 440792. DOI: 10.1101/440792 (cit. on p. 109).

[JWV16] Catherine L. Jackson, Laurence Walch, and Jean-Marc Verbavatz. „Lipids and Their Trafficking: An Integral Part of Cellular Organization“. eng. In: *Developmental Cell* 39.2 (2016), pp. 139–153. DOI: 10.1016/j.devcel.2016.09.030 (cit. on pp. 6, 9, 13).

[Kel85] R. B. Kelly. „Pathways of protein secretion in eukaryotes“. eng. In: *Science (New York, N.Y.)* 230.4721 (Oct. 1985), pp. 25–32 (cit. on p. 28).

[Kim+16] Jane J. Kim, Zhanna Lipatova, Uddalak Majumdar, and Nava Segev. „Regulation of Golgi Cisternal Progression by Ypt/Rab GTPases“. eng. In: *Developmental Cell* 36.4 (Feb. 2016), pp. 440–452. DOI: 10.1016/j.devcel.2016.01.016 (cit. on p. viii).

[Kle+09] Robin W. Klemm, Christer S. Ejsing, Michal A. Surma, et al. „Segregation of sphingolipids and sterols during formation of secretory vesicles at the trans-Golgi network“. eng. In: *The Journal of Cell Biology* 185.4 (May 2009), pp. 601–612. DOI: 10.1083/jcb.200901145 (cit. on p. 30).

[KMD11] Mary J. Klute, Paul Melançon, and Joel B. Dacks. „Evolution and diversity of the Golgi“. eng. In: *Cold Spring Harbor Perspectives in Biology* 3.8 (Aug. 2011), a007849. DOI: 10.1101/cshperspect.a007849 (cit. on p. 24).

[Küh+10] Jens Kühnle, Julian Shillcock, Ole G. Mouritsen, and Matthias Weiss. „A modeling approach to the self-assembly of the Golgi apparatus“. eng. In: *Biophysical Journal* 98.12 (June 2010), pp. 2839–2847. DOI: 10.1016/j.bpj.2010.03.035 (cit. on pp. 18, 24).

[Küh+11] Thomas Kühn, Teemu O. Ihalainen, Jari Hyväluoma, et al. „Protein Diffusion in Mammalian Cell Cytoplasm“. In: *PLoS ONE* 6.8 (Aug. 2011). DOI: 10.1371/journal.pone.0022962 (cit. on p. 3).

[Lad+99] Mark S. Ladinsky, David N. Mastronarde, J. Richard McIntosh, Kathryn E. Howell, and L. Andrew Staehelin. „Golgi Structure in Three Dimensions: Functional Insights from the Normal Rat Kidney Cell“. In: *The Journal of Cell Biology* 144.6 (Mar. 1999), pp. 1135–1149 (cit. on p. 13).

[LDK18] Lin Liu, Balraj Doray, and Stuart Kornfeld. „Recycling of Golgi glycosyltransferases requires direct binding to coatomer“. eng. In: *Proceedings of the National Academy of Sciences of the United States of America* 115.36 (2018), pp. 8984–8989. DOI: 10.1073/pnas.1810291115 (cit. on p. 102).

[Lev+10] Stephanie K. Levi, Dibyendu Bhattacharyya, Rita L. Strack, Jotham R. Austin, and Benjamin S. Glick. „The Yeast GRASP Grh1 Colocalizes with COPII and Is Dispensable for Organizing the Secretory Pathway“. In: *Traffic (Copenhagen, Denmark)* 11.9 (Sept. 2010), pp. 1168–1179. DOI: 10.1111/j.1600-0854.2010.01089.x (cit. on p. 74).

[LM10] Nick Lane and William Martin. „The energetics of genome complexity“. en. In: *Nature* 467.7318 (Oct. 2010), pp. 929–934. DOI: 10.1038/nature09486 (cit. on p. 7).

[Lor+11] Christopher Lord, Deepali Bhandari, Shekar Menon, et al. „Sequential interactions with Sec23 control the direction of vesicle traffic“. In: *Nature* 473.7346 (May 2011), pp. 181–186. DOI: 10.1038/nature09969 (cit. on p. 107).

[Lor+17] Joseph H. Lorent, Blanca Diaz-Rohrer, Xubo Lin, et al. „Structural determinants and functional consequences of protein affinity for membrane rafts“. En. In: *Nature Communications* 8.1 (Oct. 2017), p. 1219. DOI: 10.1038/s41467-017-01328-3 (cit. on p. 6).

[Los+06] Eugene Losev, Catherine A. Reinke, Jennifer Jellen, et al. „Golgi maturation visualized in living yeast“. en. In: *Nature* 441.7096 (June 2006), pp. 1002–1006. DOI: 10.1038/nature04717 (cit. on pp. vii, ix, 16, 26, 73, 74, 109).

[LRH00] J. Lippincott-Schwartz, T. H. Roberts, and K. Hirschberg. „Secretory protein trafficking and organelle dynamics in living cells“. eng. In: *Annual Review of Cell and Developmental Biology* 16 (2000), pp. 557–589. DOI: 10.1146/annurev.cellbio.16.1.557 (cit. on pp. 23, 24).

[Mar+04] Brad J. Marsh, Niels Volkmann, J. Richard McIntosh, and Kathryn E. Howell. „Direct continuities between cisternae at different levels of the Golgi complex in glucose-stimulated mouse islet beta cells“. eng. In: *Proceedings of the National Academy of Sciences of the United States of America* 101.15 (Apr. 2004), pp. 5565–5570. DOI: 10.1073/pnas.0401242101 (cit. on p. 29).

[Mar+07] Pierfrancesco Marra, Lorena Salvatore, Alexander Mironov, et al. „The biogenesis of the Golgi ribbon: the roles of membrane input from the ER and of GM130“. eng. In: *Molecular Biology of the Cell* 18.5 (May 2007), pp. 1595–1608. DOI: 10.1091/mbc.E06-10-0886 (cit. on p. 28).

[Mat+06] Kumi Matsuura-Tokita, Masaki Takeuchi, Akira Ichihara, Kenta Mikuriya, and Akihiko Nakano. „Live imaging of yeast Golgi cisternal maturation“. eng. In: *Nature* 441.7096 (June 2006), pp. 1007–1010. DOI: 10.1038/nature04737 (cit. on pp. 16, 26, 28, 74, 109).

[Maz99] Paolo Mazzarello. „A unifying concept: the history of cell theory“. En. In: *Nature Cell Biology* 1.1 (May 1999), E13. DOI: 10.1038/8964 (cit. on p. 2).

[Mis01] T. Misteli. „The concept of self-organization in cellular architecture“. eng. In: *The Journal of Cell Biology* 155.2 (Oct. 2001), pp. 181–185. DOI: 10.1083/jcb.200108110 (cit. on p. 5).

[MM04] Harvey T. McMahon and Ian G. Mills. „COP and clathrin-coated vesicle budding: different pathways, common approaches“. eng. In: *Current Opinion in Cell Biology* 16.4 (Aug. 2004), pp. 379–391. DOI: 10.1016/j.ceb.2004.06.009 (cit. on pp. vii, 9).

[MM06] Vivek Malhotra and Satyajit Mayor. „Cell biology: The Golgi grows up“. en. In: *Nature* 441.7096 (June 2006), pp. 939–940. DOI: 10.1038/441939a (cit. on p. 15).

[MO14] Shankar Mukherji and Erin K. O'Shea. „Mechanisms of organelle biogenesis govern stochastic fluctuations in organelle abundance“. eng. In: *eLife* 3 (June 2014), e02678 (cit. on p. 24).

[MR19] Erick Martins Ratamero and Stephen J Royle. „Calculating the maximum capacity of intracellular transport vesicles“. en. In: *bioRxiv* (Feb. 2019). DOI: 10.1101/555813 (cit. on p. 87).

[Orc+00] L. Orci, M. Ravazzola, A. Volchuk, et al. „Anterograde flow of cargo across the golgi stack potentially mediated via bidirectional "percolating" COPI vesicles“. eng. In: *Proceedings of the National Academy of Sciences of the United States of America* 97.19 (Sept. 2000), pp. 10400–10405. DOI: 10.1073/pnas.190292497 (cit. on pp. 103, 108).

[Orc+97] L. Orci, M. Stamnes, M. Ravazzola, et al. „Bidirectional transport by distinct populations of COPI-coated vesicles“. eng. In: *Cell* 90.2 (July 1997), pp. 335–349 (cit. on pp. 14, 103).

[Pap+15] Effrosyni Papanikou, Kasey J. Day, Jotham Austin, and Benjamin S. Glick. „COPI selectively drives maturation of the early Golgi“. eng. In: *eLife* 4 (Dec. 2015). DOI: 10.7554/eLife.13232 (cit. on pp. viii, 9, 72).

[Pfe01] Suzanne R Pfeffer. „Rab GTPases: specifying and deciphering organelle identity and function“. In: *Trends in Cell Biology* 11.12 (Dec. 2001), pp. 487–491. DOI: 10.1016/S0962-8924(01)02147-X (cit. on p. 8).

[Pfe10] Suzanne R. Pfeffer. „How the Golgi works: a cisternal progenitor model“. eng. In: *Proceedings of the National Academy of Sciences of the United States of America* 107.46 (Nov. 2010), pp. 19614–19618. DOI: 10.1073/pnas.1011016107 (cit. on pp. viii, 26).

[Pfe17] Suzanne R. Pfeffer. „Rab GTPases: master regulators that establish the secretory and endocytic pathways“. In: *Molecular Biology of the Cell* 28.6 (Mar. 2017), pp. 712–715. DOI: 10.1091/mbc.e16-10-0737 (cit. on pp. 8, 9).

[PG09] Effrosyni Papanikou and Benjamin S. Glick. „The yeast Golgi apparatus: insights and mysteries“. eng. In: *FEBS letters* 583.23 (Dec. 2009), pp. 3746–3751. DOI: 10.1016/j.febslet.2009.10.072 (cit. on p. 16).

[PG14] Effrosyni Papanikou and Benjamin S. Glick. „Golgi Compartmentation and Identity“. In: *Current opinion in cell biology* 0 (Aug. 2014), pp. 74–81. DOI: 10.1016/j.ceb.2014.04.010 (cit. on p. 13).

[PL03] Sapna Puri and Adam D. Linstedt. „Capacity of the golgi apparatus for biogenesis from the endoplasmic reticulum“. eng. In: *Molecular Biology of the Cell* 14.12 (Dec. 2003), pp. 5011–5018. DOI: 10.1091/mbc.E03-06-0437 (cit. on p. 18).

[PM06] Matthew Y. Pecot and Vivek Malhotra. „The Golgi apparatus maintains its organization independent of the endoplasmic reticulum“. eng. In: *Molecular Biology of the Cell* 17.12 (Dec. 2006), pp. 5372–5380. DOI: 10.1091/mbc.E06-06-0565 (cit. on p. 13).

[Pre+97] J. F. Presley, N. B. Cole, T. A. Schroer, et al. „ER-to-Golgi transport visualized in living cells“. eng. In: *Nature* 389.6646 (Sept. 1997), pp. 81–85. DOI: 10.1038/38001 (cit. on p. 30).

[Pyl+18] Olena Pylypenko, Hussein Hammich, I.-Mei Yu, and Anne Houdusse. „Rab GTPases and their interacting protein partners: Structural insights into Rab functional diversity“. In: *Small GTPases* 9.1-2 (Mar. 2018), pp. 22–48. DOI: 10.1080/21541248.2017.1336191 (cit. on p. 8).

[RC12] Sean O. Ryan and Brian A. Cobb. „Roles for major histocompatibility complex glycosylation in immune function“. eng. In: *Seminars in Immunopathology* 34.3 (May 2012), pp. 425–441. DOI: 10.1007/s00281-012-0309-9 (cit. on pp. 14, 74).

[SBR16] Himani Sachdeva, Mustansir Barma, and Madan Rao. „Nonequilibrium description of de novo biogenesis and transport through Golgi-like cisternae“. eng. In: *Scientific Reports* 6 (Dec. 2016), p. 38840. DOI: 10.1038/srep38840 (cit. on pp. 20, 21, 24).

[Sch+19] Jennifer Schoberer, Eva Liebminger, Ulrike Vavra, et al. „The Golgi Localization of GnTI Requires a Polar Amino Acid Residue within Its Transmembrane Domain“. eng. In: *Plant Physiology* 180.2 (June 2019), pp. 859–873. DOI: 10.1104/pp.19.00310 (cit. on p. 103).

[Sci+97] N. Sciaky, J. Presley, C. Smith, et al. „Golgi tubule traffic and the effects of brefeldin A visualized in living cells“. eng. In: *The Journal of Cell Biology* 139.5 (Dec. 1997), pp. 1137–1155 (cit. on p. 9).

[She+13] Jinbo Shen, Yonglun Zeng, Xiaohong Zhuang, et al. „Organelle pH in the Arabidopsis Endomembrane System“. English. In: *Molecular Plant* 6.5 (Sept. 2013), pp. 1419–1437. DOI: 10.1093/mp/sst079 (cit. on p. 7).

[SN11] Suda Yasuyuki and Nakano Akihiko. „The Yeast Golgi Apparatus“. In: *Traffic* 13.4 (Dec. 2011), pp. 505–510. DOI: 10.1111/j.1600-0854.2011.01316.x (cit. on p. 24).

[SO01] Harald Stenmark and Vesa M. Olkkonen. „The Rab GTPase family“. In: *Genome Biology* 2 (Apr. 2001), reviews3007. DOI: 10.1186/gb-2001-2-5-reviews3007 (cit. on p. 8).

[SR13] Pierre Sens and Madan Rao. „(Re)modeling the Golgi“. eng. In: *Methods in Cell Biology* 118 (2013), pp. 299–310. DOI: 10.1016/B978-0-12-417164-0.00018-5 (cit. on p. 24).

[SSM10] Hayley J. Sharpe, Tim J. Stevens, and Sean Munro. „A Comprehensive Comparison of Transmembrane Domains Reveals Organelle-Specific Properties“. English. In: *Cell* 142.1 (July 2010), pp. 158–169. DOI: 10.1016/j.cell.2010.05.037 (cit. on pp. 6, 102).

[Sta11] Pamela Stanley. „Golgi glycosylation“. eng. In: *Cold Spring Harbor Perspectives in Biology* 3.4 (Apr. 2011). DOI: 10.1101/cshperspect.a005199 (cit. on pp. 13, 23).

[Sud+13] Yasuyuki Suda, Kazuo Kurokawa, Ryogo Hirata, and Akihiko Nakano. „Rab GAP cascade regulates dynamics of Ypt6 in the Golgi traffic“. eng. In: *Proceedings of the National Academy of Sciences of the United States of America* 110.47 (Nov. 2013), pp. 18976–18981. DOI: 10.1073/pnas.1308627110 (cit. on pp. 9, 28).

[Suz+17] Reiko Suzuki, Ichiro Nishii, Shigeru Okada, and Tetsuko Noguchi. „3D reconstruction of endoplasmic reticulum in a hydrocarbon-secreting green alga, Botryococcus braunii (Race B)“. In: *Planta* 247 (2017), pp. 663–677. DOI: 10.1007/s00425-017-2811-8 (cit. on p. 5).

[Tak+06] Shigeo Takamori, Matthew Holt, Katinka Stenius, et al. „Molecular anatomy of a trafficking organelle“. eng. In: *Cell* 127.4 (Nov. 2006), pp. 831–846. DOI: 10.1016/j.cell.2006.10.030 (cit. on pp. 28, 87).

[Tan+18] Sayuri Tanabashi, Keiko Shoda, Chieko Saito, et al. „A missense mutation in the NSF gene causes abnormal Golgi morphology in Arabidopsis thaliana“. eng. In: *Cell Structure and Function* (Feb. 2018). DOI: 10.1247/csf.17026 (cit. on p. 72).

[TM17] Masashi Tachikawa and Atsushi Mochizuki. „Golgi apparatus self-organizes into the characteristic shape via postmitotic reassembly dynamics“. eng. In: *Proceedings of the National Academy of Sciences of the United States of America* 114.20 (May 2017), pp. 5177–5182. DOI: 10.1073/pnas.1619264114 (cit. on pp. 19, 24).

[TSS05] Matthew S. Turner, Pierre Sens, and Nicholas D. Socci. „Nonequilibrium Raftlike Membrane Domains under Continuous Recycling“. In: *Physical Review Letters* 95.16 (Oct. 2005), p. 168301. DOI: 10.1103/PhysRevLett.95.168301 (cit. on pp. 39, 48).

[Tur+12] Vito Turk, Veronika Stoka, Olga Vasiljeva, et al. „Cysteine cathepsins: From structure, function and regulation to new frontiers“. In: *Biochimica et Biophysica Acta (BBA) - Proteins and Proteomics*. Proteolysis 50 years after the discovery of lysosome 1824.1 (Jan. 2012), pp. 68–88. DOI: 10.1016/j.bbapap.2011.10.002 (cit. on p. 7).

[Van22] Antoni Van Leeuwenhoek. *Opera omnia, seu arcana naturæ, ope exactissimorum microscopiorum detecta, experimentis variis comprobata, epistolis, ad varios illustres viros, ...Antonii à Leeuwenhoek*. Editio novissima, prioribus emendatior ..., 1722 (cit. on p. 2).

[VS18a] Quentin Vagne and Pierre Sens. „Stochastic Model of Maturation and Vesicular Exchange in Cellular Organelles“. In: *Biophysical Journal* 114.4 (Feb. 2018), pp. 947–957. DOI: 10.1016/j.bpj.2017.12.018 (cit. on pp. 20, 24, 29).

[VS18b] Quentin Vagne and Pierre Sens. „Stochasticm Model of Vesicular Sorting in Cellular Organelles“. In: *Physical Review Letters* 120.5 (Feb. 2018), p. 058102. DOI: 10.1103/PhysRevLett.120.058102 (cit. on p. 20).

[VTS15] Quentin Vagne, Matthew S. Turner, and Pierre Sens. „Sensing Size through Clustering in Non-Equilibrium Membranes and the Control of Membrane-Bound Enzymatic Reactions“. eng. In: *PloS One* 10.12 (2015), e0143470. DOI: 10.1371/journal.pone.0143470 (cit. on pp. 38, 48).

[Wan+17] Peng Wang, Hong Wang, Jiangtao Gai, et al. „Evolution of protein *N*-glycosylation process in Golgi apparatus which shapes diversity of protein *N*-glycan structures in plants, animals and fungi“. en. In: *Scientific Reports* 7 (Jan. 2017), p. 40301. DOI: 10.1038/srep40301 (cit. on pp. 74, 104).

[Wil14] Herbert S. Wilf. *Generatingfunctionology*. en. Google-Books-ID: XOPMBQAAQBAJ. Elsevier, May 2014 (cit. on p. 69).

[WS10] Jen-Hsuan Wei and Joachim Seemann. „Unraveling the Golgi ribbon“. eng. In: *Traffic (Copenhagen, Denmark)* 11.11 (Nov. 2010), pp. 1391–1400. DOI: 10.1111/j.1600-0854.2010.01114.x (cit. on p. 16).

[WS17] Jen-Hsuan Wei and Joachim Seemann. „Golgi ribbon disassembly during mitosis, differentiation and disease progression“. eng. In: *Current Opinion in Cell Biology* 47 (Aug. 2017), pp. 43–51. DOI: 10.1016/j.ceb.2017.03.008 (cit. on pp. 15, 24).

[Yam+14] Koji Yamano, Adam I. Fogel, Chunxin Wang, Alexander M. van der Bliek, and Richard J. Youle. „Mitochondrial Rab GAPs govern autophagosome biogenesis during mitophagy“. eng. In: *eLife* 3 (Feb. 2014), e01612. DOI: 10.7554/eLife.01612 (cit. on p. 8).

[YHW09] Jordan T. Yelinek, Cynthia Y. He, and Graham Warren. „Ultrastructural study of Golgi duplication in Trypanosoma brucei“. eng. In: *Traffic (Copenhagen, Denmark)* 10.3 (Mar. 2009), pp. 300–306. DOI: 10.1111/j.1600-0854.2008.00873.x (cit. on pp. 30, 46).

[YW14] Masashi Yamaguchi and Cedric ODriscoll Worman. „Deep-sea microorganisms and the origin of the eukaryotic cell“. en. In: 47.1 (2014), p. 20 (cit. on p. 4).

[ZH13] Miao Zhang and Junjie Hu. „Homotypic fusion of endoplasmic reticulum membranes in plant cells“. eng. In: *Frontiers in Plant Science* 4 (Dec. 2013), p. 514. DOI: 10.3389/fpls.2013.00514 (cit. on p. 9).

[Zha+18] Liwei Zhao, Peng Liu, Gaelle Boncompain, et al. „Identification of pharmacological inhibitors of conventional protein secretion“. In: *Scientific Reports* 8 (Oct. 2018). DOI: 10.1038/s41598-018-33378-y (cit. on p. 104).

List of Figures

List of Tables